Hull Vibration Analysis of a Small Multipurpose Fishing Vessel from Newfoundland and Labrador

by © Mohamed Auf

A Thesis submitted to the School of Graduate Studies

in partial fulfillment of the requirement for the degree of

Master of Ocean and Naval Architectural Engineering

Faculty of Engineering and Applied Science

Memorial University of Newfoundland

May 2020

St. John’s, Newfoundland and Labrador

Abstract

Regarded as one of the most dangerous industries for workers, commercial fishing is a high-risk industry that provides a living for millions around the world. It is imperative for designers to analyze and obtain practical solutions for the reduction of these unnecessary hazards. The need to quantify and analyze the risk areas onboard fishing vessels has been pressed by authorities worldwide from the increasing number of injuries and fatalities in this industry. Fishing vessels are mainly known for their high levels of vibrations due to their layout and relatively small size. Vibration mitigation on fishing vessels impacts both vessel equipment and onboard crew. Benefits of reduction include protection of sensitive ship equipment and hydro-acoustic apparatus, low noise emitted to the water so as not to scare fish schools, and increased safety of the onboard crew. Fish harvesters working in these vessels are in constant prolonged exposure causing a decrease in comfort levels leading to an unsafe work environment. The approach of this study is to effectively capture the dynamics of a case study fishing vessel in terms of vibrations, providing a practical methodology for designers to implement.

Acknowledgment

First and foremost, I would like to thank my supervisor Dr. Lorenzo Moro of the Ocean and Naval Department of Memorial University of Newfoundland. His door was always open and has been tremendously patient and continually guiding me during my research. My deepest and profound gratitude goes to him for this opportunity.

I want to thank Mr. Rick Young of TriNav Marine Brokerage Inc. for the fishing vessel plans, composite hull plate sample, and various meetings throughout the research. His time and consideration are much appreciated and vital to the success of this research.

I am very grateful for my research group colleagues who have been supportive and critical to the completion of my work, namely: Giorgio Burella, Jacopo Fragasso, and Alessandro Zambon. Without their sharing of knowledge and data, the validation of the model could not have been successfully performed.

I would also like to express my appreciation for the collaboration by Prof. Marco Biot of the Department of Engineering and Architecture in University of Trieste, Italy.

Last but not least, I would like to thank my family and friends for their consistent support throughout my studies.

Table of Contents

List of Figures

List of Tables

Chapter 1: Introduction

Working and living onboard vessels can impose a vibratory strain on the human body. The tight space construction, use of lower cost and longer life materials further exploit this phenomenon, making it a toxic environment for the onboard crew. Commercial shipping is an essential industry, but poor onboard safety has negatively affected seafarer's willingness to partake in such a dangerous vocation. Considered the most extended series of consistent analysis on seafarer employment ratio, in Britain commercial seafarers dropped an astoundingly from 208 per 100,000 persons in 1921 to only 11 per 100,000 in the 1996-2005 period (Roberts, 2008). The reason behind it is simply that the fatality rate among seafarers may reach up to ten times more than the average onshore worker (Roberts & Hansen, 2002).

The latest FAO statistics indicate that the world fishing fleet consists of 4.5 million vessels, of which two-thirds are engine-powered, and directly employ approximately 60 million people (FAO (Food & Agriculture Organisation), 2017). The economic value of the fisheries sector is about 140 billion USD, with a progressive yearly increase in human consumption (FAO (Food & Agriculture Organisation), 2018). As such, the fisheries sector may be considered a pivotal global market connecting the livelihoods of millions of people, yet insufficient action is taken by the worldwide community to decrease risks associated with these occupations.

The International Labor Organization estimates that 24,000 fatalities occur worldwide per year. Fish workers also sustain very high rates of non-fatal injuries worldwide, yet they are

most likely under-reported (FAO (Food & Agriculture Organisation), 2001). Studies also demonstrate that risk patterns formed from the injuries sustained from varying fishing vessel types and fish harvesting activities is possible (Jaremin & Kotulak, 2004). These risk patterns are also modified by weather, water temperature, presence of potentially harmful marine life, concluding to the fact that fishing is consistently shown to be among the highest of industries in terms of risk.

Numerous ergonomic studies have been performed, highlighting the increasingly harmful effects of vibration resonance on the human body on board vessels (Subashi et al., 2008). In general, onboard crew is exposed to low-frequency whole-body vibration, i.e. exposure of the entire body on all three axes (Kingma et al., 2003) as well as impulse shock loads such as slamming and whipping (Dessi & Ciappi, 2010; Kapsenberg, 2011). Low-frequency motions can result in motion sickness, body instability, fatigue, and increased health risk, while high-frequency vibrations create discomfort and possible cause degraded performance and health (American Bureau of Shipping, 2016).

Generally, studies show a trend that vibratory accelerations in the 1-80 Hz range directly affect the spine, resulting in lower back disorders (Jensen & Jepsen, 2014). Research has shown an increased pressure in the cerebrospinal fluid caused by acceleration of $\pm 0.4 m/s^2$ and rolling of ±8 degrees onboard trawlers (Torner et al., 1994). Twisting motions, a persistent motion for seafarers in a tight space unbalanced environment, was suggested to be a prime factor causing lower back pain (Hoogendoorn et al., 2000). Further studies indicate increased fatigue, and reduced sleep quality are highly linked to vibratory accelerations either directly (Haward et al., 2009), or indirectly through the reduced oxygen

exchange due to constant physical strain onboard (Wertheim et al., 2002). Some researchers also took to the study of resonances within the human body, concluding that for thoracic and abdominal organs the resonance frequency is from 3-9 Hz, while visual disturbances due to resonance of the eyeball may occur around 60-90 Hz (Jensen & Jepsen, 2014).

Later studies show that a condition that affects many seafarers named Sopite syndrome, defined as "inordinate sleepiness, lassitude or drowsy inattention induced by vibrations, low-frequency oscillatory motion (e.g., ship motion) or general travel stress", could be hazardous in their workplace due to their reliance on physical activity. Common symptoms among seafarers, similar to motion sickness, are motion-induced fatigue, causing lack of motivation, excessive tiredness, and reluctance to work are also tied to onboard vibrations also (Haward et al., 2009).

From these studies and more, seafarers are subject to the effect of these vibratory accelerations for prolonged periods, resulting in an overall deterioration of their physical and mental health. Safety procedures and guidelines often take seafarers' physical condition for granted, so much so that despite increasingly stringent onboard protocols, the International Maritime Organization statistics show that approximately 80% of accidents onboard cargo ships are caused by human factors (Oldenburg et al., 2010).

As such, recent attention in the maritime industry was devoted to the field of onboard comfort and habitability in terms of vibration levels. ISO standards 6954:2000 (recently updated to 20283-5:2016 (International Organization for Standardization (ISO), 2016)) and 2631-1/2 address mechanical vibration and shock guidelines with regards to habitability in

passenger/merchant ships and buildings respectively (International Organization for Standardization (ISO), 1997, 2000). Based on these standards, various classification societies offer comfort grading requirements for different vessel types (American Bureau of Shipping, 2016; Asmussen et al., 2001). These habitability guides are usually focused on passenger ships, recreational luxury crafts, supply vessels, and navy ships and do not offer adequate criteria targeted for the highest risk category of vessels, the fishing vessel. However, recently, the industry is becoming increasingly aware of classifying vibration onboard fishing vessels separately due to its high risk of occupational health and safety (Maritime and Coastguard Agency, 2007).

Many studies have been performed to minimize the noise and vibration levels aboard vessels in terms of structural safety and ergonomic-personal wellbeing, particularly in the context of luxury transportation (American Bureau of Shipping, 2006; Asmussen et al., 2001; Norwood & Dow, 2013; Ojak, 1988; Pais et al., 2017). The development of floating floors (Moro et al., 2016), and resilient mounts (Biot & Moro, 2012) aim to decouple ship structures from the onboard sources. The use of viscoelastic materials has proven to provide a viable means to dampen the effects of noise and vibration on board (Fragasso et al., 2017; Vergassola et al., 2018). However, a more dependable process, from a control hierarchy perspective, would be the elimination of vibration during the design of fishing vessels as proposed in this study, rather than the use of corrective methods post-manufacturing.

The main aim of this study is to provide designers with a practical procedure to implement during the design phase of fishing vessels. In a broad sense, the process is to apply typical

modal analysis and frequency response functions to the complex structure through the aid of numerical methods. Research has proven that Finite Element (FE) analysis is a viable technique for such a study and provides agreeable results to experimental measurements for ship structures (American Bureau of Shipping, 2014; Bašić & Parunov, 2013; Chen, 2002; Koona et al., 2008; Norwood & Dow, 2013; Pais et al., 2017). Modal analyses will provide a means and measure to identify and evaluate the fishing vessels' response from a vibration point of view. The design procedure entails the characterization of sources, modeling of ships' structure, simulation of its dynamics, analysis of its response, and finally the identification of critical areas. Once these vital areas are highlighted, methods of mitigation can be applied to the simulation at the design phase of the vessel.

The main objective of the presented research is to develop a design procedure to simulate vibration levels on a fishing vessel. Other objectives of this study may be summarized as follows:

- Effective dynamic modeling of a fishing vessel using FE analysis;
- Determination of an overall structural damping ratio that can be used to predict vibration levels on board;
- Analyze the vessel's dynamic responses for identification of critical areas

Chapter 2: Literature Review

Marine vessels are a complex system of conjoined structural and mechanical assemblies, excited by many dynamic forces, whether transient or periodic, and further affected by highly variable sea and operating conditions. Vibrations rising from said dynamic forces affect the vessels' structural fatigue as well as crew comfort, ultimately compromising safety as discussed in the previous chapter. However, designers often regarded the dynamic response of these structures too problematic, with its plethora of variables, to consider in their designs, let alone predict. Researchers acknowledged the importance of studying and predict the response of vibrations onboard vessels as early as World War II, though they were focused on solutions for singular vibration problems rather than on the ship as a whole (Ship Structure Committee, 1990).

Once international traction was gained concerning vibration levels on board, and their detrimental health effects on the onboard crew, international agencies and classification societies developed criteria and guidelines for the acceptable limits. The originator for the categorization of vibration levels was the International Organization of Standardization and specifically standards ISO 2631-1 and ISO 6954:1984 address the evaluation of human exposure to vibrations, and vibrations in merchant ships respectively (International Organization for Standardization (ISO), 1984, 1997). The latter provided guidelines based on single amplitude peak resonances of velocity at discrete frequencies and represented in an acceptability chart. The chart is shown below in Figure 2.1.

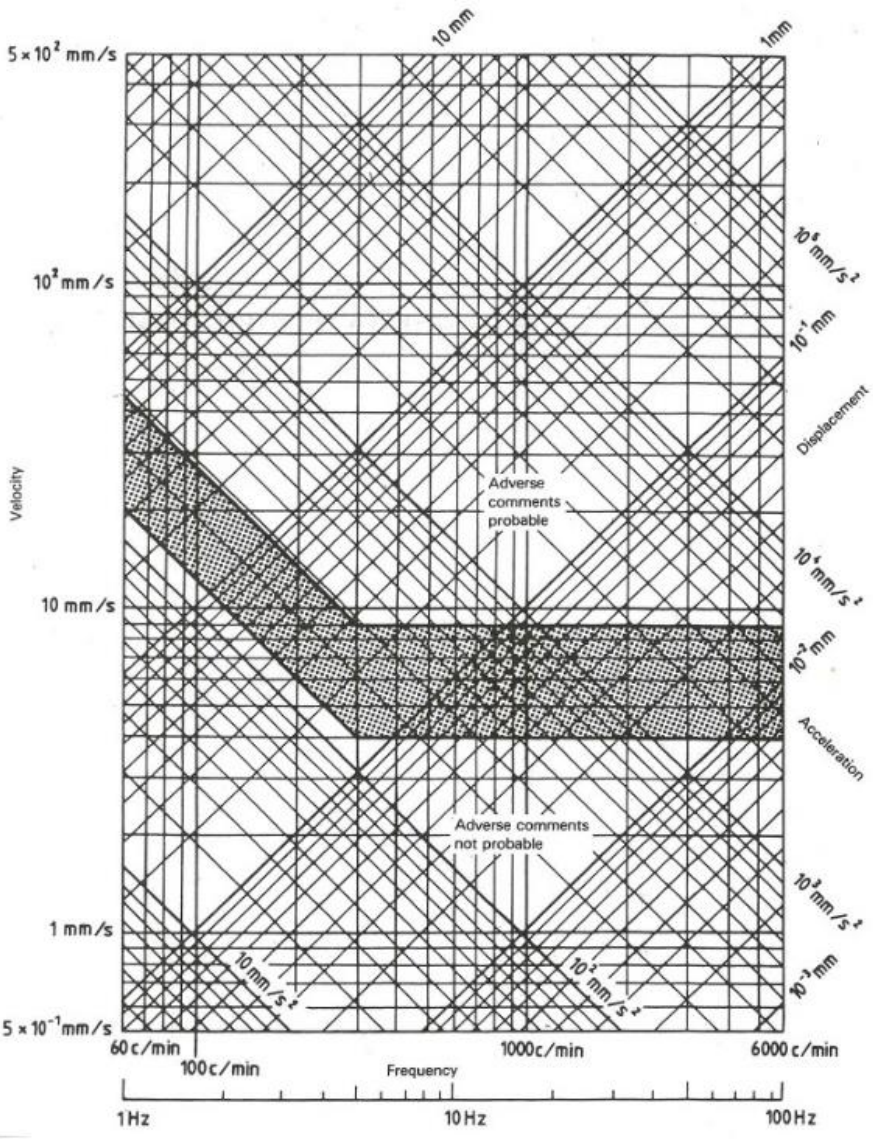

Figure 2.1: ISO 6954:1984 guidelines for acceptable vibration levels

Unfortunately, the criteria shown in Figure 2.1 contradicts guidelines described in ISO 2631-1, which lead to the more recent revision of ISO 6954:2000. The newly revised ISO 6954:2000 is a weighted root mean square average approach for all frequencies from 1 to 80 Hz. This new development makes the assessment of measurements easier for comparison but combines all excitation sources into the response rendering individual

excitation analysis useless. ISO 6954:2000 may be summarized in Table 2.1, as shown below (International Organization for Standardization (ISO), 1997, 2000). Area Classifications depicted in Table 2.1 were categorized as follows: 'A' is passenger cabins, 'B' is crew accommodation areas, and 'C' is working areas.

Table 2.1: ISO 6954:2000 guidelines based on overall frequency weighted RMS values from 1-80Hz for different areas on a merchant ship

	Area Classification					
	A		B		C	
	mm/s²	*mm/s*	*mm/s²*	*mm/s*	*mm/s²*	*mm/s²*
Values above which adverse comments are probable	143	4	214	6	286	8
Values below which adverse comments are probable	71.5	2	107	3	143	4

Note 1: The zone between upper and lower values reflect the shipboard vibration environment commonly experienced and accepted.
Note 2: Values are of acceleration are given in mm/s²

The most recent update to improve comfort and onboard working conditions resulted in ISO 20283-5:2016, which has further abridged and integrated onboard vibration limits and increased categorization of spaces onboard to uphold these limits. Table 2.2 below shows the upper limit vibration level in terms of velocity and acceleration for each location type (International Organization for Standardization (ISO), 2016).

Table 2.2: ISO 20283-5:2016 guidelines for acceptable vibration limits onboard

	Velocity (mm/s)	Acceleration (mm/s²)
Crew Spaces		
Crew Accommodation	3.5	125
Workspaces	6.0	214
Offices	4.5	161
Navigation Bridge	5.0	179
Engine Control Room	5.0	179
Open-deck Recreation Spaces	4.5	161
Passenger Spaces		

Cabins and Public Spaces	3.5	125
Open-deck Recreation Spaces	4.5	161

Although seemingly comprehensive, ISO standards for evaluating vibration do not cover all vessel types. ISO 6954:1984 states its applicability to both turbine and diesel-driven merchant ships of length between perpendiculars of 100 meters or greater (International Organization for Standardization (ISO), 1984). In the revised ISO 6954:2000, the scope of vessels was increased to include passenger ships alongside merchant ships with no mention of length criteria (International Organization for Standardization (ISO), 2000). The final revision, ISO 20283-5:2016, applies to passenger and merchant ships, as its predecessor, but imposes further distinction to include ships with intended voyages of 24 hours or more (International Organization for Standardization (ISO), 2016). In spite of the limited scope of ship types, designers and researchers alike still use the ISO standards as a guideline even though their relevance may be compromised by varying vessel types.

Classification societies continually adopt the most recent ISO standards and produce their own rules for the assessment of onboard comfort. Through their studies, classification societies usually provide a more explicit mandate on the ships applicable to these comfort assessments and award different levels of certifications of compliance to vessels based on said assessment. For instance, Lloyd's Register states accommodation comfort is a function of ship type and layout and thus provides guidelines only to passenger ships (e.g., cruise, ro-ro ferries) or cargo ships (e.g. container ships, tankers) (LLoyd's Register, 2019). DNV-GL provides comfort guidelines that apply to all ship types, but guidelines are based on the ISO 6954:2000 rather than its reviewed version of 2016 (DNV GL, 2017). Although

providing the most comprehensive guide for habitability on ships, ABS rules apply to tankers, bulk carriers, container, cargo, or passenger vessels (American Bureau of Shipping, 2016). Though the certifications of compliance and comfort assessments are performed by these main societies, they must be requested by the owner and are purely optional.

Another common factor among classification societies is the use of FE analysis as a viable tool to predict onboard vibrations. To the extent that they have published specific detailed guidelines for vibration prediction using FE software, citing recommended practices to obtain viable results (American Bureau of Shipping, 2018; DNV GL, 2016). Although the use of FE analysis for vibrations is not a new concept, it is certainly reassuring for classification societies in the naval field to endorse FE analysis' practicality for vibration studies.

On the other hand, there is increasing use of FE analysis for vibration within the academic naval field. Though in the past, vibration study was typically performed using analytical methods (and often by hand), the development of powerful processors has made handling complex structures and performing simulations possible with high accuracy. This makes the use of FE analysis for ships and ship structures very attractive for researchers; due to the vessels' complex nature and avoiding the difficulty in analysis without using it. Studies are generally focused on the characterization of the onboard excitation sources, dynamic response of the vessel, and proposed mitigation techniques to employ on the vessel.

Research on the characterization of onboard excitation sources is typically focused on the most prominent source on a vessel, the propeller. Propellers create pressure pulses on the

ship hull from the induced rotary forces of the shaft lines. There are three methods for quantifying these pressure pulses: empirical methods (e.g. (Holden et al., 1980)), advanced theoretical approaches (e.g. panel, lifting surface, CFD), and experimental methods (Norwood & Dow, 2013). Reciprocating machinery, such as main engine and generator, have also been studied to provide a method to characterize their dynamic effects onboard (Biot et al., 2015). Studies were then expanded to characterize main engines that are installed on resilient mounts, which is a typical configuration in most vessels (Biot & Moro, 2012).

The dynamic response of the vessel, in terms of vibrations, has been the point of interest for researchers for several decades. With the onset of readily available commercial FE analysis software packages, vibration prediction has become a popular tool. Some researchers tackle the vessel globally to calculate dynamic properties of the vessel in both free and forced vibration analyses obtaining valuable insight on the ship (Deng et al., 2014; Moro et al., 2013; Norwood & Dow, 2013; Yucel & Arpaci, 2013) while others focus on local ship structures to lay the groundwork for understanding vibration transmission and eventually its mitigation (Alberto Ferrari & Rizzuto, 2003).

The thorough study investigation of vibration onboard using FE analysis discussed in the previous paragraph leads to the study of vibration control and mitigation. Much research was devoted to vibration control onboard in a general sense, such as (Daniela-Elena, 2013; Lin et al., 2009), highlighting approaches that may be taken in a vibration study of a vessel. Vibration mitigation studies, however, focus on local structure damping, assuming that the vessel's critical areas have been previously assessed. These studies such as (Bhattacharya

et al., 2002; A. Ferrari & Rizzuto, 2007; Fragasso et al., 2017; Johnson & Kienholz, 1982; Koona et al., 2008) employ the use of viscoelastic materials, either in the free layer damping or constrained layer damping configurations, and provide guidelines on effectiveness of each in terms of vibration attenuation.

Despite the availability of all the literature mentioned above, there is barely any research, classification society guidelines, or international standards available for assessing vibrations on fishing vessels. Fishing vessels are unique in terms of method of construction and materials used compared to other commercial merchant vessels. They are most often constructed by hand, in an uncontrolled environment, and often stray from design plans. The most common material for hulls and decking of fishing vessels are composite fiber-reinforced plastics that are formed via a hand lay-up technique. Many of these vessels are also motorized and constructed to minimize space. All of these factors have a high degree of variance and make pre-construction vibration assessments almost impossible. Seafarers are at risk from these vibratory accelerations affecting their mortality, quality of life, and livelihoods. This highlights the need for the world's community needs to focus on providing practical guidelines for the assessment of vibrations for fishing vessels, specifically in hopes of alleviating its notoriety as one of the most dangerous industries in the world.

Chapter 3: Methodology

The development of a numerical model to accurately capture the dynamic behavior of fishing vessels, in terms of onboard vibrations, is the foundation of this research. This chapter presents the approach taken to achieve the real-life dynamics of a fishing vessel using the FE method. Producing a FE model to predict onboard vibration requires a great deal of attention and detail towards input parameters and geometry as discussed in Section 3.3. As of typical structural vibration analysis problems, the free vibration analyses in the frequency domain were performed as in Section 3.4 which lead to the identification of the ship's global modes in dry and wet conditions. In Section 3.5 the forced frequency response of the vessel's structures was analyzed using excitation sources (as in Section 3.5.1) and also using a unitary force in a mobility study (as in Section 3.5.2). The excitation sources were then modeled based on experimental data, and equivalent response functions were obtained. The results of the forced vibration analysis were then validated against the experimental data acquired as described in Section 3.2. The validation was used to determine the fishing vessel overall structural damping ratio as shown in Section 3.5.2. A summary of the overall procedure taken is shown in Figure 3.1 below.

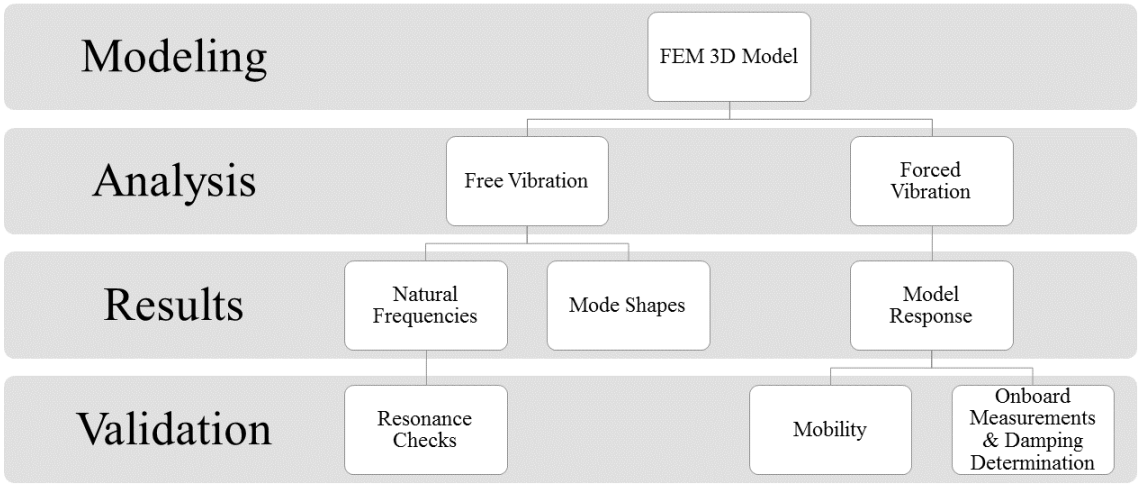

Figure 3.1: Flow Chart of Methodology

3.1. Vessel Case Study

The fishing vessel technical drawings were obtained from a local designer in St. John's, Newfoundland. The aim is to create a model for an existing vessel in operation to provide a practical outcome for design methodology in terms of ship vibrations. The case study vessel's side view is shown below in Figure 3.2.

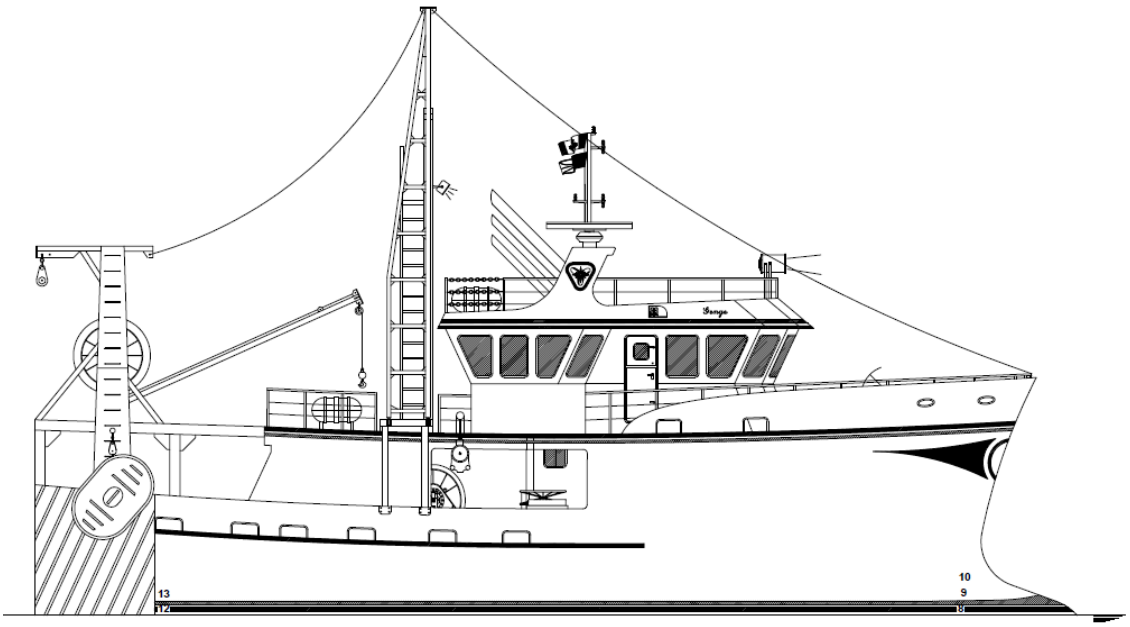

Figure 3.2: Case Study Fishing Vessel Side View (curtesy of TriNav Marine Design Inc.)

The case study fishing vessel is a multipurpose fishing vessel employed for fishing cod, shrimp, and crab equipped with its appropriate machinery. The main vessel dimensions are shown below in Table 3.1.

Table 3.1: Case Study Fishing Vessel Particulars

Case Study Fishing Vessel Particulars	
Length OVERALL	20.88m
Length AT DWL	20.62m
Breadth MOULDED	7.32m
Depth TOP OF KEEL TO TOP OF MAIN DECK AMIDSHIPS	4.01m
Depth TOP OF KEEL TO TOP OF MAIN DECK AMIDSHIPS	4.31m
Construction Material	GRP Composite
Design Draft AFT	3.61m
Design Draft FORWARD (HULL)	2.38m
Rake of Keel	1.24m (over 20.88m)
Deck Camber	0.91m
Main Deck Sheer AFT	6.1m
Upper Deck Sheer FWD	3.05m
Fuel Oil Capacity	Approx. 18180 liters
Fresh Water Capacity	Approx. 3400 liters

Gross Tonnage	Less than 150 GT
Design/Construction Rules	ABS (Reinforced Plastic Vessels) / TC SFV Regulations

3.2. Onboard Measurements

The numerical model was built based on the case-study fishing vessel and validated using measurements taken at sea. The onboard experimental measurements were taken during regular operation at sea using accelerometers to capture vibrations at critical points within the crew quarters on this ship.

Locations of high structural stiffness were selected for mounting accelerometers to exclude unwanted input vibrations and reduction of undesirable background noise. These locations were chosen to evaluate onboard comfort (such as the worker cabins) and to record the vibration source excitation output to be used in the FE model. The sources output velocity levels were measured by placing the accelerometers on beam foundations for the engine and generator, and the beam and hull area directly above the propeller as the point of nearest measurement (Moro et al., 2013). Figure 3.3 shows the general arrangement of the vessel and highlights the measurement points.

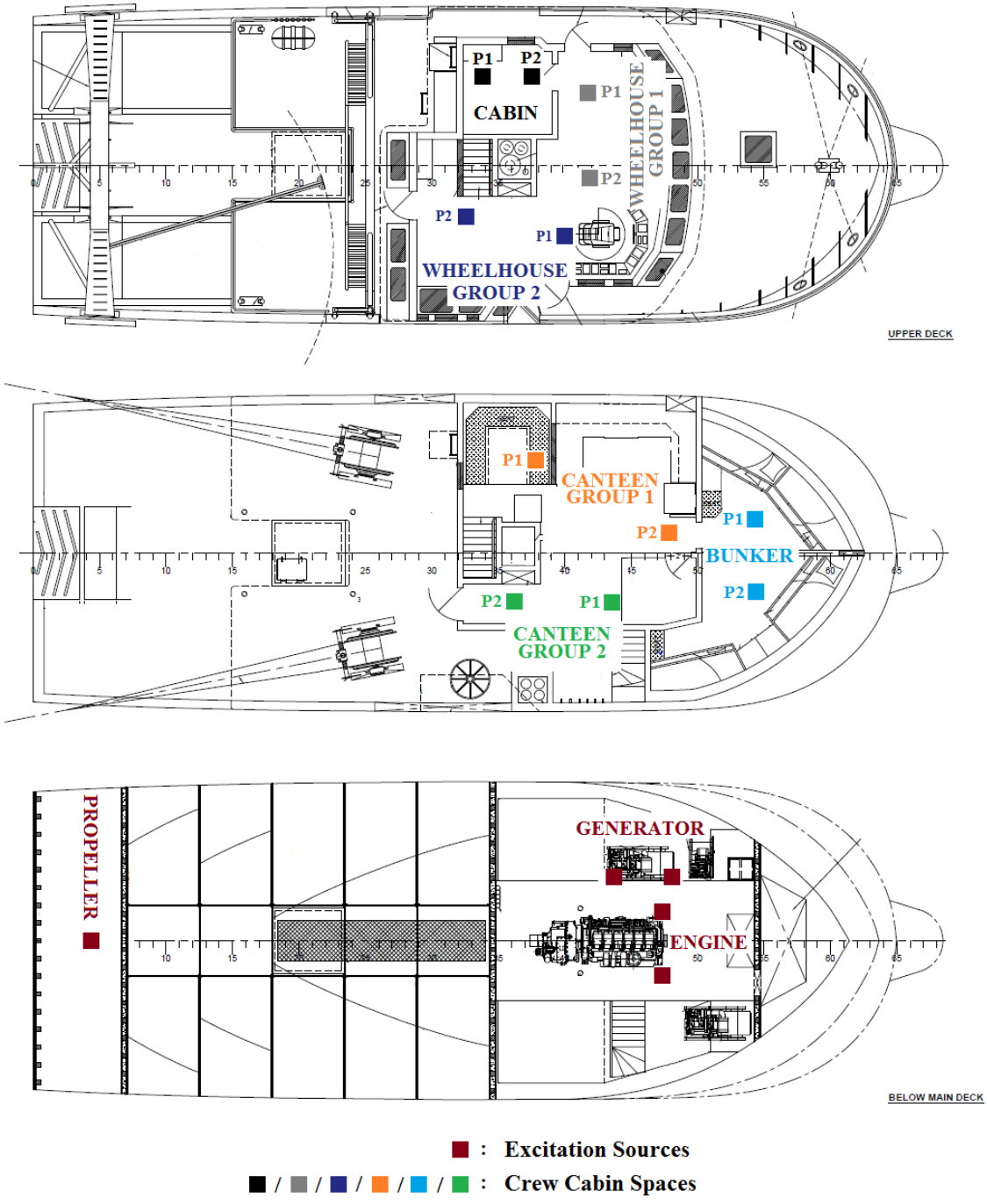

Figure 3.3: Map of Measurement Points on Vessel

The data was acquired alongside sea trials for acoustic measurements in a Newfoundland and Labrador case study (Burella et al., 2019) as the vessel was steaming at 1596 RPM as per ISO 6954:1984 Mechanical Vibration and Shock standard. Although the ISO 6954:1984 was withdrawn and replaced with ISO 6954:2000, the study adopted the former due to the desire to observe the effect of each vibration source individually rather than a holistic approach as described in the latter standard.

Time-domain measurements of one-minute span were recorded using ICP® Accelerometers (model number 352C33) controlled by a National Instruments® NI 9234 dynamic signal acquisition module connected via USB to a Panasonic® Toughbook laptop computer. Even though the scope of the present study was up to the 80 Hz range, a sampling rate of 52.6 kHz was used to address structure-borne noise for future initiatives. The acquired signal was then filtered to obtain the vibration levels in the frequency range of interest.

LabVIEW® was used to post-process recorded measurements into the required format for validation with the FE analysis. The measurements were recorded three times at each point and then post-processed by averaging to increase the overall quality of the dynamic structural representation. The averaged signals were then converted into the frequency domain employing a Hanning window filter. Vibration level amplitudes were expressed in root mean square (R.M.S.) values to allow for a direct comparison with the FE simulation results (Pais et al., 2017).

3.3. Finite Element Modeling

The engineering drawings for the case-study fishing vessel were used to create a detailed numerical model using finite elements. The FE method was chosen to analyze vibrations as it is a proven method to effectively model the size and complexity of a fishing vessel, such as the case study vessel, in terms of degrees of freedom and number of components. FE analysis is also capable of solving the free and forced vibration problems of such a model for the required frequency range. The model was constructed and analyzed using the MSC.Patran® and MSC.Nastran® suite. The finalized model is shown below in Figure 3.4.

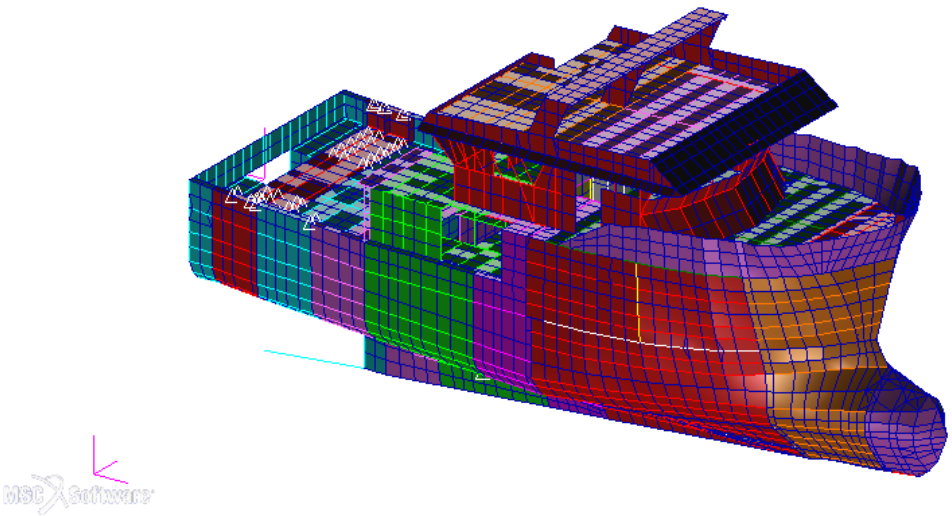

Figure 3.4: FE Model of Case Study Fishing Vessel

3.3.1. Finite Element Modeling

Appropriate material definition and application is of pivotal importance to the FE model to correctly mimic the structural behavior of the case study fishing vessel. The case study

fishing vessel is made primarily of glass/fiber-reinforced composites and wood. The former is very difficult to model due to its complex nature of alternating laminations of randomly oriented fibers in resin (chopped strand matt) and woven directional sheets (woven roving) in resin. The manufacturing process of these composites for fishing vessels is often performed by hand in an uncontrolled environment, which also introduces irregularities and discontinuities throughout the structure. Consequently, a sample of the composite material was obtained and tested to reverse engineer its dynamic behavior and use it as an input to the FE model. The material properties and respective material model definitions used in the FE model are shown below in Table 3.2.

Table 3.2: Material Properties for FE Model

Material	Properties	Material Definition
Aluminum	$E = 71.00\ GPa$ $\nu = 0.33$ $\rho = 2700\ kg/m^3$	Linear Elastic Isotropic
Steel	$E = 200\ GPa$ $\nu = 0.26$ $\rho = 7850\ kg/m^3$	Linear Elastic Isotropic
Chopped Strand Matt (CSM) (Naughton et al., 1985)	$E = 8\ GPa$ $\nu = 0.33$ $\rho = 1400\ kg/m^3$	Linear Elastic Isotropic
Woven Roving (WR) (Naughton et al., 1985)	$E_{11} = 20\ GPa$ $E_{22} = 20\ GPa$ $G_{12} = 2\ GPa$ $G_{23} = 2\ GPa$ $G_{13} = 2\ GPa$ $\rho = 1750\ kg/m^3$	Linear Elastic 2D Orthotropic
Douglas Fir (Ross & USDA Forest Service., 2010)	$E_{11} = 12.7\ GPa$ $E_{22} = 0.93\ GPa$ $G_{12} = 0.93\ GPa$ $G_{23} = 0.14\ GPa$ $G_{13} = 0.75\ GPa$ $\rho = 650\ kg/m^3$	Linear Elastic 2D Orthotropic
Plywood	$E_{11} = 7.96\ GPa$	Linear Elastic

(Janowiakt et al., 2007)	$E_{22} = 4.2\ GPa$ $G_{12} = 0.72\ GPa$ $G_{23} = 57\ MPa$ $G_{13} = 1.06\ GPa$ $\rho = 650\ kg/m^3$	2D Orthotropic
Spruce (Ross & USDA Forest Service., 2010)	$E_{11} = 110.7\ GPa$ $E_{22} = 0.7\ GPa$ $G_{12} = 0.5\ GPa$ $G_{23} = 23\ MPa$ $G_{13} = 0.62\ GPa$ $\rho = 800\ kg/m^3$	Linear Elastic 2D Orthotropic

Further to the list of materials incorporated into the FE model shown in Table 3.2, the case study fishing vessel composite layup differs depending on the physical location. Figure 3.5 is an excerpt from the case study vessel plans identifying the different layups configurations, each defined with its composite material definition in the FE model.

AREA	OUTSIDE (MINIMUM)	INSIDE (MINIMUM)	TOTAL
HULL SIDES	10 CSM, 8 WR + VINEER (3 CSM)	4 CSM, 2 WR	27 LAYERS, 52.10 oz / sq. ft
HULL BOTTOM	10 CSM, 8 WR + VINEER (3 CSM)	4 CSM, 2 WR	27 LAYERS, 52.10 oz / sq. ft
HULL IWO RUDDER	14 CSM, 12 WR	4 CSM, 2 WR	32 LAYERS, 64.24 oz / sq. ft
HULL IWO STERN POST	16 CSM, 14 WR		30 LAYERS, 57.76 oz / sq. ft
TUCK	12 CSM, 9 WR + VINEER (3 CSM)	4 CSM, 2 WR	30 LAYERS, 61.24 oz / sq. ft
KEEL	14 CSM, 12 WR	4 CSM, 2 WR	32 LAYERS, 64.24 oz / sq. ft
STEM (in way of bulb)	14 CSM, 12 WR	7 CSM, 5 WR	28 LAYERS, 52.08 oz / sq. ft
HULL IWO DEADWOODS	16 CSM, 14 WR		30 LAYERS, 57.76 oz / sq. ft
MAIN DECK	4 CSM, 2 WR		6 LAYERS, 11.32 oz / sq. ft
UPPER DECK	3 CSM, 1 WR		4 LAYERS, 7.16 oz / sq. ft
HOUSE FRONT	3 CSM, 1 WR		4 LAYERS, 7.16 oz / sq. ft
HOUSE SIDES	2 CSM		2 LAYERS, 3.00 oz / sq. ft
HOUSE TOP	3 CSM		3 LAYERS, 4.50 oz / sq. ft
MAIN DECK SHELF		4 CSM, 2 WR	6 LAYERS, 11.32 oz / sq. ft
UPPER DECK SHELF FORWARD		4 CSM, 2 WR	6 LAYERS, 11.32 oz / sq. ft
LONGITUDINAL STIFFENERS IN LAZARETTE, ENG ROOM & FOC'SLE		4 CSM, 2 WR	6 LAYERS, 11.32 oz / sq. ft
LONGITUDINAL STIFFENERS IN IN FISH HOLD		5 CSM, 4 WR BELOW BILGE 4 CSM, 2 WR ABOVE BILGE	9 LAYERS, 16.98 oz / sq. ft 6 LAYERS, 11.32 oz / sq. ft
LONGITUDINAL STIFFENERS IN TWEEN DECK FORWARD		4 CSM, 2 WR	6 LAYERS, 11.32 oz / sq. ft
TRANSVERSE DEEP WEB FRAMES IN ENGINE ROOM		6 CSM, 4 WR BELOW BILGE 4 CSM, 2 WR ABOVE BILGE	10 LAYERS, 19.64 oz / sq. ft 6 LAYERS, 11.32 oz / sq. ft
TRANSVERSE DEEP WEB FRAMES IN LAZARETTE		5 CSM, 4 WR BELOW BILGE 4 CSM, 2 WR ABOVE BILGE	9 LAYERS, 16.98 oz / sq. ft 6 LAYERS, 11.32 oz / sq. ft
TRANSVERSE DEEP WEB FRAMES FORE PEAK		5 CSM, 3 WR BELOW BILGE 4 CSM, 2 WR ABOVE BILGE	8 LAYERS, 15.48 oz / sq. ft 6 LAYERS, 11.32 oz / sq. ft
TRANSVERSE DEEP WEB FRAMES FORE PEAK (in bulb ballast tank)		7 CSM, 5 WR BELOW BILGE	12 LAYERS, 23.80 oz / sq. ft
FISH PENS		2 CSM EACH SIDE	4 LAYERS, 6.00 oz / sq. ft
BULKHEADS		2 CSM EACH SIDE	4 LAYERS, 6.00 oz / sq. ft
TRANSOM	10 CSM, 8 WR	4 CSM, 2 WR	24 LAYERS, 47.60 oz / sq. ft
DEEP FLOORS		4 CSM, 2 WR EACH SIDE	6 LAYERS, 11.32 oz / sq. ft
BULWARKS	7 CSM, 5 WR + VINEER (3 CSM)	4 CSM, 2 WR	21 LAYERS, 39.62oz / sq. ft
SHELTER SIDES	3 CSM	2 CSM	5 LAYERS, 7.50 oz / sq. ft
SHAFT TUNNEL		4 CSM, 2 WR EACH SIDE	6 LAYERS, 11.32 oz / sq. ft

Figure 3.5: Composite Layup Configurations

3.3.2. Hull Sample Composite Validation

Due to the complexities associated with the modeling laminated fiberglass composites on such a large structure, a validation study was performed on a sample of the hull to validate its dynamic properties. The study consists of an experimental frequency response analysis of the hull sample using an impact hammer and updating the material properties in an equivalent FE analysis. The hull composite sample was labeled into a grid to define the location of the accelerometers and exciting force, as shown below in Figure 3.6, for the experimental frequency response analysis.

Figure 3.6: Labeled Composite Hull Sample

The plate was excited at a selected point, named the reference point (Point 6 in Figure 3.6), employing an impact hammer (ICP Impact Hammer Model 086C03), of which its force is measured in its inbuilt quartz force sensor. The resulting vibrations of the plate on the selected point and adjacent points were measured by accelerometers (ICP Accelerometer Model 352C33), which were securely mounted on the plate. The input force and vibrations

were acquired using a National Instruments Data Acquisition System (NI 9234) and processed on a laptop with National Instruments LabVIEW® script. The hull sample was examined in a free-free boundary condition, which was mimicked in the experimental setup using long, flexible nylon wires, as shown below in Figure 3.7.

Figure 3.7: Experimental Setup for Composite Hull Plate

Three accelerometers were recorded at a time; therefore, the procedure was repeated until the vibrations of all points were recoded against the reference point. The accelerometer readings, along with their respective forces, were then superimposed to create a complete spectrum representing the plate dynamic behavior. For obtaining accurate frequency response functions, at each singular point, the modal hammer was struck three times and

the LabVIEW® script averages value of the responses recorded. The signal coherence function was calculated for each frequency response function (FRF) in order to verify its quality. While measuring, an accelerometer was placed on the stiff supporting structure in order to monitor the vibration energy lost in the experiment and validate the free-free boundary conditions of the sample.

The equivalent FE model was then created based on the same experimental setup, as shown in Figure 3.8 below. The same shell elements and material model were used as the FE model for the vessel's hull, MSC.Nastran® 's CQUAD4, which are compatible with composite laminates. A convergence study was performed for element size and compatible element formulations, which lead to a mesh size of 0.02 meters and using standard CQUAD4 formulation for thin laminates. A unitary force was applied to the reference point, and MSC.Nastran® solver was set to SOL108 for Frequency Response using Direct formulation to recreate the experimental setup up to 1kHz range.

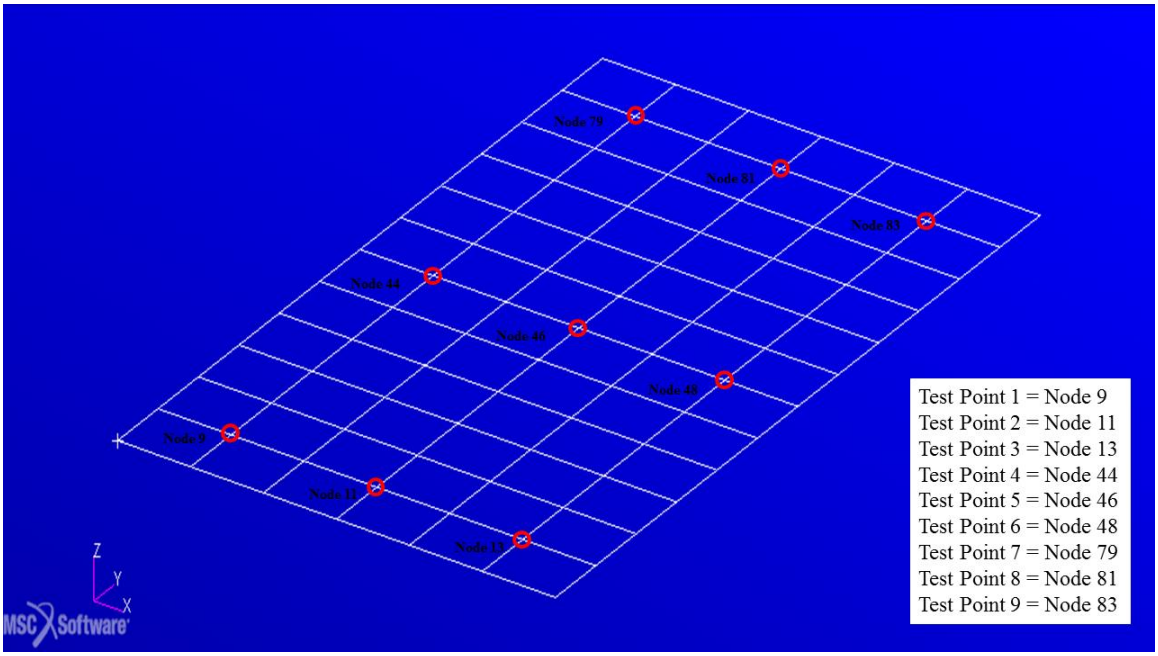

Figure 3.8: Finite Element Model of Composite Hull Sample

The material model initially employed in the finite element model was based on theoretical application of the composite rule of mixtures approach for both CSM and WR fiberglass laminae to obtain initial values of stiffnesses. Since the rule of mixtures approach varies largely from experimental measurements, sometimes reaching 50 percent error (Nielsen, 1970; Reddy, 1997; Rejab et al., 2008; Sai et al., 2013; Smarslok et al., 2012), the material's stiffness was updated based on the dynamic properties obtained in the aforementioned experimental setup. This model updating procedure is to ensure the natural frequency of the FE model is a true representation of the dynamics of the hull plate. The density of the material was obtained from the fishing vessel case study design plans and confirmed using the weight and dimensions of the composite hull plate sample.

3.3.3. Meshing

A total of 13,876 elements and 8,571 nodes were used to construct the discretized model resulting in 51,426 degrees of freedom. The mesh size was calculated based on the American Bureau of Shipping Guidance Notes (American Bureau of Shipping, 2014) as well as DNV GL Class Guidelines for Finite Element Analysis (DNV GL, 2016). The mesh size must adequately represent the deformation wave of the highest frequency observed by the structure and be feasible in terms of modeling and calculation times. In theory, a wave-shaped deformation can be characterized by a minimum of five grid points, but in practice it is usually ten grid points (Moro et al., 2013). Thus, a mesh size of approximately 0.4 meters was used, which is a good measure to observe structural vibrations without over-stiffening the model. The finalized number of elements and their respective types are shown below in Table 3.3. In Table 3.3, the lumped mass elements (CONM2) are the elements used to model the fishing vessel's non-structural masses, as described in the following Section (Section 3.3.4).

Table 3.3: Finite Element Model Element List

Element Description	MSC.Nastran® Element Type	Number of Elements
Bar	CBAR	2953
Beam	CBEAM	429
Quadrilateral Shell	CQUAD4	8561
Triangular Shell	CTRIA3	551
Lumped Mass Point	CONM2	155

3.3.4. Added Masses and Non-Structural Masses

Inertial forces of the surrounding fluid on the fishing vessel were taken into account as hydrodynamic added mass as they significantly affect the ships' vibration response (Bašić & Parunov, 2013). This fluid-structure interaction was modeled using the Boundary Element Method, which applies 4-noded acoustic elements to the hull of the vessel and is the most accurate way to model frequency-dependent added-mass. This method was implemented in MSC.Nastran® using the command of MFLUID. The Helmholtz method used by MSC.Nastran® solves Laplace's Equation by distributing a set of sources over the outer boundary, representing the surrounding water, each producing a simple solution to the differential equation. The values of the sources determine the effective pressures and by extension, the forces on the boundary element grid points (MSC Software, 2004). The result is a matrix equation representing the virtual mass matrix, as derived below.

Assuming σ_j is the value of a point source of fluid (units are volume flow rate per area) located at a location r_j, and is considered acting over an area A_j, the vector velocity $\dot{u}_i$ at any other point r_i is defined as shown below in Equations (3.1) and (3.2).

$$\dot{u}_i = \sum_j \int_{A_j} \frac{\sigma_j e_{ij}}{|r_i - r_j|^2} dA_j \qquad (3.1)$$

$$p_i = \sum_j \int_{A_j} \frac{\rho \sigma_j e_{ij}}{|r_i - r_j|} dA_j \qquad (3.2)$$

where e_{ij} is the unit vector in the direction from point j to point i, and p_i is the pressure at any point i in terms of the density ρ. The results of integrating Equations (3.1) and (3.2)

over the FE surfaces are collected into matrices $[\chi]$ and $[\Lambda]$ to form Equations (3.3) and (3.4) as shown below.

$$\{\dot{u}\} = [\chi][\sigma] \tag{3.3}$$

$$\{F\} = [\Lambda]\{\dot{\sigma}\} \tag{3.4}$$

where F are the forces at the grid points.

The mass matrix now be defined by integrating Equation (3.2) to obtain $[\Lambda]$ and substituting into Equations (3.3) and (3.4) as shown below in Equation (3.5).

$$\{F\} = [M^f][\ddot{u}] \tag{3.5}$$

Thus, yielding a virtual mass matrix, $[M^f]$, to be defined as shown below in Equation (3.6).

$$[M^f] = [\Lambda][\chi]^{-1} \tag{3.6}$$

For proper calculation of the virtual added mass on the hull, the normal shell directions must be directed outwards, as shown below in Figure 3.9.

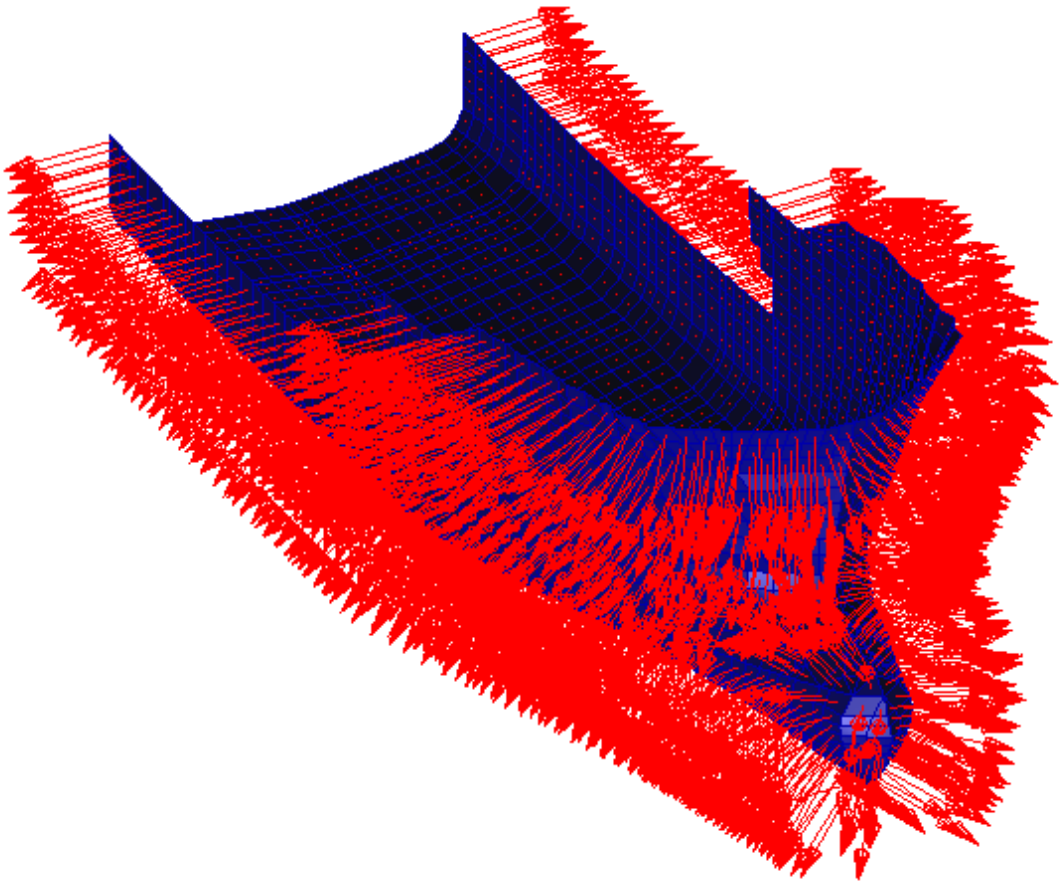

Figure 3.9: Hull Shell Normal Direction

Masses onboard that do not affect the stiffness of the vessel were classified as non-structural masses. Such masses were modeled as lumped mass points and were distributed across their appropriate structural load-bearing members. Examples of such masses are deck machinery, main engine, generators, and tanks. Figure 3.10 shows the highlighted triangular elements which represent the non-structural masses across a longitudinal section of the vessel.

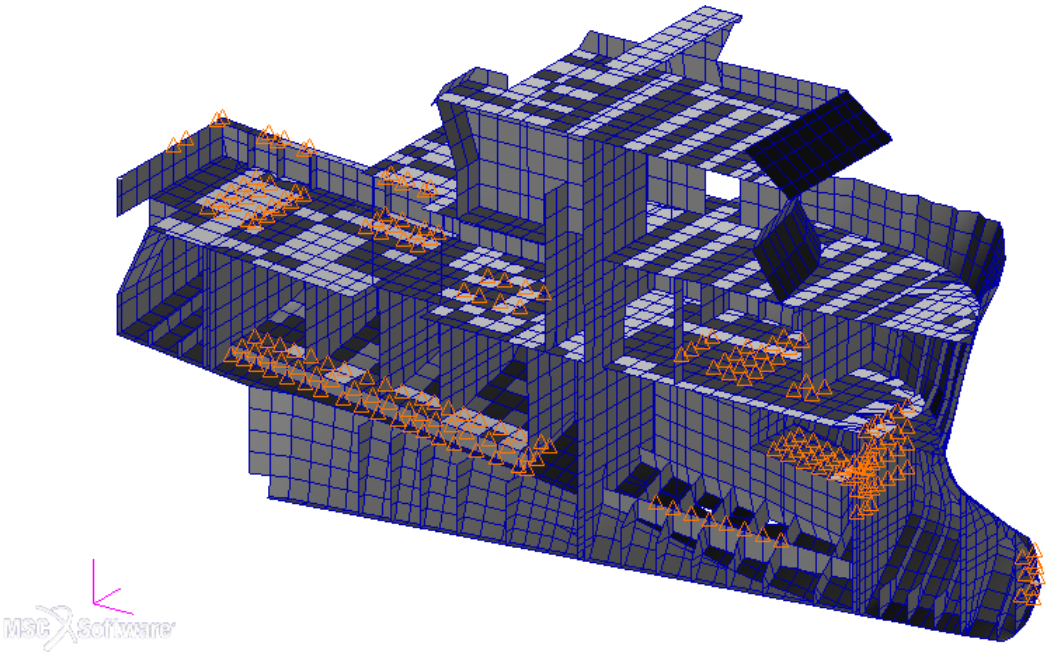

Figure 3.10: Non-structural Masses On-Board

3.4. Free Vibration Analysis

The FE model was then used to generate the global vibration modes and natural frequencies of the vessel. These natural frequencies are obtained in MSC.Nastran® by solving the eigenvalue problem and obtaining the eigenvalues and corresponding graphical mode shapes (eigenvectors). The eigenvalues are obtained by solving the system equation of motion shown in Equation (3.7):

$$[M]\{\ddot{u}(t)\} + [C]\{\dot{u}(t)\} + [K]\{u(t)\} = \{F\} \qquad (3.7)$$

where $[M]$ is the mass matrix, $[C]$ is the damping matrix, $[K]$ is the stiffness matrix, $[F]$is the harmonic forces matrix, and $u(t)$ is a vector representing displacements of the FE model.

For free vibration, the damping and forces matrixes are zero. The eigenvalue problem solution would be as shown in Equation (3.8):

$$[K]\{\Phi\} = \omega^2\{M\}\{\Phi\} \qquad (3.8)$$

where $[K]$ is the symmetric stiffness matrix, $[M]$ is the diagonal mass matrix, $[\Phi]$ is the column mode shape matrix, and ω is the natural frequency.

Equation (3.8) is solved by normal mode analysis. Normal modes are scaled characteristic shapes of the structure used for comparison to excitation frequencies to determine resonances.

The high modal density of complex structures makes it time-consuming to identify local and global modes within the vessel. To alleviate this phenomenon, static condensation, or also known as Guyan condensation, was applied to limit the number of degrees of freedom analyzed by the solver without losing accuracy. The static condensation technique was preferred to dynamic condensation techniques (e.g. Craig-Bampton Method) as the frequency range of the analysis was low (0-80 Hz) and the Guyan condensation is easier to implement in FEA. Key global structural nodes were selected to create a complementary set of degrees of freedom across the vessel to coordinate the eigenvalue solutions to reduce local modes from appearing. This complementary set is called the o-set and omits these degrees of freedom from the dynamic analysis through a reduction process. The process then distributes the o-set mass, stiffness, and damping to the a-set DOFs by using a transformation that is based on a partition of the stiffness matrix (MSC Software, 2013). The basic dynamic equation before the reduction is given by Equation (3.9) as shown below.

$$\begin{bmatrix} \bar{M}_{aa} & M_{ao} \\ M_{oa} & M_{oo} \end{bmatrix} \begin{Bmatrix} \ddot{u}_a \\ \ddot{u}_o \end{Bmatrix} + \begin{bmatrix} \bar{B}_{aa} & B_{ao} \\ B_{oa} & B_{oo} \end{bmatrix} \begin{Bmatrix} \dot{u}_a \\ \dot{u}_o \end{Bmatrix} + \begin{bmatrix} \bar{K}_{aa} & K_{ao} \\ K_{oa} & K_{oo} \end{bmatrix} \begin{Bmatrix} u_a \\ u_o \end{Bmatrix} = \begin{Bmatrix} \bar{P}_a \\ P_o \end{Bmatrix} \quad (3.9)$$

Where $u_a, \dot{u}_a, \ddot{u}_a$ are the displacements, velocities, and accelerations of the analysis (a) set, to be retained, $u_o, \dot{u}_o, \ddot{u}_o$ are the displacements, velocities, and accelerations of the omit (o) set, to be eliminated, M, B, K are the mass, damping, and stiffness matrices (assumed to be real and symmetric), $\bar{P}_a, P_o$ the applied loads, and the bar quantities ($\bar{P}_a$, etc.) indicate unreduced values.

We further simplified Equation (3.9) by ignoring the mass and damping effects and solve the lower partition to obtain Equation (3.10) as shown below.

$$\{u_o\} = -[K_{oo}^{-1}]([K_{oa}]\{u_a\} + \{P_o\}) \quad (3.10)$$

The two parts of Equation (3.10) become the Guyan matrix (G_o), and the static corrective displacement (u_o^o) as shown below in Equations (3.11) and (3.12), respectively.

$$[G_o] = -[K_{oo}^{-1}]([K_{oa}] \quad (3.11)$$

$$[u_o^o] = -[K_{oo}^{-1}]\{P_o\} \quad (3.12)$$

The exact static solution system is then obtained by substituting Equation (3.10) through Equation (3.12) into the upper partition terms of Equation (3.9), resulting in the reduced equations shown below in Equations (3.13) through to (3.16).

$$[K_{oa}]\{u_a\} = \{P_a\} \quad (3.13)$$

$$\{u_o\} = [G_o]\{u_a\} + \{u_o^o\} \quad (3.14)$$

Where:

$$[K_{aa}] = [K_{aa}] + [K_{ao}][G_o] \quad (3.15)$$

$$\{P_a\} = \{P_a\} + [G_o^T]\{P_o\} \tag{3.16}$$

Now by approximating the vectors $\ddot{u}_o$ and $\dot{u}_o$ and using transformations to a new coordinate system, the new reduced dynamic system equation (ignoring damping for simplification) is shown below in Equation (3.17).

$$\begin{aligned}[\bar{M}_{aa} + M_{ao}G_o]\{\ddot{u_a}\} + [\bar{K}_{aa} + K_{ao}G_o]\{u_a\} \\ - [K_{ao}K_{oo}^{-1}] + [M_{ao} + M_{oo}G_o]\{\ddot{u}_a\} \\ = \{\bar{P}_a\} - [K_{ao}][K_{oo}^{-1}]\{P_o\}\end{aligned} \tag{3.17}$$

The hydrodynamic added mass was included in a separate analysis to view its effect on the dynamic characteristics of the vessel, then compared with the Guyan condensation results. The reason behind comparing separate analyses is that boundary elements (such as those employed by MFLUID command in MSC.Nastran® for hydrodynamic added mass) cannot be used with Guyan condensation. Furthermore, Guyan condensation is needed to analyze the FE model for global modes.

3.5. Forced Vibration Analysis

To obtain the vessel's dynamic frequency response using excitation forces, the forced vibration equation of motion, Equation (3.7), is solved using some simple manipulation and Laplace transformation to obtain Equation (3.18) shown below (Brandt, 2011).

$$(ms^2 + cs + k)U(s) = F(s) \tag{3.18}$$

Equation (3.18) leads to the definition of the transfer function, $H(s)$, which is a ratio of $F(s)$ and $U(s)$ as and written in its standard form to become the following Equation (3.19).

$$H(s) = \frac{U(s)}{F(s)} = \frac{\frac{1}{m}}{s^2 + s2\zeta\omega_n + {\omega_n}^2} \quad (3.19)$$

Where ω_n is the undamped natural frequency and $\zeta$is the damping ratio given by the following Equations (3.20) and (3.21), respectively.

$$\omega_n = \sqrt{\frac{k}{m}} \quad (3.20)$$

$$\zeta = \frac{c}{2\sqrt{km}} \quad (3.21)$$

Frequency response analysis was used to compute the structural response of steady-state oscillatory excitations using the transfer functions, as described above. The three-dimensional FE model was subjected to oscillatory excitations obtained from direct measurements on-board the vessel at sea. Measurements were processed to spectra for each vibration source given in root mean square (RMS) value of velocity, as shown below in Figure 4.4, Figure 4.5, and Figure 4.6. The spectra were then fed into the FE model excitation nodes as frequency-dependent loads with their corresponding values.

3.5.1. Excitation Sources

The primary excitation sources on board a fishing vessel are the diesel engines (main engine and generators), propeller(s), and auxiliary machinery (e.g., winches). The forces and moments generated from a marine diesel engine can have a substantial effect on vibration levels onboard. These forces and moments are made from the combustion process coupled with the inertia of mass in motion, which may cause resonance in the engine foundation structure and ships' hull. Excitations from the propeller are either shaft forces or pressure pulses on the hull. Propeller shaft forces, or bearing forces, are the most

significant factor for vibration of the shaft line. However the most crucial excitation for comfort analysis usually comes from pressure pulses acting on the ship hull above the propeller (American Bureau of Shipping, 2006).

The forcing vector in the equation of motion for forced vibration as described above in Equation (3.7) requires an accurate dynamic description. An accurate approach to capture this dynamic behavior is to collect accelerations at the sources as described in Section 3.2, and then feed the data into the FE model as boundary conditions. Onboard marine vibration excitation sources are generally located in bottom of the vessel, as shown below in Figure 3.11, and therefore the vibration travels from bottom of the vessel upwards.

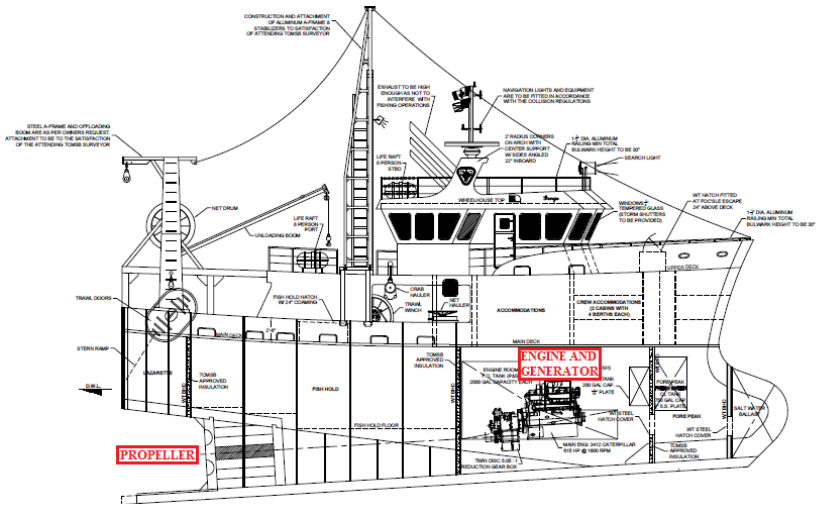

Figure 3.11: Excitation Sources Location on Fishing Vessel

These sources inherently have excitation frequencies corresponding to their typical operating regimes (typically rotations per minute or RPM). These excitation frequencies and their orders (or multiples of that frequency) are usually values of interest that need to be taken into consideration during design to avoid resonances (Lloyd's Register, 2015). The fundamental excitation frequency values were calculated as per (Gloza, 2008; Moro

et al., 2013) and may be summarized into Equations (3.22), (3.23), (3.24), and (3.25) below.

$$f_{engine(N)} = \frac{n_{engine} * N}{s * 60} \quad (3.22)$$

$$f_{generator(N)} = \frac{n_{generator} * N}{s * 60} \quad (3.23)$$

$$f_{propeller(N)} = f_{engine(1)} * r_{gearbox} * N \quad (3.24)$$

$$f_{shaft(N)} = f_{propeller(N)} * Z \quad (3.25)$$

Where $f_{engine(N)}$, $f_{generator(N)}$, $f_{propeller(N)}$, $f_{shaft(N)}$ are the fundamental frequencies of N order, n_{engine}, $n_{generator}$ are the rotation rate of the respective reciprocating engines in RPM, $r_{gearbox}$ is the main engine gearbox reduction ratio, and Z is the number or propeller blades.

3.5.2. Model Validation

The FE model was validated through two distinct methods. Firstly, a mobility analysis was performed to check the proper element connectivity and to understand the dynamic response of the vessel. Mobility is a form of experimental modal analysis comprising of the ratio between measured frequency response in terms of velocity of a structure and a recorded input driving force applied to said structure. The result of this ratio is a transfer function describing the structures' dynamic properties (Brandt, 2011).

The mobility transfer function mathematical formulation is derived using the equation describing the frequency response of a system, Equation (3.19), and substituting the

relation $s = j\omega = j2\pi f$ to obtain Equation (3.26) and further some algebraic manipulation to simplify to Equation (3.27) as shown below.

$$H(f) = \frac{U(f)}{F(f)} = \frac{\frac{1}{m}}{-\omega^2 + j2\zeta\omega_n\omega + {\omega_n}^2} \tag{3.26}$$

$$H(f) = \frac{U(f)}{F(f)} = \frac{\frac{1}{k}}{1 - \left(\frac{f}{f_n}\right)^2 + j2\zeta\left(\frac{f}{f_n}\right)} \tag{3.27}$$

Where $\left(\frac{f}{f_n}\right)$ is the relative frequency. Through differentiation of Equation (3.27), which in the frequency domain corresponds to a multiplication by $j2\pi f (= jw)$, we obtain mobility, $H_v(f)$, with units of $\frac{m}{Ns} = \frac{s}{kg}$ which is given by Equation (3.28) below.

$$H_v(f) = \frac{V(f)}{F(f)} = j2\pi f \frac{\frac{1}{k}}{1 - \left(\frac{f}{f_n}\right)^2 + j2\zeta\left(\frac{f}{f_n}\right)} \tag{3.28}$$

Usually, mechanical mobility analysis is performed when vibration sources are unknown to the system, therefore identifying local resonances at critical locations using an impulse or harmonic excitation. In this case study, a unity impulse force was used to excite the system such that the observed dynamic response could be scaled for further investigation of different excitation sources.

Once the mechanical mobility analysis provides consistent results, the determination of the overall damping ratio corresponding to the case study vessel's dynamic characterization is needed. The difficulty is often observed when evaluating the frequency response of ship vibrations due to the different types of damping affecting the structure (Pais et al., 2017).

Damping is the irreversible energy loss in a system, and in terms of vibration energy, it is usually lost in the form of thermal energy. This lost energy can be due to the structures' inherent material damping and or external structural properties such as friction or connections. The types of damping associated with ship vibrations are generally considered to be a combination of structural damping, cargo damping, and hydrodynamic damping. For the forced vibration analysis, it is assumed that their effects can be lumped together into an equivalent viscous damping ratio, ζ, also known as critical damping or simply damping ratio, and is given by Equation (3.29) below (Yucel & Arpaci, 2013).

$$\zeta = \frac{c}{c_{cr}} \tag{3.29}$$

Where c is the damping coefficient and c_{cr} is the critical damping coefficient defined by Equation (3.30) below.

$$c_{cr} = 2\sqrt{km} \tag{3.30}$$

where k is the stiffness, and m is the mass.

In the case of complex ship structures, literature has provided empirical formulas for estimation of the damping value to be used in the vibration frequency analyses. In general, the damping coefficient is increased as vibration frequency increases. Germanischer Lloyd produced such a relationship between the damping ratio and frequency for container ships for the purpose of FE dynamic simulations (Asmussen et al., 2001). However, no literature was found for smaller vessels, such as in the presented case study. Thus following (Pais et al., 2017), the critical damping coefficient was estimated using the onboard vibration measurements in the different areas of the vessel and iteratively comparing them to linear

forced vibration analyses with various critical damping values. A MATLAB® code was developed to post-process data obtained from MSC.Nastran® and compare them to onboard measurements at each location of interest (as shown in Figure 3.3).

Chapter 4: Results

This chapter shows the results combined from analyses procedures for validation as summarized in Figure 3.1. Firstly, the hull sample composite plate analysis results from experimental study and FE analysis (as described in Section 3.3.2) are presented for comparison and validation of the dynamic composite behaviour. Secondly, a free vibration analysis was performed to obtain the natural frequencies and corresponding normal modes of the fishing vessel's structures in both wet and dry configurations (as described in Section 3.4). Thirdly, in preparation to perform the forced vibration analysis, the excitation source frequencies were then analytically calculated (as described in Section 3.5.1) and measurements of said sources obtained (see Section 3.2). Fourthly, the FE model response in a mobility analysis is shown to ensure model structural validity (as described in Section 3.4). Finally, via excitation from onboard measurements and comparison of experimental onboard measurements with FE analysis (as described in Section 3.5), the dynamic response of the fishing vessel was analyzed to obtain an accurate estimate of structural damping (as described in Section 3.5.2).

4.1. Hull Sample Composite Plate Validation

After the FE material model was updated according to the experimental analysis as described earlier in Section 3.3.2, and the recorded difference between both was approximately 20%. The results demonstrate the dynamic behavior up to 900 Hz from both the experimental and FE analyses, and can be shown below in Figure 4.1 and Figure 4.2

respectively. Figure 4.1 and Figure 4.2 are the frequency response functions of the plate, which is a measure between the applied force and the resulting response, and is commonly used to identify the dynamic mechanical properties of structures.

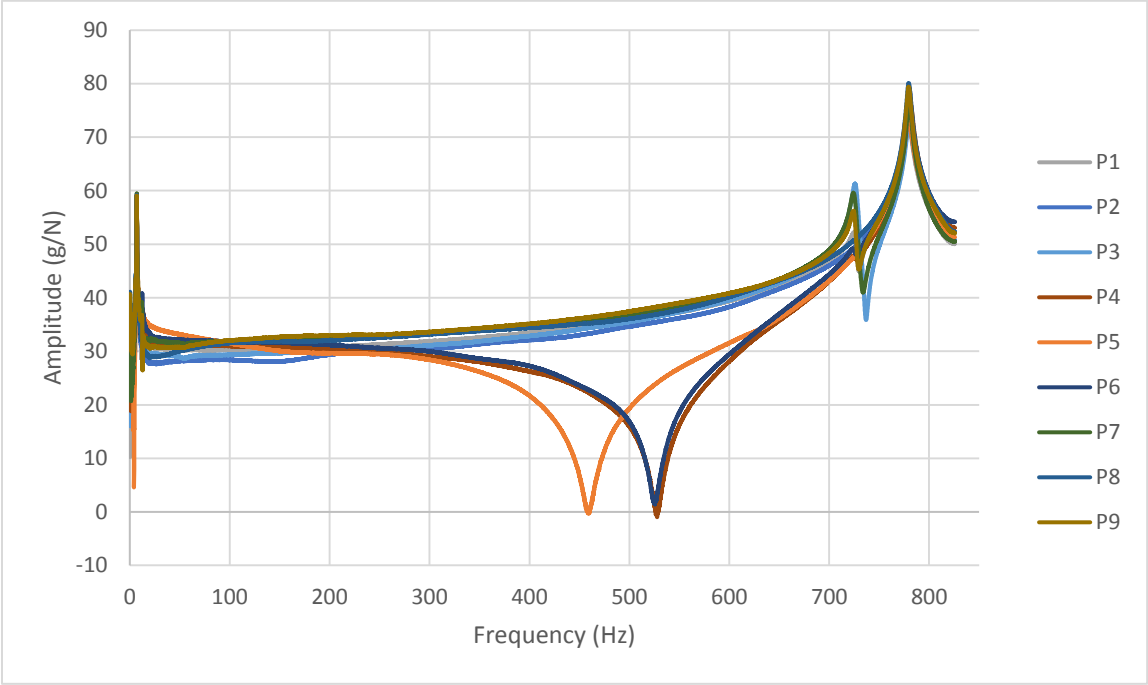

Figure 4.1: Experimental Frequency Response of Composite Hull Sample

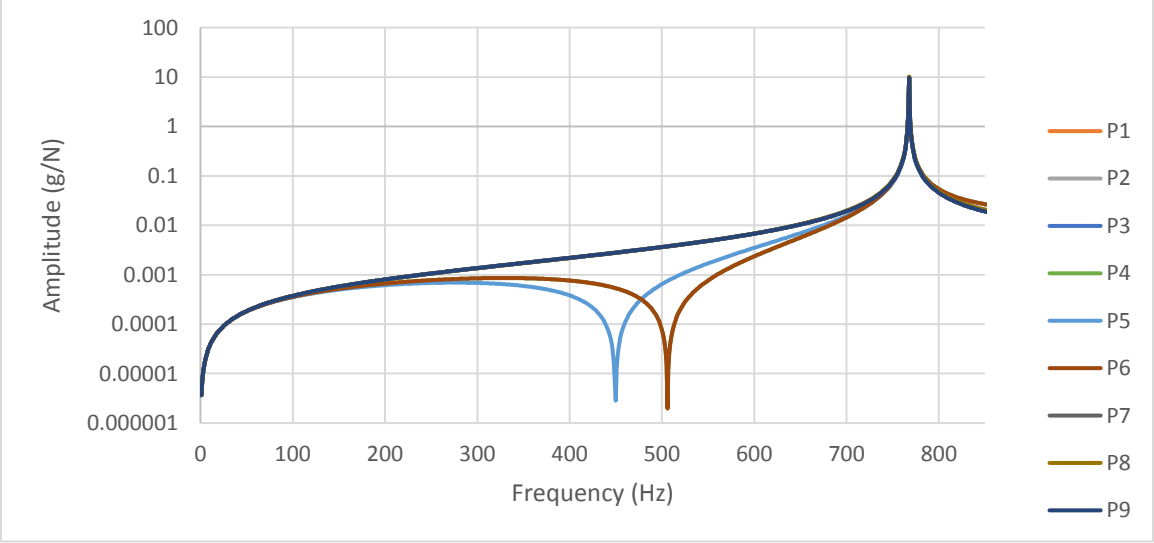

Figure 4.2: Finite Element Frequency Response of Composite Hull Sample

4.2. Free Vibration Analysis

The global natural frequencies and modes of the fishing vessel were analyzed in both wet, with the hydrodynamic added mass on the hull, and dry, with Guyan static condensation but no hydrodynamic added mass, configurations using MSC.Nastran® and post-processed using MSC.Patran®. Significant resonance frequencies are usually found up to the 15Hz range for most ship structures (Asmussen et al., 2001). Therefore, the global natural frequencies for the wet and dry configurations were tabulated and compared in Table 4.1 below.

Table 4.1: Global Natural Frequencies

Wet (Hz)	Dry (Hz)	Mode Type	Difference
6.1947	6.9765	Torsion	11.2%
10.1330	-	Bending	N/A
13.1700	14.4680	Torsion and Bending	9.0%
14.3220	15.7960	Torsion	9.3%
18.8040	18.2280	Bending and Torsion	-3.2%

The vessel mode shapes were extracted from MSC.Patran®, and their graphical representations are all shown in Appendix A. Figure 4.3 shows a graphical comparison of the first global mode of vibration in both wet and dry cases.

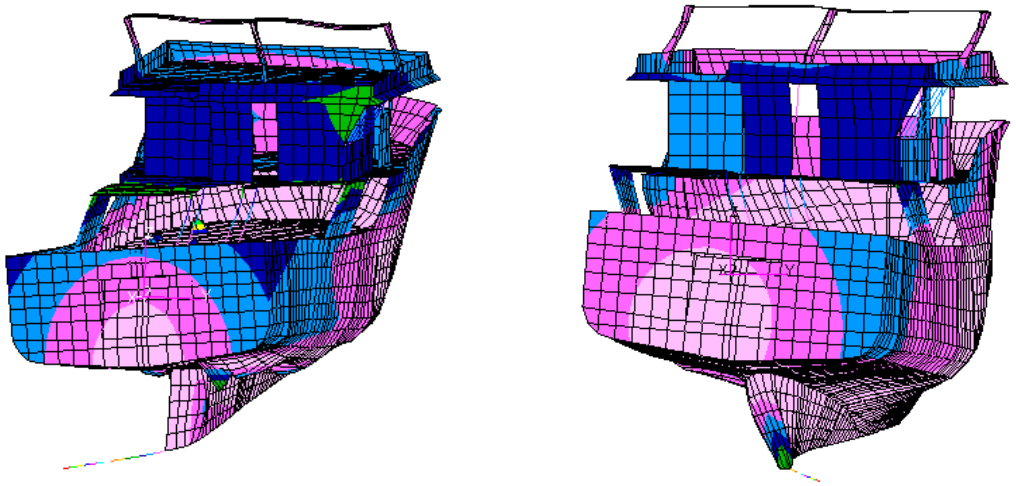

Wet Torsional Mode at 6.1947 Hz Dry Torsional Mode at 6.9765 Hz

Figure 4.3: Global Mode Shape Comparison of First Mode

4.3. Excitation Frequencies and Measurements

The fundamental excitation frequency values for the onboard sources were calculated as described above in Section 3.5.1 and are shown as the first row of values in Table 4.2 below. The following values in each respective column represent the harmonics of these vibration sources.

Table 4.2: Vessel Excitation Fundamental Natural Frequencies (Hz)

Main Engine	Propeller Shafting	Generator	Propeller
13.3	4.47	30.6	17.88
26.6	8.94	61.2	35.76
39.9	13.41	91.8	53.64
53.2	17.88	122.4	71.62
66.5	22.35	153	89.5
…	…	…	…

As described earlier in Section 3.2, accelerometers were placed on excitation source mounts (engine and generator) or on the nearest area of high structural stiffness (propeller). Results from these measurements were extracted using LabVIEW® and are shown below in Figure 4.4, Figure 4.5, and Figure 4.6. These velocity levels were then applied to the FE model as boundary conditions, to simulate enforced motions.

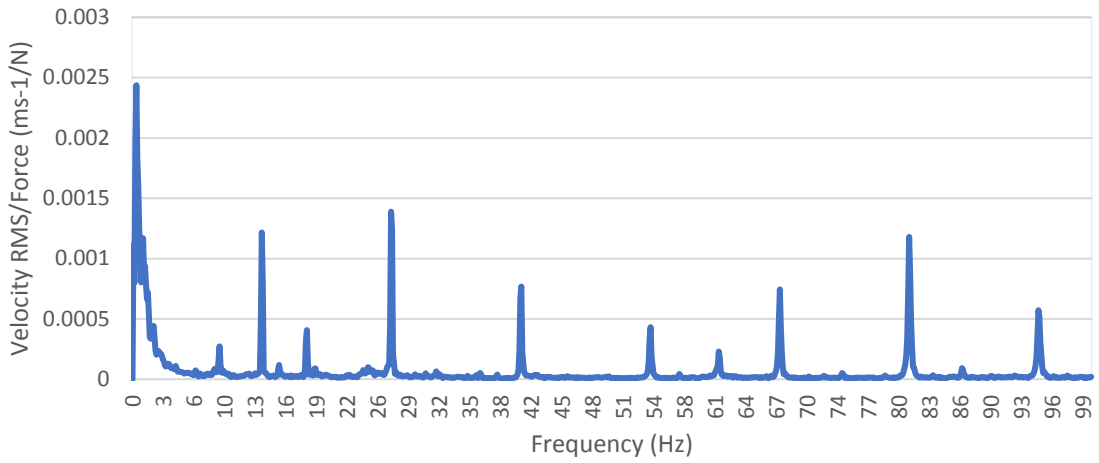

Figure 4.4: Engine Onboard Measurements

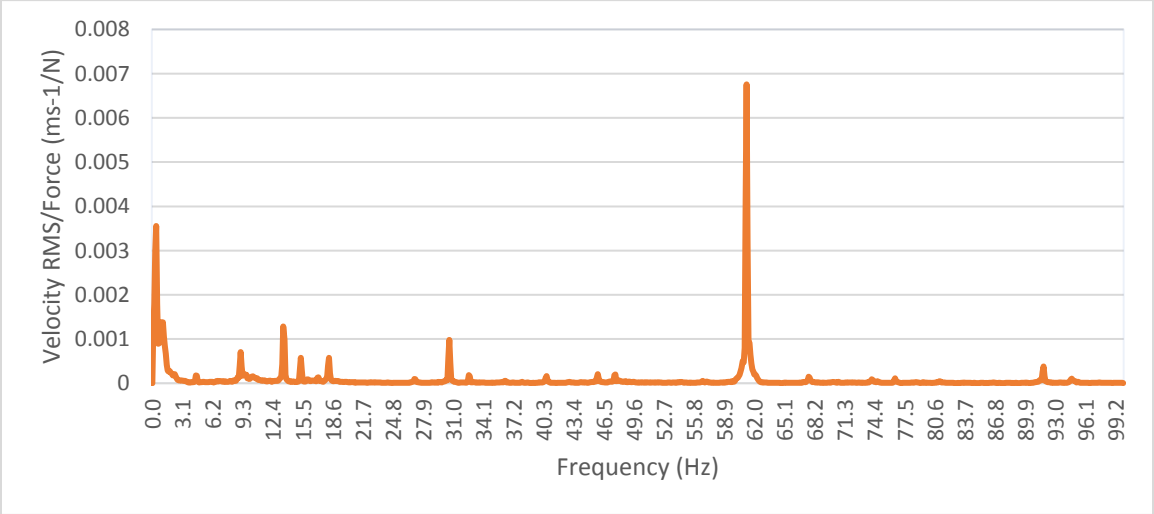

Figure 4.5: Generator Onboard Measurements

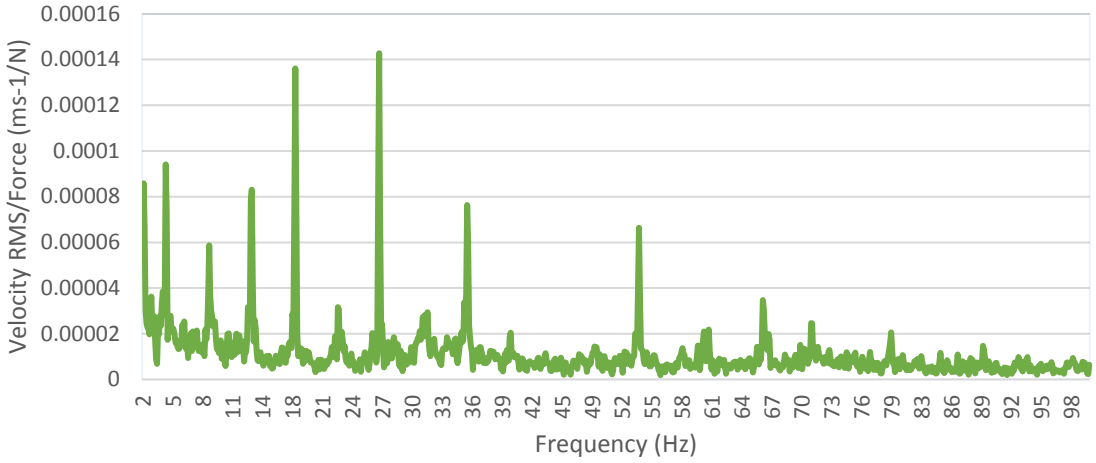

Figure 4.6: Propeller Onboard Measurements

4.4. Forced Vibration Analysis

This section displays results for forced vibration analyses, namely the mobility analysis and the damping determination iterative process. In the former analysis, a unitary force is employed to visualize transmission of vibration from excitation source to points of interest (see Section 3.4), while in the latter analysis excitation forces obtained from measurements shown in the above section were employed as the forcing function.

4.4.1. Mobility Analysis

Using MSC.Nastran® in conjunction with a MATLAB® script for post-processing, the mobility of the fishing vessel was calculated in terms of each primary onboard vibration source (namely the propeller, generator, and engine). In each case a unitary force was applied at either the source of vibration, such as engine or generator mounts, or the immediate affecting area, such as the hull area above propeller (Lloyd's Register, 2015).

The mobility transfer functions were calculated, and results were plotted for each of the pre-identified regions shown in Figure 3.3. Each of these areas was indexed in the FE model by nine adjacent nodes to correctly capture the local vibration and identify or eliminate outliers if local resonances appear. The velocities of these nine nodes were then averaged to observe the local vibratory response of the area as a whole. Figure 4.7, Figure 4.8, and Figure 4.9 show mobility results for the set of nodes representing Cabin 1 (see Figure 3.3) resulting from the unitary excitation of the propeller, generator, and engine, respectively. The complete set of results for all the pre-identified areas can be found in Appendix B.

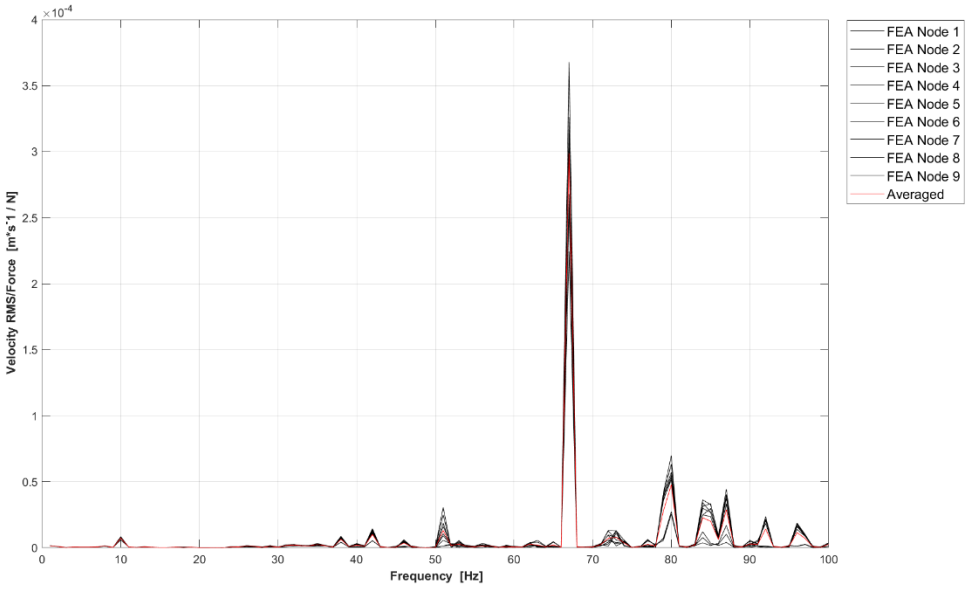

Figure 4.7: Mobility – Propeller to Cabin Point 1

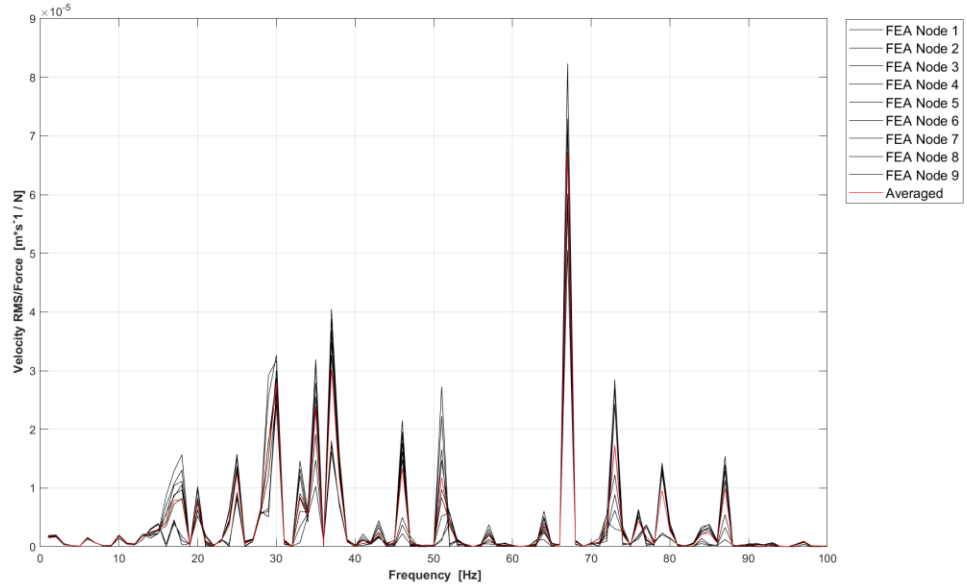

Figure 4.8: Mobility - Generator to Cabin Point 1

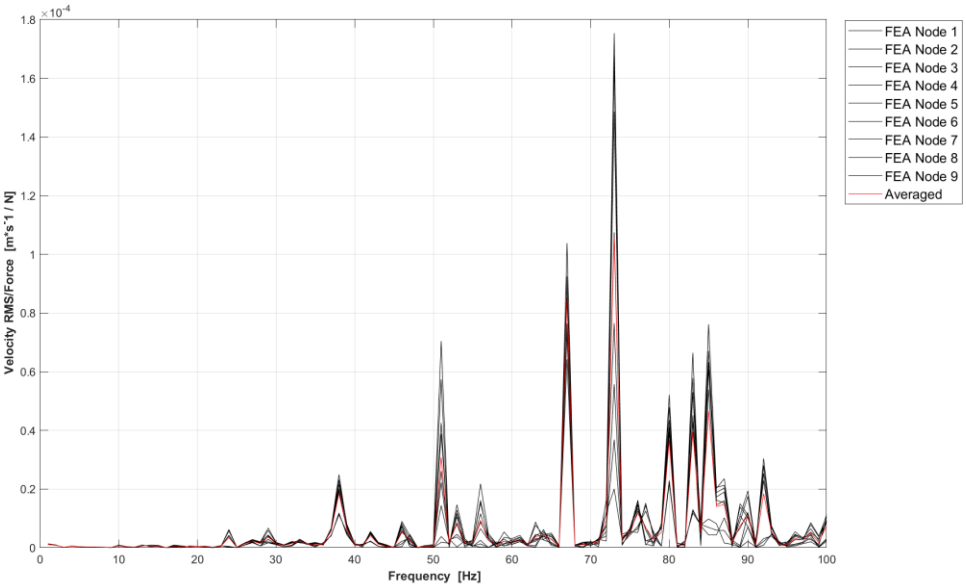

Figure 4.9: Mobility - Engine to Cabin Point 1

4.4.2. Model Validation

MSC.Nastran® was used to evaluate the vibration levels of the pre-identified areas highlighted in Figure 3.3, given the input of each vibration source individually (engine, generator, and propeller) and then all together. The analysis was performed singularly to observe the effects of each of the vibration sources independently. Using a MATLAB® script, each of these analyses was then re-iterated with varying values of structural damping and compared with the experimentally measured onboard vibration levels. The following Figure 4.10, Figure 4.11, Figure 4.12, and Figure 4.13 are a preview of these results in graphical form for each of the excitation sources with a varying structural damping coefficient (identified by critical damping C_{Cr}) per the pre-identified location of Wheelhouse Group 1 Point 1 (see Figure 3.3).

The complete output of these results for all locations and various excitation sources can be found in Appendix C. The solid black line represents the measurements taken aboard the vessel in the corresponding measurement points, and its vertical axis is on the right of the chart. The left vertical axis represents the remainder of results obtained from the FE model with varying critical damping coefficients.

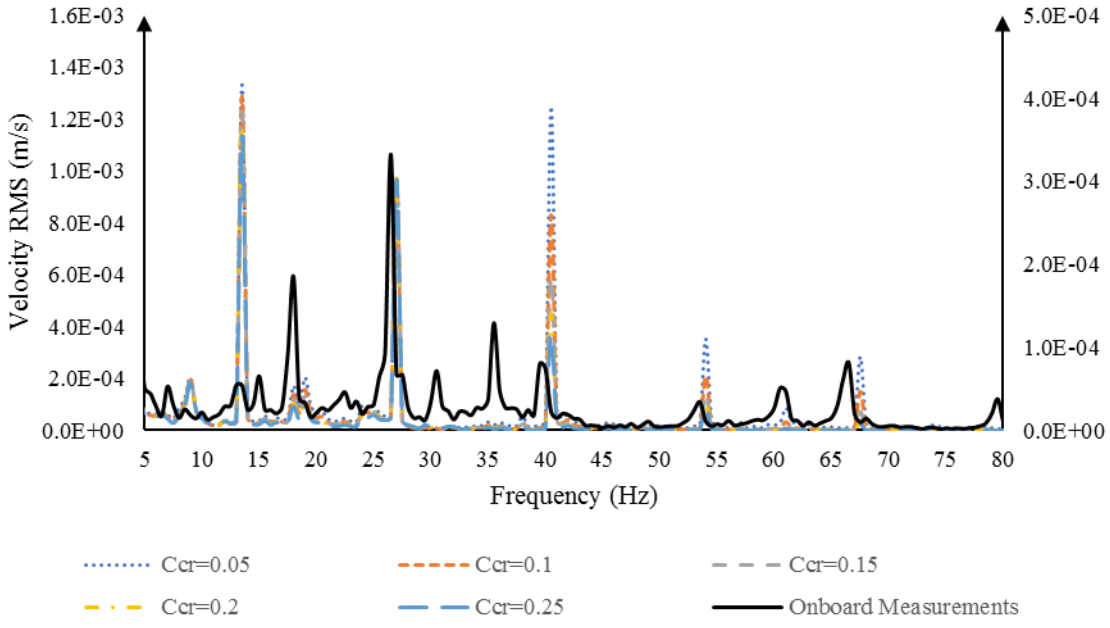

Figure 4.10: Onboard Measurements against Finite Element with Varying Damping (Engine Excitation) - Wheelhouse G1 P1

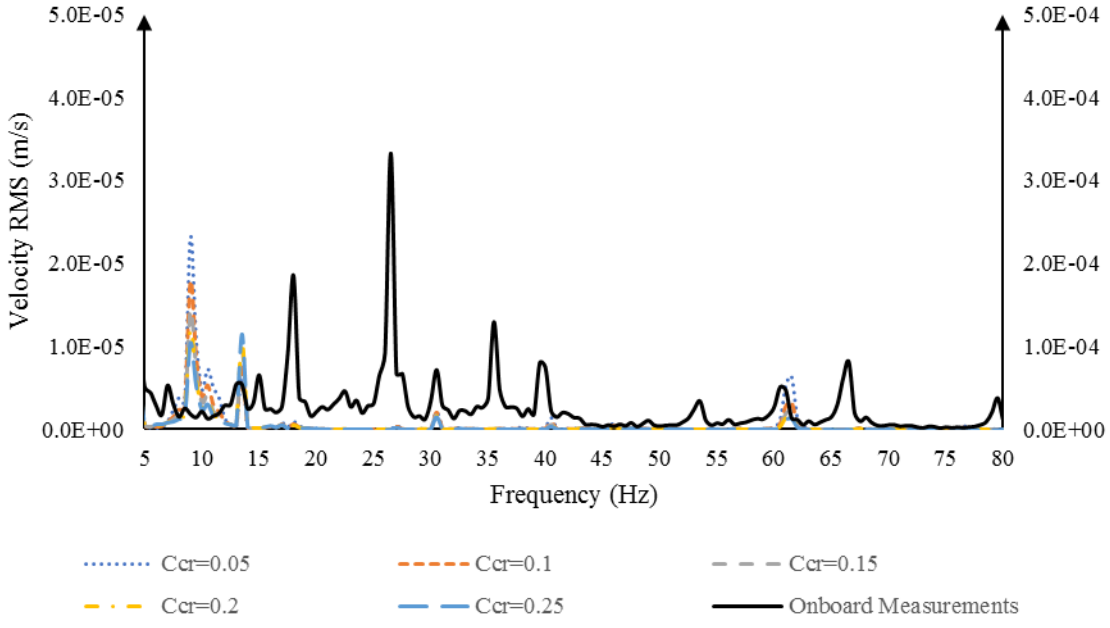

Figure 4.11: Onboard Measurements against Finite Element with Varying Damping (Generator Excitation) - Wheelhouse G1 P1

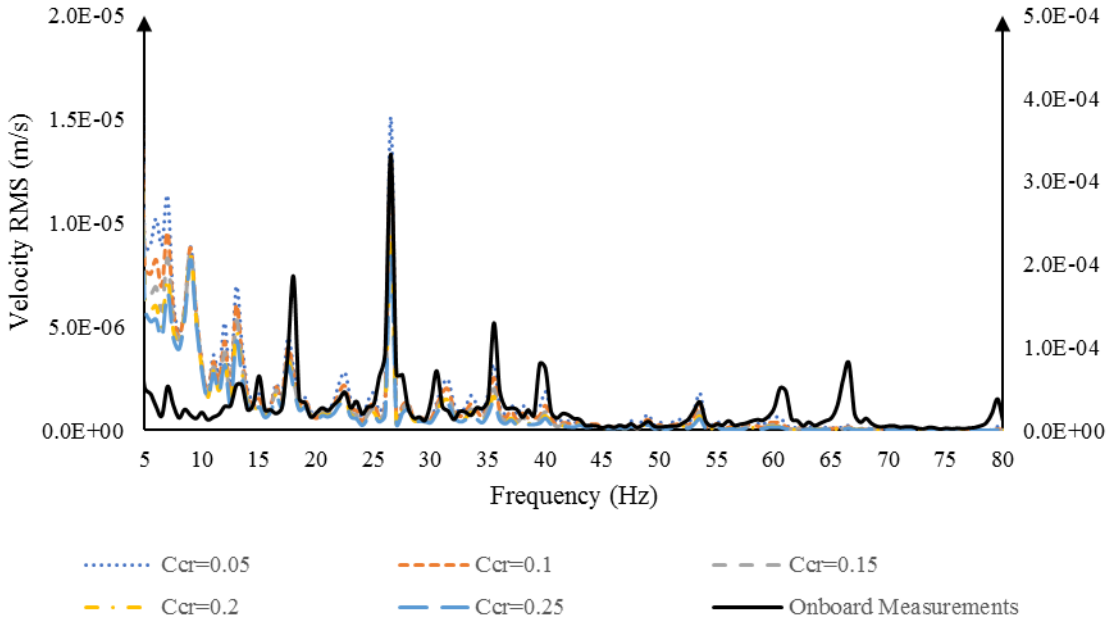

Figure 4.12: Onboard Measurements against Finite Element with Varying Damping (Propeller Excitation) - Wheelhouse G1 P1

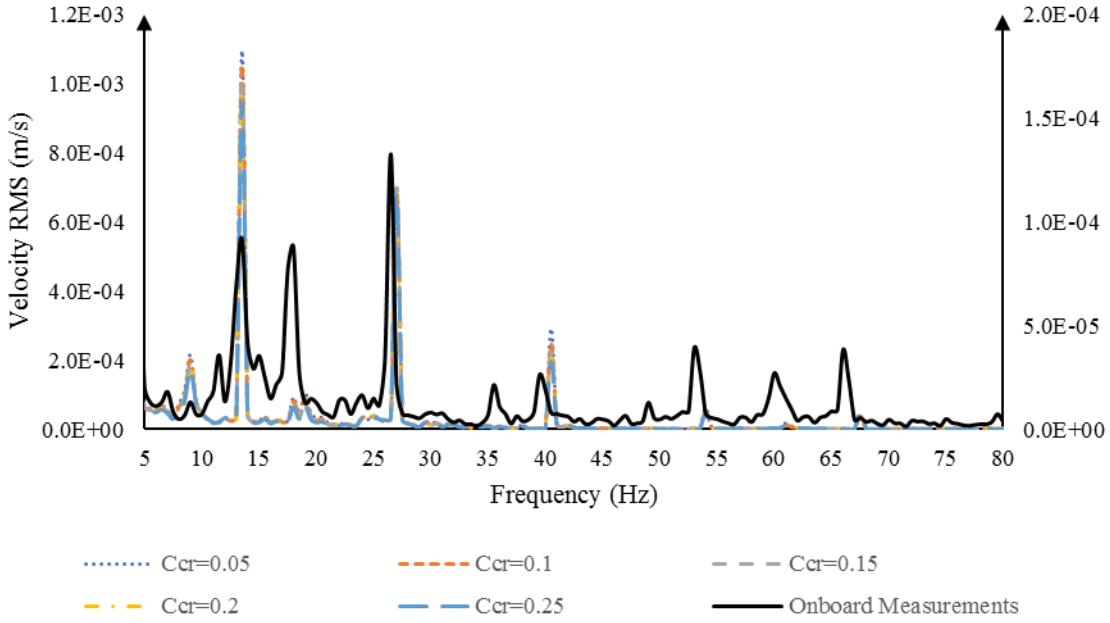

Figure 4.13: Onboard Measurements against Finite Element with Varying Damping (All Source Excitation) - Wheelhouse G1 P1

Chapter 5: Discussion

As no studies on vibration, vibration exposure, and methods to mitigate such exposures were found in the literature review, this study provides a practical methodology for researchers and designers to pave the road in this field. Following the documents' outline, the results from the composite plate experimental comparative study will be discussed first, followed by the onboard measurements of the case study fishing vessel. Then an overview of the results from the free and forced vibration results will be discussed, along with a more detailed hypothetical study of a specific location onboard to serve as a guideline for future vibration analyses.

The composite hull plate experimental analysis proved necessary to mimic the dynamic behavior of a fiber reinforced laminate in FE analysis. Using the results shown in Section 4.1, the FE model stiffnesses for both chopped strand matt and woven roving were reduced approximately 20% to align with results from the experimental study. The small peaks shown in Figure 4.1 are attributed to resonances of two different modes in different directions.

The recorded data measurements from sea trials of the case study fishing vessel proved to be interesting. When compared with ISO 6954:1984 lower limit of 4 mm/s (see Section 3.2 for reasoning behind selection of this standard), the vessel maximum peak vibration levels seem to be well away from vibrations whose "adverse effects on human habitability is not probable" as shown in Table 5.1 below. Table 5.1 reveals that although vibration values are below the lower limit defined in ISO 6954:1985, the average difference is a mere 6%.

Table 5.1: Recorded Measurements Against ISO 6954:1984 Standard

Location	Peak Value	Difference from ISO Standard
Wheelhouse Group 1 Point 1	3.33E-04	8.33%
Wheelhouse Group 1 Point 2	3.47E-04	8.68%
Wheelhouse Group 2 Point 1	1.62E-04	4.04%
Wheelhouse Group 2 Point 2	7.02E-05	1.75%
Canteen Group 1 Point 1	9.52E-04	23.81%
Canteen Group 1 Point 2	1.43E-04	3.57%
Canteen Group 2 Point 1	1.32E-04	3.31%
Canteen Group 2 Point 2	5.50E-05	1.38%
Bunker Point 1	2.45E-04	6.13%
Bunker Point 2	2.87E-04	7.16%
Cabin Point 1	8.04E-05	2.01%
Cabin Point 2	1.33E-04	3.32%

The first step to analyze the dynamics of the vessel is a review of the vessel's natural frequencies. The difference arising from using a wetted hull versus a dry one signifies the importance of the hydrodynamic mass surrounding the ship. In general, the effect of the hydrodynamic added mass varies in frequency and mode type, and it is evident from this study that it is a necessity to be included in dynamic FE analysis. Table 4.1 depicts a significant maximum difference value of approximately 11% between dry and wet natural frequencies, which is agreeable to results from literature (Bašić & Parunov, 2013; Pais et al., 2017). Also apparent from Table 4.1 is that the error decreases substantially with increasing frequency, meaning added mass is a significant factor especially in low frequencies. Finally, Table 4.1 shows that the first mode in both dry and wet conditions is a torsional one. This means that this case study vessel is structurally weak in the transverse

direction, since most vessels should exhibit their first mode shape in the bending configuration.

Since the global natural frequencies have been determined, a resonance "check" against the primary excitation harmonics was performed to avoid unwanted stimulation of the structure (American Bureau of Shipping, 2006; Menzel et al., 2008). The sources excitation frequencies and their harmonics from Table 4.2 pitted against the wet global natural frequencies are shown below in Table 5.2. Of concern is the resonance and near resonance conditions highlighted in bold in Table 5.1. Rectification of these resonant conditions usually come in the form of either changing the engine operating conditions (namely the RPM) or the number of propeller blades employed on the vessel (Lloyd's Register, 2015). Typically, such a study is performed at the design stage of the vessel construction and translated to the stability booklet into operating configurations for the vessel in the lightweight and loaded conditions for the onboard crew to operate the ship safely.

Table 5.2: Resonance Check of Global Natural Frequencies (Hz)

Wet Global Natural Frequencies	Main Engine	Propeller Shafting	Generator	Propeller
6.1947	**13.31**[1]	4.47	30.6	**17.88**[2]
10.1330	26.6	8.94	61.2	35.76
13.1700[1]	39.9	**13.41**[1]	91.8	53.64
14.3220	53.2	17.88	122.4	71.62
18.8040[2]	66.5	22.35	153	89.5

[1] Resonance or near resonance occurrence between global structure, main engine, and propeller shafting.
[2] Resonance or near resonance occurrence between global structure and propeller.

A closer look into the frequencies attributed to maximum peak values shown in Table 5.1 alongside the above Table 5.2, shows that the peak values can be traced back to a certain excitation frequency. Table 5.3 below shows each peak value and its corresponding frequencies, pointing out a general trend that most of these peak values occur at the first or second order excitation frequency of either the engine or propeller.

Table 5.3: Peak Measurements Corresponding to Excitation Frequencies

Location	Peak Value	Frequency
Wheelhouse Group 1 Point 1	3.33E-04	26.5
Wheelhouse Group 1 Point 2	3.47E-04	26.5
Wheelhouse Group 2 Point 1	1.62E-04	18
Wheelhouse Group 2 Point 2	7.02E-05	26.5
Canteen Group 1 Point 1	9.52E-04	60
Canteen Group 1 Point 2	1.43E-04	18
Canteen Group 2 Point 1	1.32E-04	18
Canteen Group 2 Point 2	5.50E-05	9
Bunker Point 1	2.45E-04	35.5
Bunker Point 2	2.87E-04	35.5
Cabin Point 1	8.04E-05	26.5
Cabin Point 2	1.33E-04	26.5

Once the main frequencies to avoid have been identified, we now turn our detailed attention to the mobility analysis. The mobility analysis was performed with independent source excitation to locate and visualize the transmissibility of vibration from source to local structure. Of particular interest are the frequencies that excite the local structure, which are identified as peaks on a frequency response function. To serve as an example to elaborate the kind of information extracted from the mobility analysis, Figure B.1 is selected.

Figure B.1 shows the mobility from the propeller to the Bunker Point 1 (as identified in Figure 3.3) and highlights many facts. Firstly, a local resonance mode of approximately 66

Hz is apparent by a disproportionate peak translating to high transmissibility of vibration. This local resonance is of concern since this frequency is excited by the engine and possibly from the propeller also as depicted in Table 5.2. A closer look into the mobility for the same location, but with the engine's excitation in Figure B.13, shows high transmissibility from the engine to the same room. Combining these two figures leads us to understand that Cabin Point 1 is a highly susceptible location onboard for vibration. Figure 5.1 below is a side by side comparison of Figure B.1 and Figure B.13 with a red circle highlighting the local resonance mode at the two different excitations.

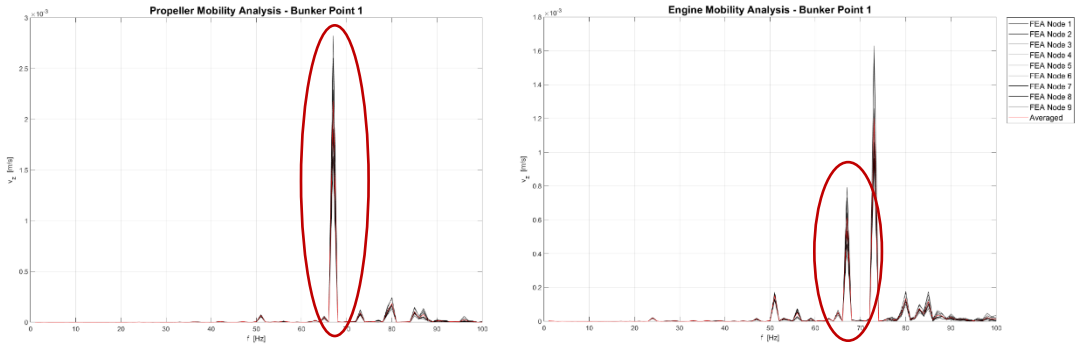

Figure 5.1: Cabin Point 1 Mobility Analysis Example

Another point to consider once analyzing mobility frequency is the measure of disparity between each nodal response. An example of such a phenomenon can be shown in Figure B.14. As the frequency increases, one can observe a difference in the intensity of the responses of the different nodes, indicating that the local substructure is undergoing a local resonance that excites these close group nodes to a varying degree. Figure 5.2 below highlights such a local resonance apparent in Figure B.14. In the case that the behavior of each node is not matching the same pattern to the rest, it may be a sign of a problem in the model's nodal connectivity.

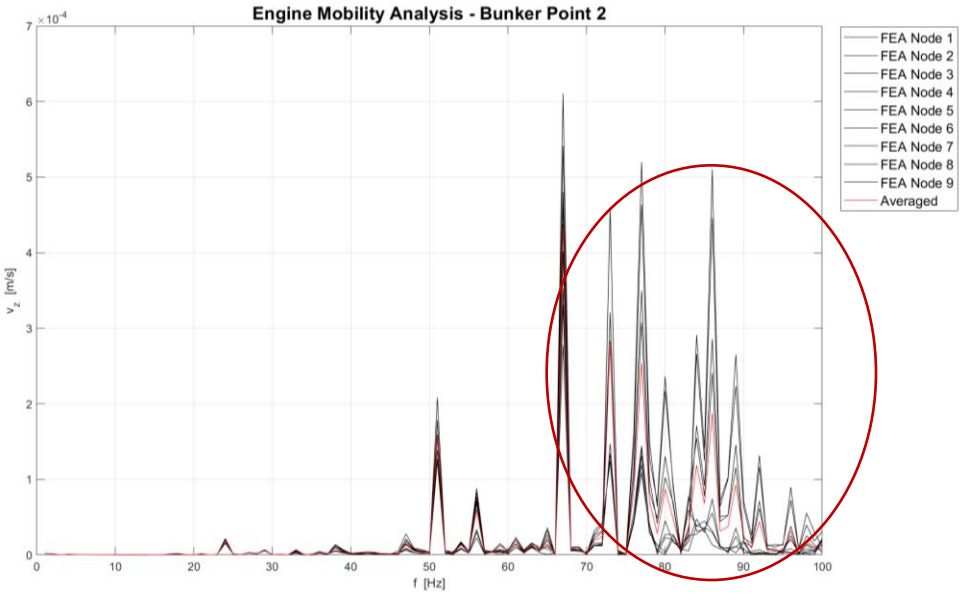

Figure 5.2: Mobility Nodal Disparity Phenomenon

Finally, we turn to the final phase of the research, the damping determination analysis, which is summed up in Appendix C. Based on the results obtained from the FE analysis, it is difficult to determine a single damping ratio to provide agreeable results in all frequency ranges. This is due to the excessive simplifications undergone to perform a frequency-dependent analysis on a global scale. Although the use of a single damping ratio was justified by main classification societies rules and guidelines and previous literature for larger and different vessel types, no literature is available for fishing vessels. Though using available literature for identification of damping, a general trend of an overestimated effect of damping in the high frequencies, and an opposite underestimated effect in the high frequencies. It is therefore recommended to use a critical damping coefficient 0.2 for a fishing vessel such as in the case study. This value creates an overestimate in the response which may be used as a safety factor to counteract the simplifications of the FE model, and

further provide a reasonable base for understanding a fishing vessels' dynamics for designers.

Further to the point above, we observed a difference in amplitudes between the FEA results and the measured onboard results. The difference varies depending on frequency which suggests that we need properly simulate the local damping coefficient for each area of the vessel. The difference between experimental and numerical data was high, but the aim of our analysis was to identify a global damping coefficient to characterize the global response of the vessel. This global damping coefficient would incorporate a safety factor to provide a realistic and general guideline allowing it to be applied to other fishing vessels.

Another general observation is that peaks of primary harmonics in the FE analysis are slightly shifted (by approximately 1-2 Hz) compared to the onboard measurements. This phenomenon is attributed to slightly varying rates of RPM during normal operation of a reciprocating engine. Despite this, the ship's overall dynamic behavior was effectively captured within the FE analysis results.

Chapter 6: Conclusion and Future Work

Throughout this research, the modeling and analysis of ship vibrations using FE analysis were performed to provide design level guidelines for the industry. Outcomes from the research show particular importance to the modeling phase of the vessel. Vessel geometry, material model, excitation loading, and added masses were studied and applied concerning a ship's onboard vibrations.

Vessel analysis results were highly dependent on the damping model used, and in this case study, a rudimentary proportional viscous damping was applied. FE analysis results proved reasonable agreement against experimental onboard measurements, and the identification of onboard "hot spots" were made possible.

Although the case study fishing vessel proved to be not harmful for the onboard crew according to ISO standards, the guidelines highlighted in this study ensures the successful output of meaningful results in terms of onboard vessel vibrations.

Expansion on this project to provide more agreeable results would entail further study in the following:

1. The damping model needs to be revisited depending on the scope of the future work.
    a. Should the scope require a detailed localized response of a particular location in the vessel, a localized damping model damping should be employed and needs to be frequency dependent and applied as such in the numerical model. This can be achieved by onboard experimental activities

that aim to measure transfer functions between machinery and locations of interest. In this way we can map out the locally frequency dependant damping.

b. In the case of a global understanding of the dynamic response of the vessel, such as the present work, experimental analysis needs to be applied on several vessels. Using the data from multiple vessels, a statistical analysis would provide viable guidelines for dynamic characterization of fishing vessels on a global scale.

2. A more detailed look into the material model of the composite structures onboard, since composite fiber-reinforced plastics are both temperature and frequency-dependent, may aid in more agreeable results. Operating conditions were likely very cold when measurements were taken, and frequency dependency requires a more advanced damping model than the overall structural damping (Hanselka, H and Hoffmann, 1999). Studies also show that composite material aging and its effects on the stiffness should be considered using a reduced elasticity modulus (Ascione et al., 2016).
3. More attention may be placed on the use of simplified equivalent structural models to stiffened plates on a global scale (Battaglia et al., 2017). This would in effect reduce model degrees of freedom thus simplifying modelling process without compromising data integrity. A reduction in computational time for the numerical analysis would also be an added benefit to employing these equivalent models.

The literature review shows that this is an understudied topic in naval architecture. We should extend this analysis to other fishing vessels, measure vibration exposures, identify solutions if needed, and expand on effects of vibration such as vibration-induced fatigue. The industry is in dire need of practical ways to address these issues to lead to increased comfort and physical well-being for seafarers.

Bibliography

American Bureau of Shipping. (2006). *Guidance Notes on Ship Vibration* (Vol. 2006, Issue April). https://ww2.eagle.org/content/dam/eagle/rules-and-guides/current/conventional_ocean_service/147_shipvibration/Ship_Vibration_GN_e-Jan15.pdf

American Bureau of Shipping. (2014). *Guidance Notes on Safehull Finite Element Analysis of Hull Structures* (Vol. 2004, Issue February).

American Bureau of Shipping. (2016). *Guide For Crew Habitability On Ships* (Issue February). http://www.eagle.org/eagleExternalPortalWEB/ShowProperty/BEA Repository/Rules&Guides/Current/102_CrewHabitabilityonShips/Pub102_CrewHabitability

American Bureau of Shipping. (2018). *Guidance Notes on Ship Vibration* (Issue February).

Ascione, L., Caron, J.-F., Correia, J. R., Corte, W. De, Godonou, P., Knippers, J., Moussiaux, E., Mottram, T., Oppe, M., Silvestre, N., Thorning, P., & Trom, L. (2016). *Prospect for New Guidance in the Design of FRP*. European Composites Industry Association. https://doi.org/10.2788/22306

Asmussen, I., Menzel, W., & Mumm, H. (2001). *Ship Vibration*. Germanischer Lloyd.

Bašić, J., & Parunov, J. (2013). Analytical and numerical computation of added mass in ship vibration analysis. *Brodogradnja*, *64*(2), 1–11.

Battaglia, G., Matteo, A. Di, Pirrotta, A., & Micale, G. (2017). Dynamic response of equivalent orthotropic plate model for stiffened plate: numerical-experimental

assessment. *Procedia Engineering*, *199*, 1423–1428. https://doi.org/https://doi.org/10.1016/j.proeng.2017.09.387

Bhattacharya, B., Tomlinson, G. R., & House, J. R. (2002). Vibration suppression of structures with viscoelastic inserts. *Proceedings of the Institution of Mechanical Engineers, Part C: Journal of Mechanical Engineering Science*, *216*(10), 983–996. https://doi.org/10.1243/095440602760400959

Biot, M., Boote, D., Brocco, E., Moro, L., Pais, T., & Delle Piane, S. (2015). Numerical and Experimental Analysis of the Dynamic Behavior of Main Engine Foundations. In *The Twenty-fifth International Ocean and Polar Engineering Conference* (p. 6). International Society of Offshore and Polar Engineers. https://doi.org/

Biot, M., & Moro, L. (2012). Experimental Study of a Resilient Mounting for Marine Diesel Engines. *In Proceedings of the IMDC 2012 Conference, April*.

Brandt, A. (2011). Noise and Vibration Analysis: Signal Analysis and Experimental Procedures. In *Noise and Vibration Analysis: Signal Analysis and Experimental Procedures*. https://doi.org/10.1002/9780470978160

Burella, G., Moro, L., & Colbourne, B. (2019). Noise sources and hazardous noise levels on fishing vessels: The case of Newfoundland and Labrador's fleet. *Ocean Engineering*, *173*(December 2018), 116–130. https://doi.org/10.1016/j.oceaneng.2018.12.062

Chen, N. Z. (2002). *Finite Element Analysis of a Fishing Vessel Built of Composite Materials*. *January*. https://doi.org/10.13140/RG.2.1.1539.4807

Daniela-Elena, M. (2013). Vibration Control of Complex Ship Structures. *Constanta*

Maritime University's Annals, 17, 107–115.

Deng, L., Song, F., Li, M., Song, B., & Shu, Q. (2014). *Static and Dynamic Finite Element Analysis of the Whole Ship Structural of Inland Waterway Bulk Carrier*. *562*, 996–1000. https://doi.org/10.4028/www.scientific.net/AMM.556-562.996

Dessi, D., & Ciappi, E. (2010). Comparative analysis of slamming events and induced response for different types of ships. *11th International Symposium on Practical Design of Ships and Other Floating Structures, PRADS 2010*, *1*, 362–371.

DNV GL. (2016). *Class Guideline: Finite Element Analysis* (Issue DNVGL-CG-0127).

DNV GL. (2017). *Rules for Classification: Ships* (Issue July).

FAO (Food & Agriculture Organisation). (2001). Safety At Sea As an Integral Part of Fisheries Management Safety. In *Fisheries Bethesda* (Issue 966).

FAO (Food & Agriculture Organisation). (2017). *Fisheries and Aquaculture Statistics 2017*. https://doi.org/10.1109/BMEI.2010.5639447

FAO (Food & Agriculture Organisation). (2018). *The State of World Fisheries and Aquaculture 2018 - Meeting the sustainable development goals*. https://doi.org/10.1093/japr/3.1.101

Ferrari, A., & Rizzuto, E. (2007). Measuring damping properties of viscoelastic materials for marine applications. *Advancements in Marine Structures - Proceedings of MARSTRUCT 2007, The 1st International Conference on Marine Structures*.

Ferrari, Alberto, & Rizzuto, E. (2003). Vibrational Behaviour of a Deck Panel of a Fast Ferry. *FAST 2003 The 7th International Conference on Fast Sea Transportation*, 27–32.

Fragasso, J., Moro, L., Mendoza Vassallo, P. N., Biot, M., & Badino, A. (2017). Experimental characterization of viscoelastic materials for marine applications. *Progress in the Analysis and Design of Marine Structures - Proceedings of the 6th International Conference on Marine Structures, MARSTRUCT 2017*, 87–96. https://doi.org/10.1201/9781315157368-12

Gloza, I. (2008). Vibration and radiated noise of a small ship. *Hydroacoustics*, *11*, 87–96.

Hanselka, H and Hoffmann, U. (1999). Damping Characteristics of Fibre Reinforced Polymers. *Technische Mechanik*, *10*, 91–101.

Haward, B. M., Lewis, C. H., & Griffin, M. J. (2009). Motions and crew responses on an offshore oil production and storage vessel. *Applied Ergonomics*, *40*(5), 904–914. https://doi.org/10.1016/j.apergo.2009.01.001

Holden, K. O., Fagerjord, O., & Frostad, R. (1980). *EARLY DESIGN-STAGE APPROACH TO REDUCING HULL SURFACE FORCES DUE TO PROPELLER CAVITATION*.

Hoogendoorn, W. E., Bongers, P. M., de Vet, H. C., Douwes, M., Koes, B. W., Miedema, M. C., Ariens, G. A., & Bouter, L. M. (2000). Flexion and rotation of the trunk and lifting at work are risk factors for low back pain: results of a prospective cohort study. *Spine*, *25*(23), 3087–3092. https://doi.org/10.1097/00007632-200012010-00018

International Organization for Standardization (ISO). (1984). *ISO 6954:1984 Mechanical Vibration and Shock – Guidelines for the overall evaluation of vibration in merchant ships*. ISO.

International Organization for Standardization (ISO). (1997). *ISO 2631-1 Mechanical Vibration and Shock: Evaluation of Human Exposure to Whole-body Vibration*. ISO.

International Organization for Standardization (ISO). (2000). *ISO 6954:2000 Mechanical Vibration and Shock – Guidelines for the Measurement, Reporting and Evaluation of Vibration with Regard to Habitability on Passenger and Merchant Ships*. ISO.

International Organization for Standardization (ISO). (2016). *ISO 20283-5:2016 Mechanical vibration — Measurement of vibration on ships — Part 5: Guidelines for measurement, evaluation and reporting of vibration with regard to habitability on passenger and merchant ships*. ISO.

Janowiakt, J. J., Hindman, D. P., & Manheck, H. B. (2007). Orthotropic Behavior of Lumber Composite Materials. *Wood and Fiber Science*, *33*(4), 580–594. https://wfs.swst.org/index.php/wfs/article/viewFile/1350/1350

Jaremin, B., & Kotulak, E. (2004). Mortality in the Polish small-scale fishing industry. *Occupational Medicine (Oxford, England)*, *54*(4), 258–260. https://doi.org/10.1093/occmed/kqh054

Jensen, A., & Jepsen, J. R. (2014). Vibration on board and health effects. *International Maritime Health*, *65*(2), 58–60. https://doi.org/10.5603/IMH.2014.0013

Johnson, C., & Kienholz, D. (1982). Finite Element Prediction of Damping in Structures with Constrained Viscoelastic Layers. *AIAA Journal*, *20*(9), 1284–1290. https://doi.org/10.2514/3.51190

Kapsenberg, G. K. (2011). Slamming of ships: where are we now? *Philosophical Transactions of the Royal Society A: Mathematical, Physical and Engineering Sciences*, *369*(1947), 2892–2919. https://doi.org/10.1098/rsta.2011.0118

Kingma, I., Delleman, N. J., & Van Dieën, J. H. (2003). The effect of ship accelerations

on three-dimensional low back loading during lifting and pulling activities. *International Journal of Industrial Ergonomics*, *32*(1), 51–63. https://doi.org/10.1016/S0169-8141(03)00029-5

Koona, R., Kumar, G., & Ranganath, S. (2008). Optimization of Surface Damping Treatments for Vibration Control of Marine Structure. *Experimental Analysis of Nano and Engineering Materials and Structures*, 747–748. https://doi.org/10.1007/978-1-4020-6239-1_371

Lin, T. R., Pan, J., O'Shea, P. J., & Mechefske, C. K. (2009). A study of vibration and vibration control of ship structures. *Marine Structures*, *22*(4), 730–743. https://doi.org/10.1016/j.marstruc.2009.06.004

Lloyd's Register. (2015). *General Overview of Ship Structural Vibration Problems*.

LLoyd's Register. (2019). Rules and Regulations for the Classification of Ships. In *Notice No. 9* (Issue July).

Maritime and Coastguard Agency. (2007). *The Merchant Shipping and Fishing Vessels Regulations (Control of Vibration at Work)*. *353*(February), 1–25.

Menzel, W., Moctar, E., & Mumm, H. (2008). Advanced thinking on tricky excitations. *Naval Architect*, *MAR.*, 64–69.

Moro, L., Biot, M., Brocco, E., Lorenzo, F. De, Nicolás, P., & Vassallo, M. (2013). Hull Vibration Analysis of River Boats. *International Conference IDS2013-Amazonia*, *July*, 1–19.

Moro, L., Brocco, E., Badino, A., Vassallo, P. N. M., Clericuzio, A., & Biot, M. (2016). Design Procedure for the Development of New Floating Floors to Improve Comfort

on Ships. *PRADS 2016 - Proceedings of the 13th International Symposium on PRActical Design of Ships and Other Floating Structures*.

MSC Software. (2004). *MSC.Nastran Advanced Dynamic Analysis User's Guide* (Issue MSC.Nastran Version 70).

MSC Software. (2013). *MSC Nastran Dynamic Analysis User's Guide: Vol. MSC Nastra* (2013.1).

Naughton, B. P., Panhuizen, F., & Vermeulen, A. C. (1985). The Elastic Properties of Chopped Strand Mat and Woven Roving in G.R. Laminae. *Journal of Reinforced Plastics and Composites*, *4*(2), 195–204. https://doi.org/10.1177/073168448500400204

Nielsen, L. E. (1970). Generalized equation for the elastic moduli of composite materials. *Journal of Applied Physics*, *41*(11), 4626–4627.

Norwood, M. N., & Dow, R. S. (2013). Dynamic analysis of ship structures. *Ships and Offshore Structures*, *8*(3–4), 270–288. https://doi.org/10.1080/17445302.2012.755285

Ojak, W. (1988). Vibrations and Waterborne Noise on Fishery Vessels. *Journal of Ship Research*, *32*(2), 112–133.

Oldenburg, M., Baur, X., & Schlaich, C. (2010). Occupational risks and challenges of seafaring. *Journal of Occupational Health*, *52*(5), 249–256. https://doi.org/10.1539/joh.K10004

Pais, T., Moro, L., Boote, D., & Biot, M. (2017). Vibration analysis for the comfort assessment of superyachts. *Journal of Marine Science and Application*, *16*(3), 323–

333. https://doi.org/10.1007/s11804-017-1420-z

Reddy, J. N. (1997). *Mechanics of Laminated Composite Plates and Shells: Theory and Analysis*.

Rejab, M. R. M., Theng, C. W., Rahman, M. M., Noor, M. M., & Rose, A. N. M. (2008). *An Investigation into the Effects of Fibre Volume Fraction on GFRP Plate Abstract — This paper presents the mechanical properties of Glass Fibre Reinforce Plastic*. 136–142.

Roberts, S. (2008). Fatal work-related accidents in UK merchant shipping from 1919 to 2005. *Occupational Medicine (Oxford, England)*, *58*, 129–137. https://doi.org/10.1093/occmed/kqm149

Roberts, S., & Hansen, H. L. (2002). An analysis of the causes of mortality among seafarers in the British merchant fleet (1986–1995) and recommendations for their reduction. *Occupational Medicine (Oxford, England)*, *52*, 195–202. https://doi.org/10.1093/occmed/52.4.195

Ross, R. J., & USDA Forest Service., F. P. L. (2010). *Wood Handbook: Wood as an Engineering Material*. https://doi.org/10.2737/FPL-GTR-190

Sai, V. S., Satyanarayana, M. R. S., Murthy, V. B. K., Rao, G. S., & Prasad, A. S. (2013). An Experimental Simulation to Validate FEM to Predict Transverse Young ' s Modulus of FRP Composites. *Advances in Materials Science and Engineering*, *2013*.

Ship Structure Committee. (1990). *Practical Guide for Shipboard Vibration Control and Attenuation*.

Smarslok, B. P., Haftka, R. T., & Ifju, P. G. (2012). Correlation model for composite elastic

properties using only measurements from a single specimen. *Probabilistic Engineering Mechanics*, *29*, 64–69. https://doi.org/https://doi.org/10.1016/j.probengmech.2011.08.008

Subashi, G. H. M. J., Matsumoto, Y., & Griffin, M. J. (2008). Modelling resonances of the standing body exposed to vertical whole-body vibration: Effects of posture. *Journal of Sound and Vibration*, *317*(1–2), 400–418. https://doi.org/10.1016/j.jsv.2008.03.019

Torner, M., Almstrom, C., Karlsson, R., & Kadefors, R. (1994). Working on a moving surface--a biomechanical analysis of musculo-skeletal load due to ship motions in combination with work. *Ergonomics*, *37*(2), 345–362. https://doi.org/10.1080/00140139408963651

Vergassola, G., Boote, D., & Tonelli, A. (2018). On the damping loss factor of viscoelastic materials for naval applications. *Ships and Offshore Structures*, *13*(5), 466–475. https://doi.org/10.1080/17445302.2018.1425338

Wertheim, A. H., Kemper, H. C. G., & Heus, R. (2002). Maximal oxygen uptake during cycling is reduced in moving environments; consequences for motion-induced fatigue. *Ergonomics*, *45*(3), 186–202. https://doi.org/10.1080/00140130110116623

Yucel, A., & Arpaci, A. (2013). Free and forced vibration analyses of ship structures using the finite element method. *Journal of Marine Science and Technology (Japan)*, *18*(3), 324–338. https://doi.org/10.1007/s00773-012-0210-1

Appendix A: Global Mode Shapes

Appendix A.1. Dry Global Mode Shapes

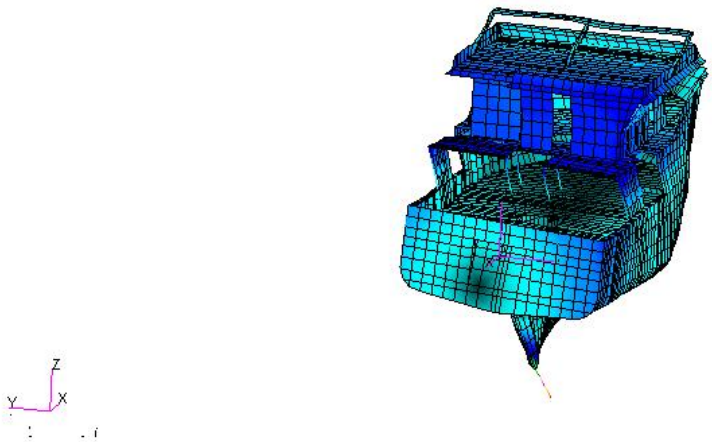

Figure A.1: Dry Global Mode Shape, Mode 1, Torsional, 6.9765 Hz

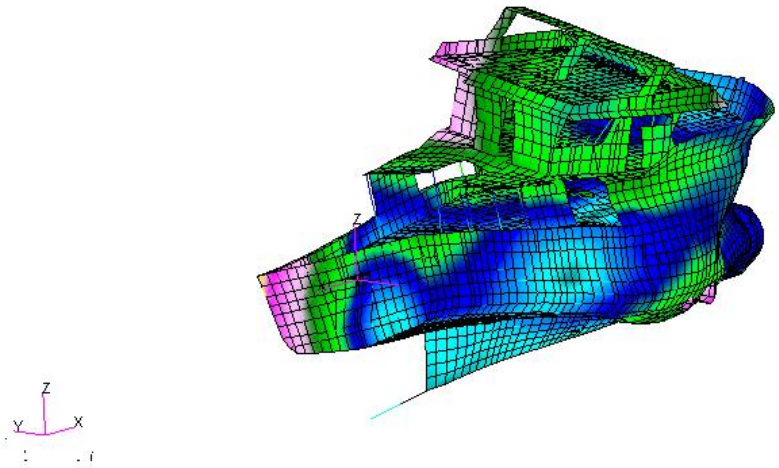

Figure A.2: Dry Global Mode Shape, Mode 2, Torsional, 9.4006 Hz

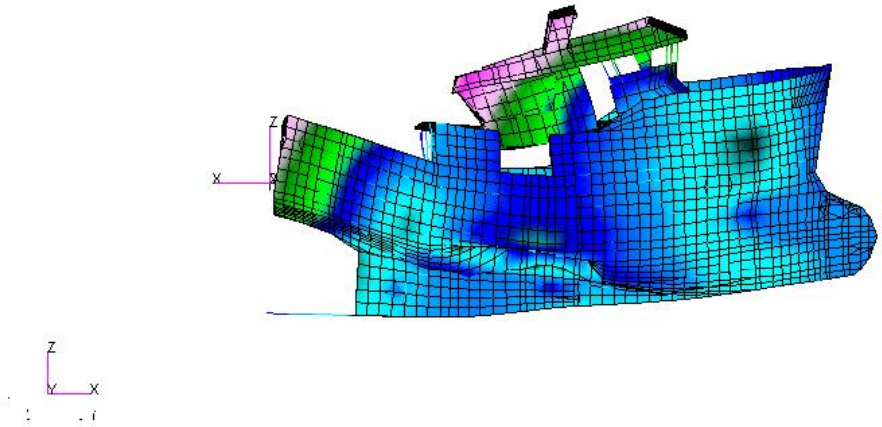

Figure A.3: Dry Global Mode Shape, Mode 3, Bending, 9.7671 Hz

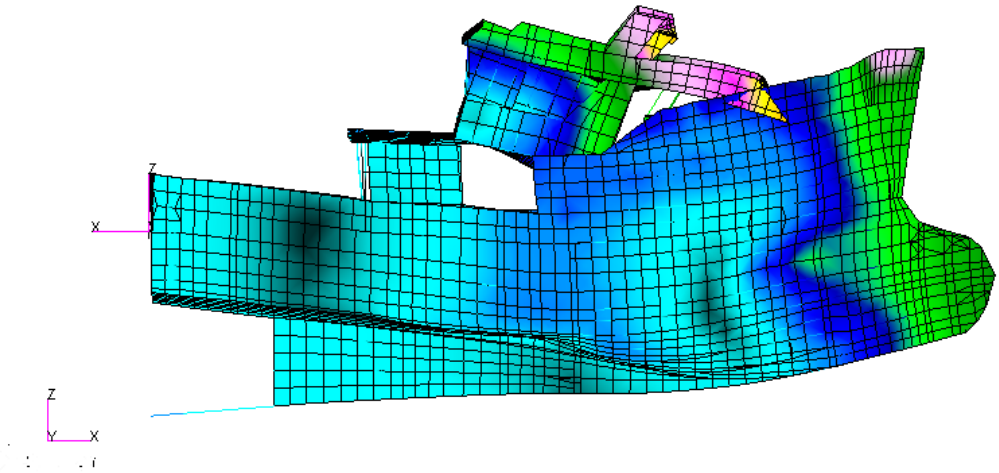

Figure A.4: Dry Global Mode Shape, Mode 4, Bending, 11.1280 Hz

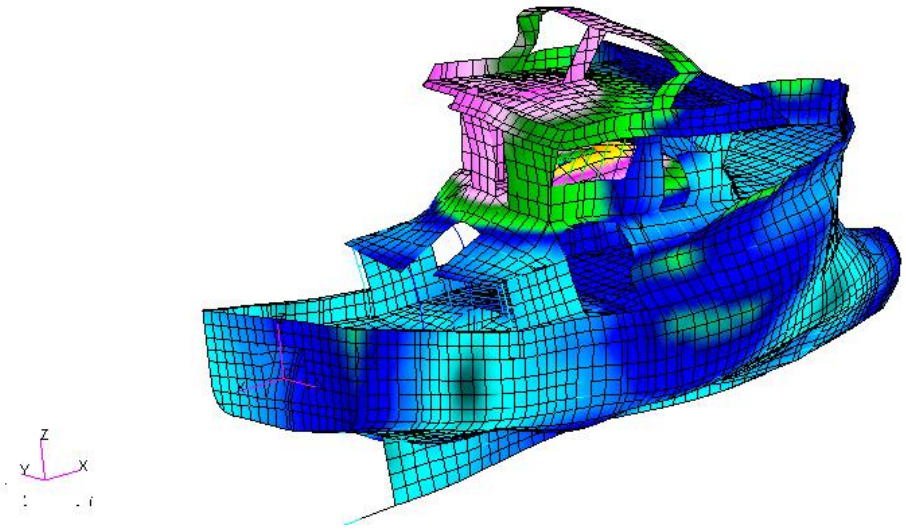

Figure A.5: Dry Global Mode Shape, Mode 5, Torsion and Bending, 14.4680 Hz

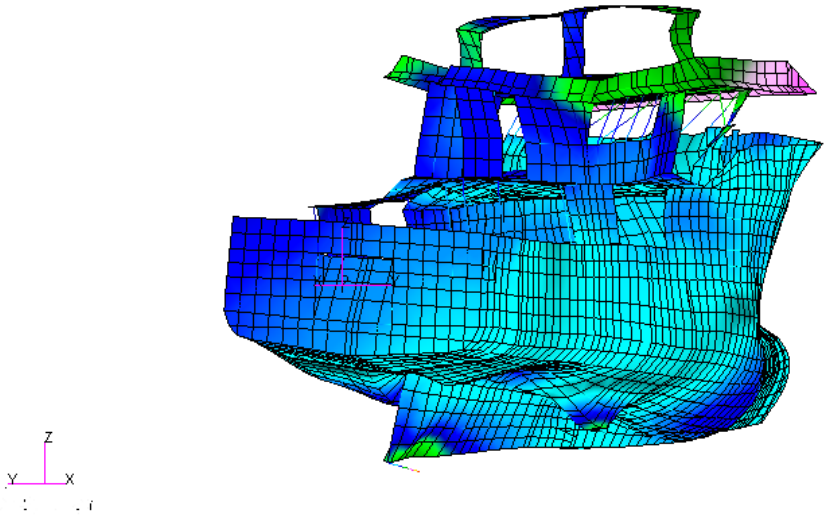

Figure A.6: Dry Global Mode Shape, Mode 6, Torsional, 15.7960Hz

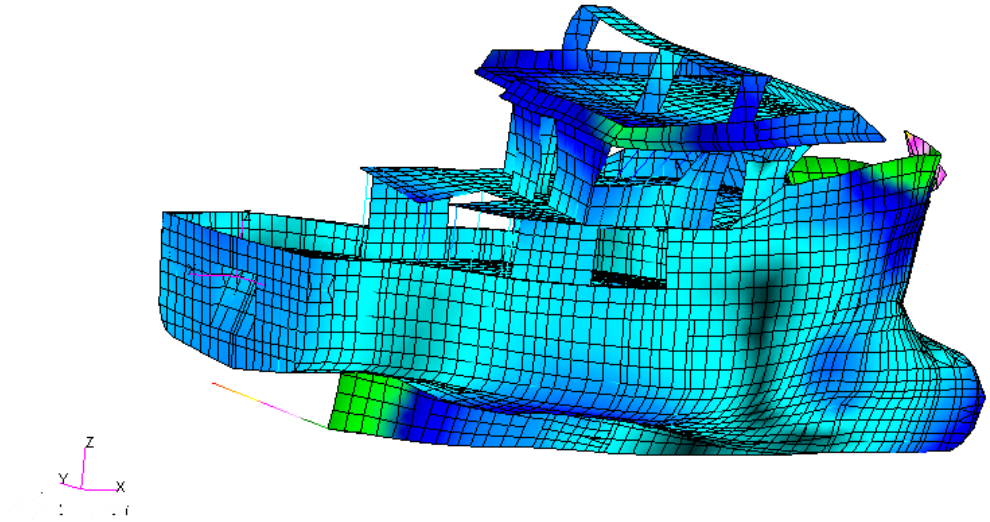

Figure A.7: Dry Global Mode Shape, Mode 7, Torsion and Bending, 18.2280 Hz

Appendix A.2. Wet Global Mode Shapes

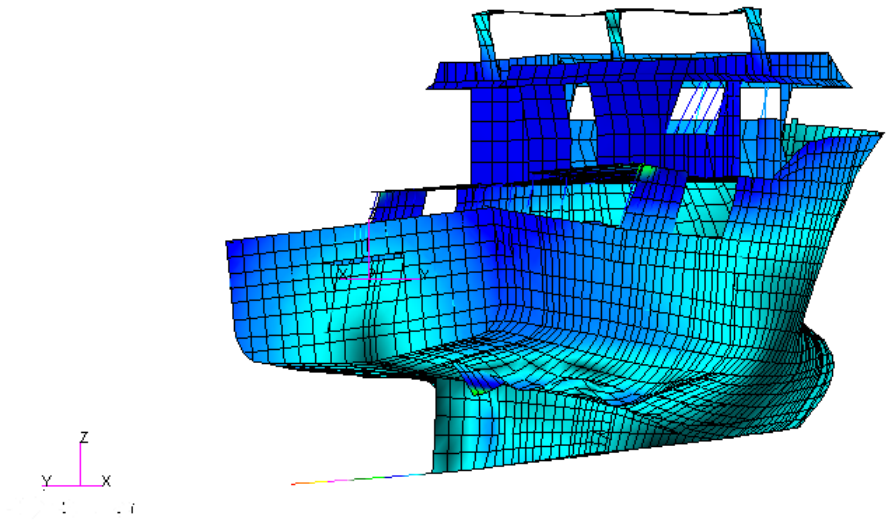

Figure A.8: Wet Global Mode Shape, Mode 1, Torsional, 6.1947 Hz

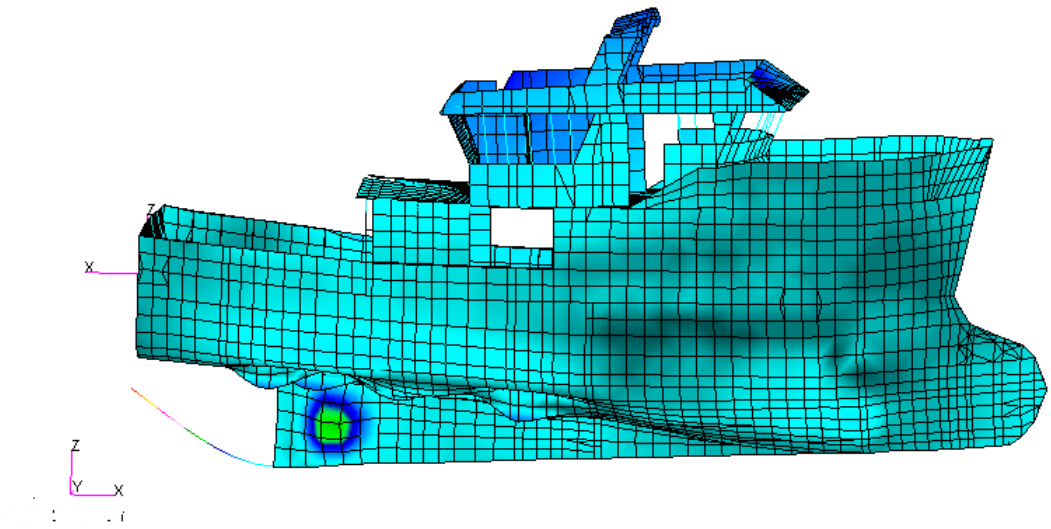

Figure A.9: Wet Global Mode Shape, Mode 2, Bending, 10.1330 Hz

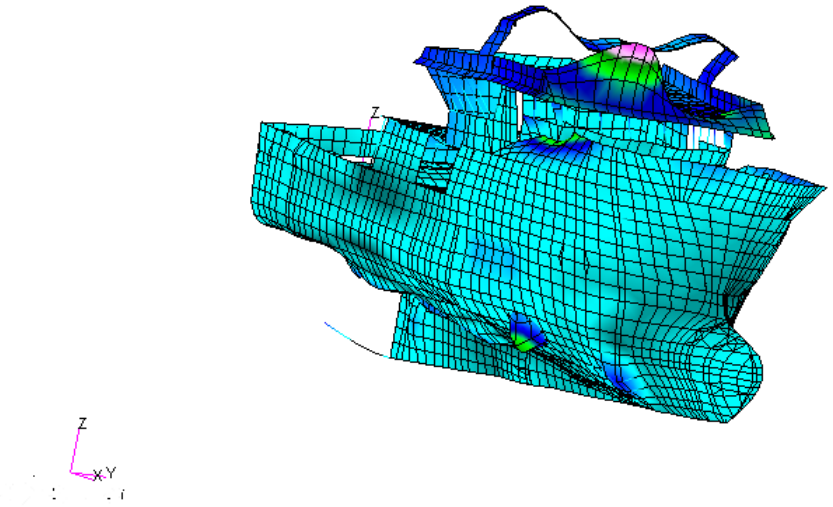

Figure A.10: Wet Global Mode Shape, Mode 3, Torsion and Bending, 13.1700 Hz

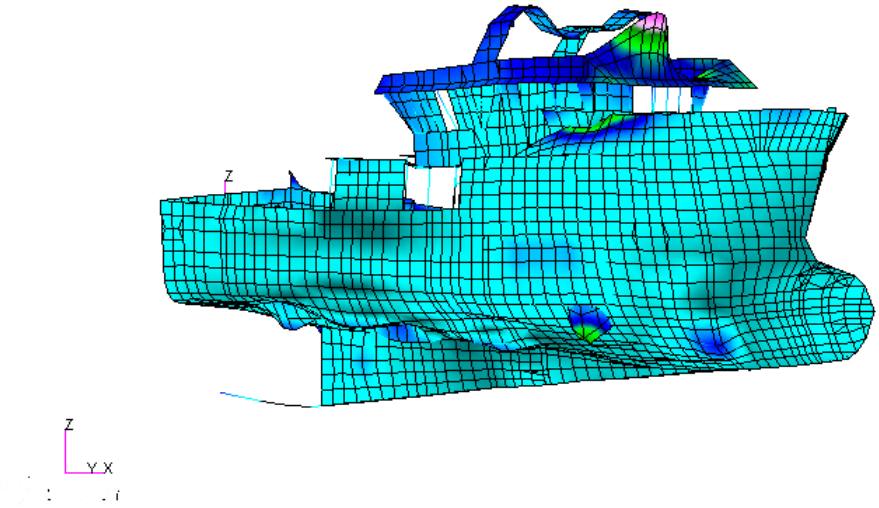

Figure A.11: Wet Global Mode Shape, Mode 4, Torsional, 14.3220 Hz

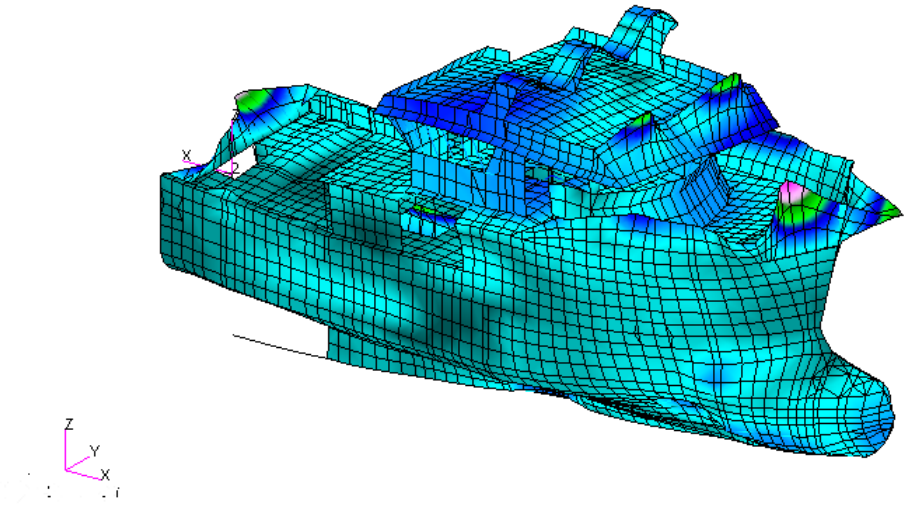

Figure A.12: Wet Global Mode Shape, Mode 5, Torsion and Bending, 18.8040 Hz

Appendix B: Mobility Analysis

Appendix B.1. Propeller Mobility

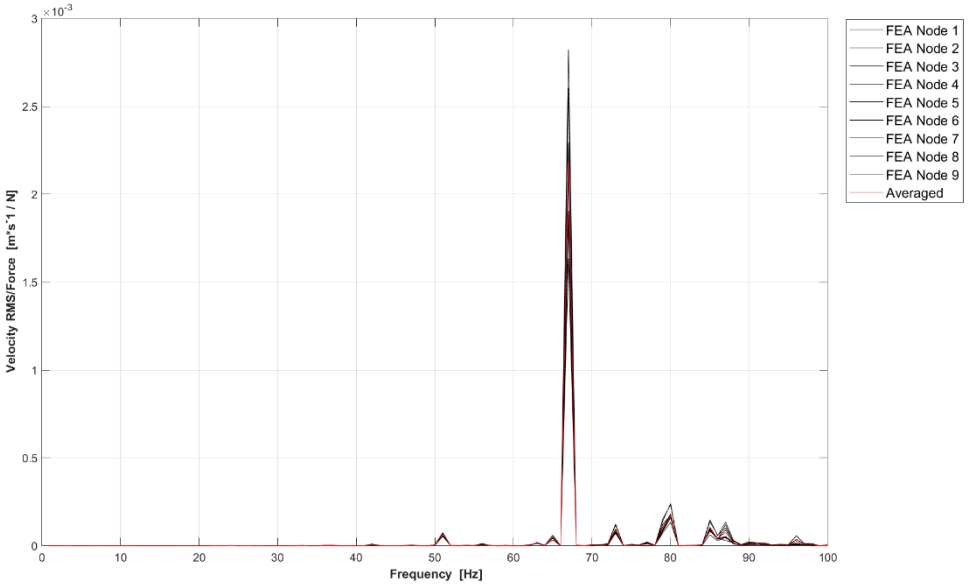

Figure B.1: Mobility - Propeller to Bunker Point 1

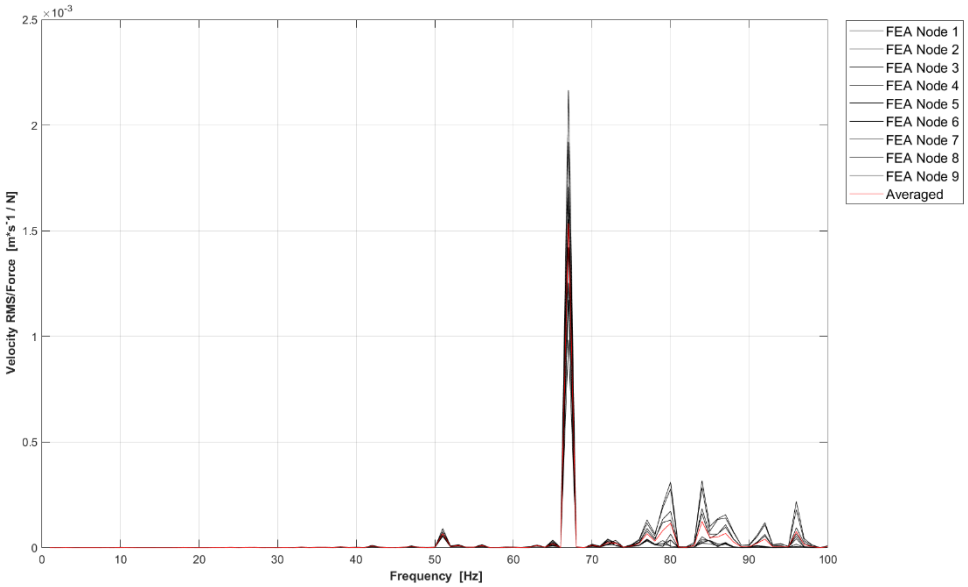

Figure B.2: Mobility - Propeller to Bunker Point 2

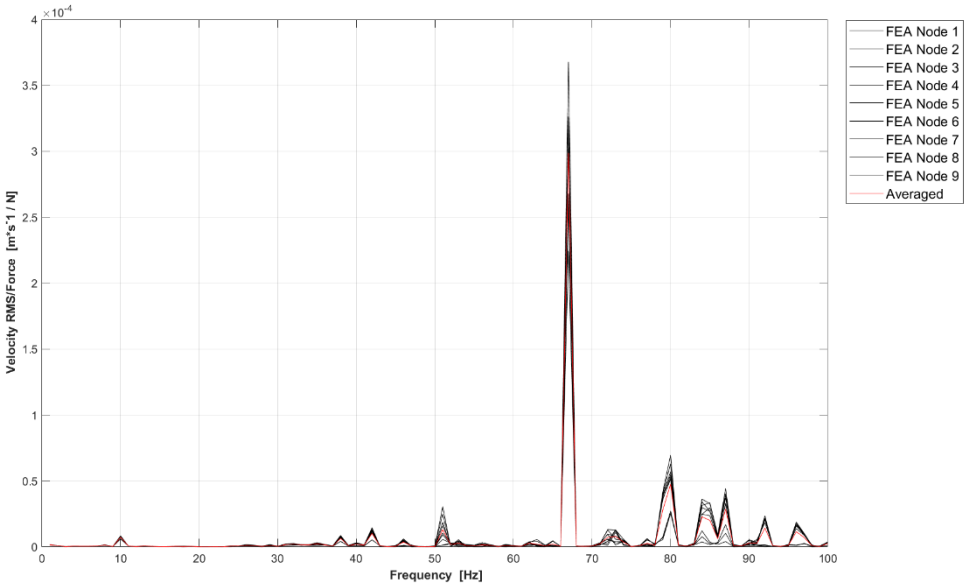

Figure B.3: Mobility - Propeller to Cabin Point 1

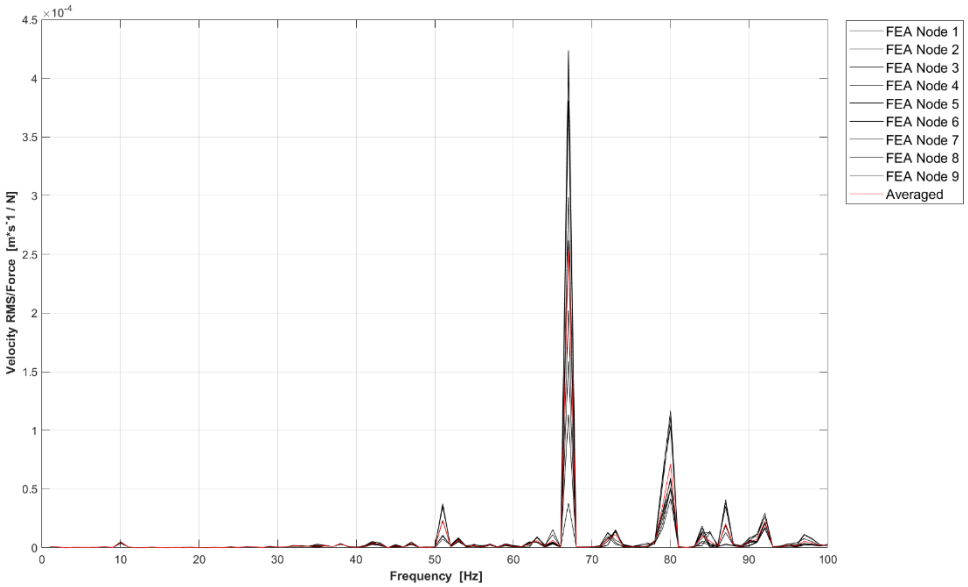

Figure B.4: Mobility - Propeller to Cabin Point 2

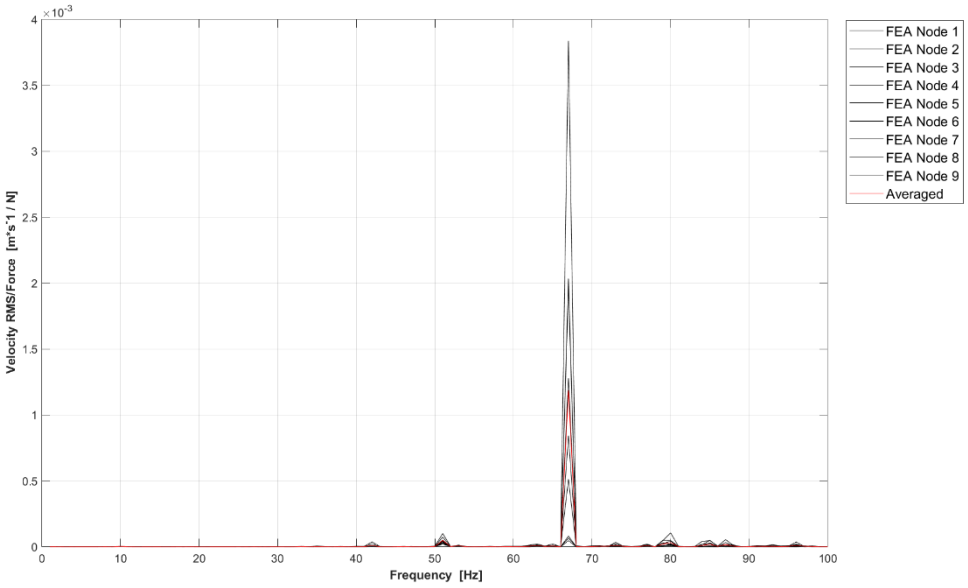

Figure B.5: Mobility - Propeller to Canteen Group 1, Point 1

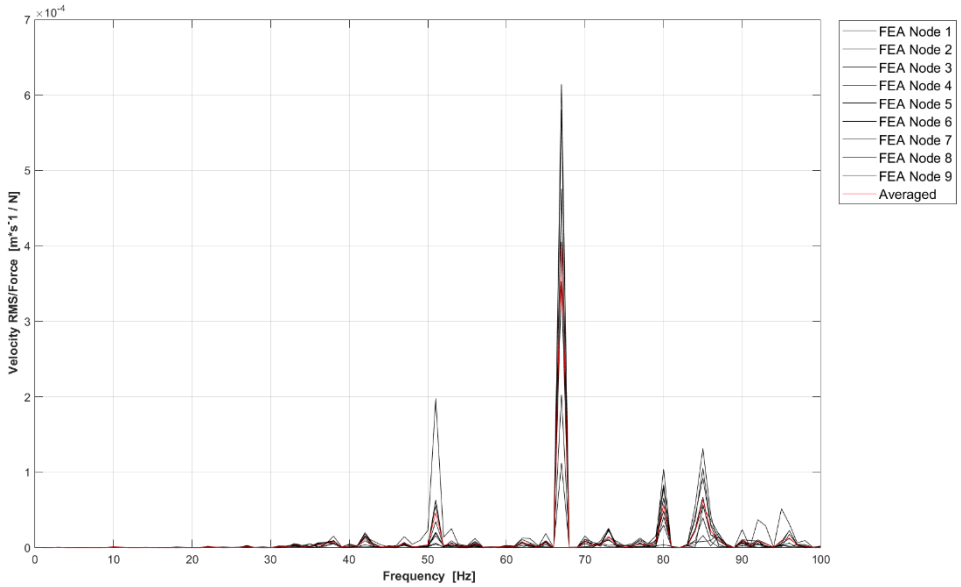

Figure B.6: Mobility - Propeller to Canteen Group 1, Point 2

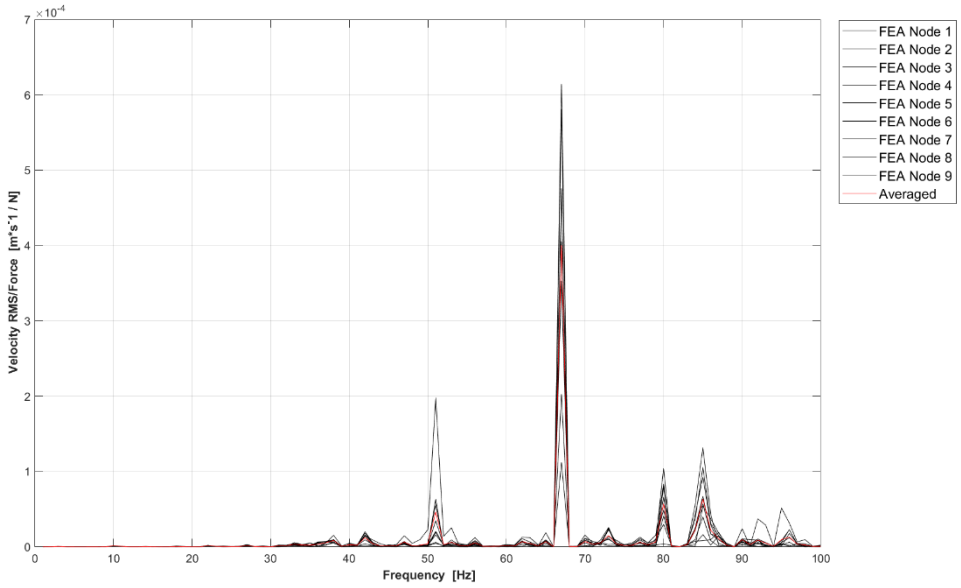

Figure B.7: Mobility - Propeller to Canteen Group 2, Point 1

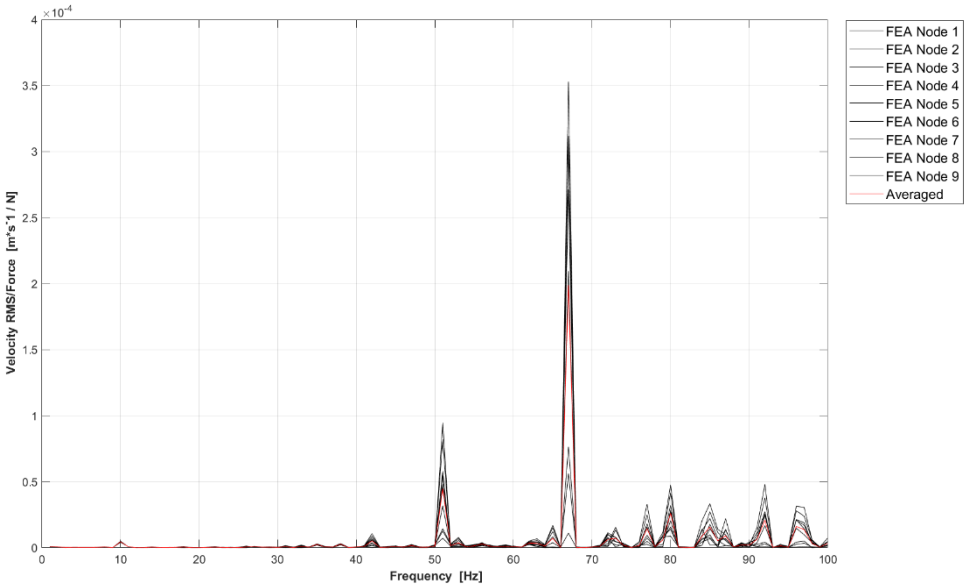

Figure B.8: Mobility - Propeller to Canteen Group 2, Point 2

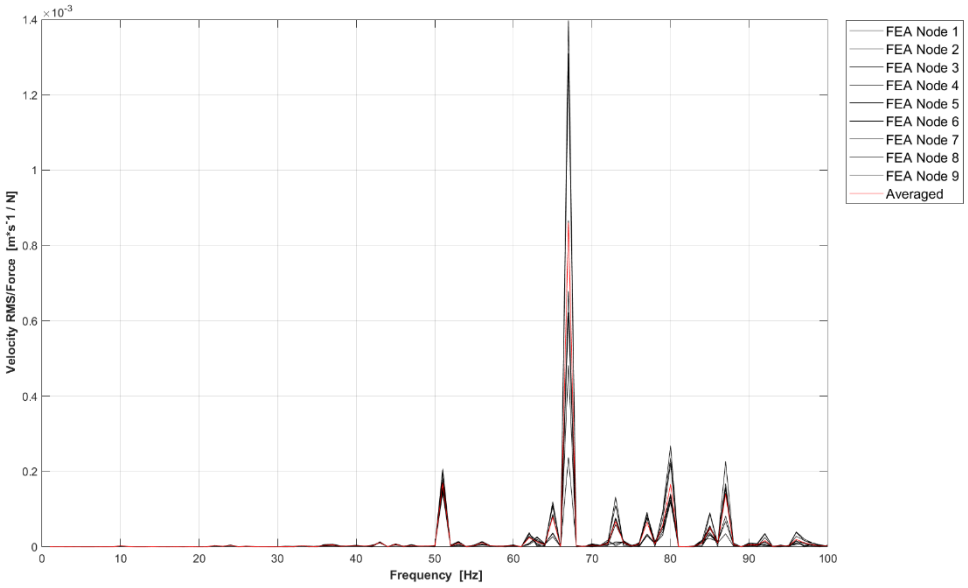

Figure B.9: Mobility - Propeller to Wheelhouse Group 1, Point 1

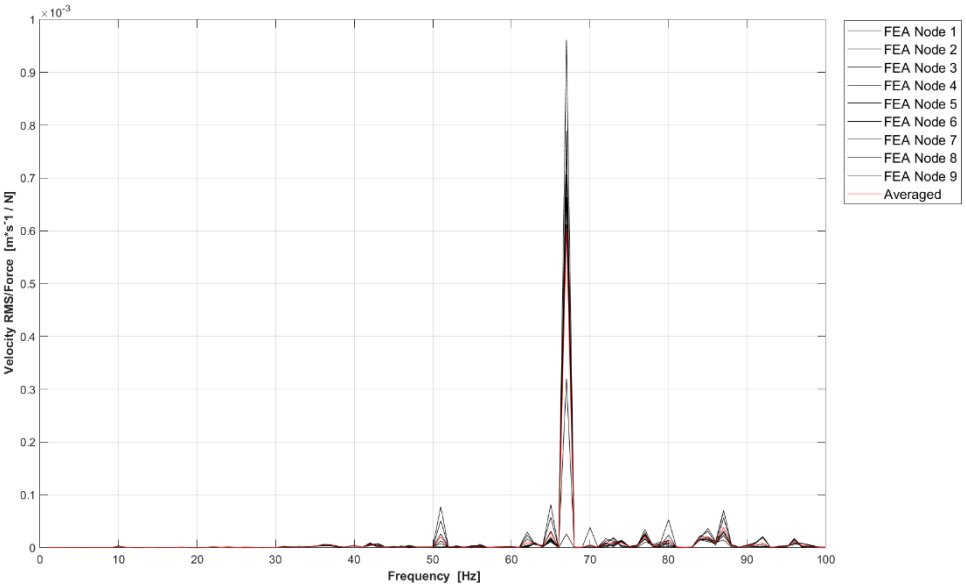

Figure B.10: Mobility - Propeller to Wheelhouse Group 1, Point 2

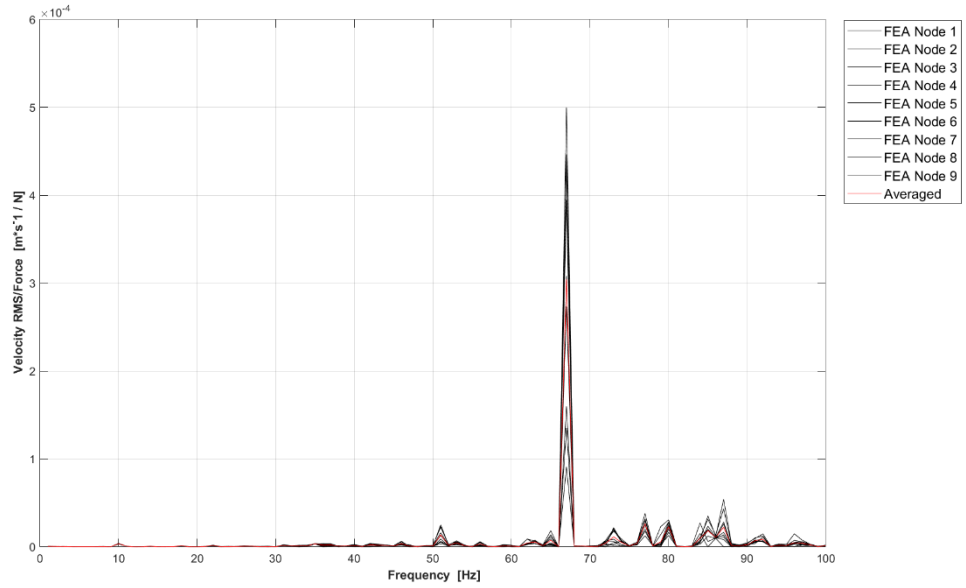

Figure B.11: Mobility - Propeller to Wheelhouse Group 2, Point 1

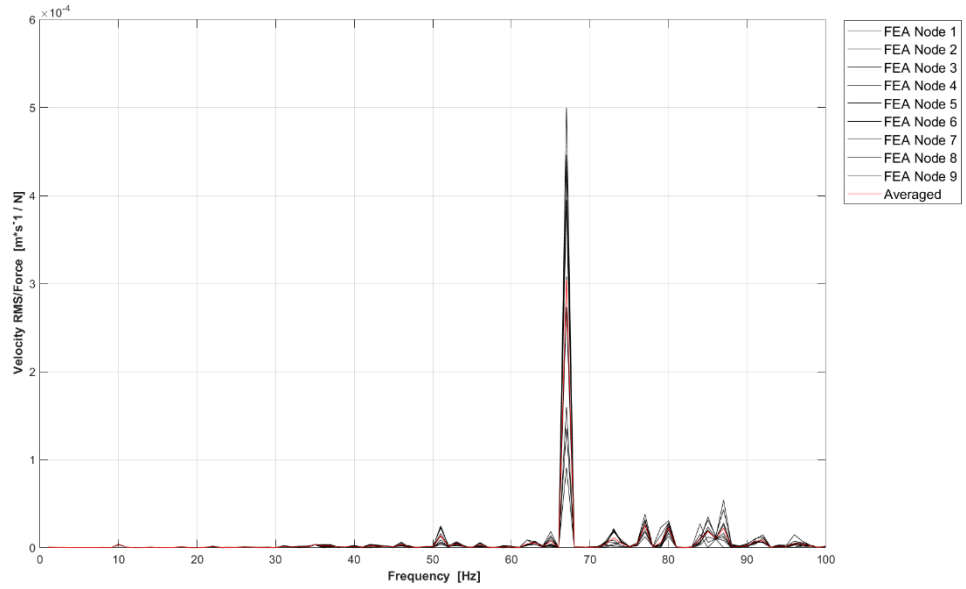

Figure B.12: Mobility - Propeller to Wheelhouse Group 2, Point 2

Appendix B.2. Engine Mobility

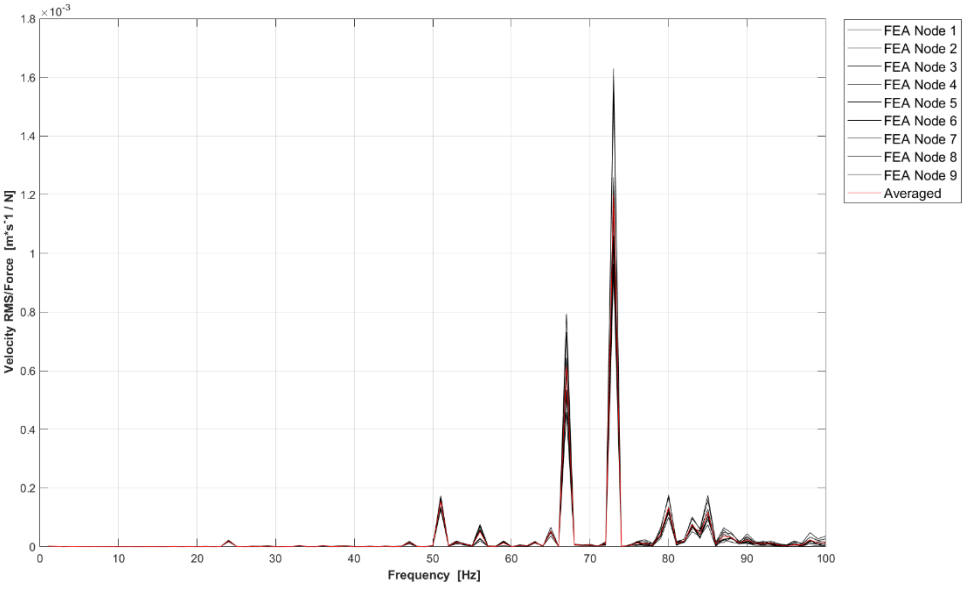

Figure B.13: Mobility - Engine to Bunker Point 1

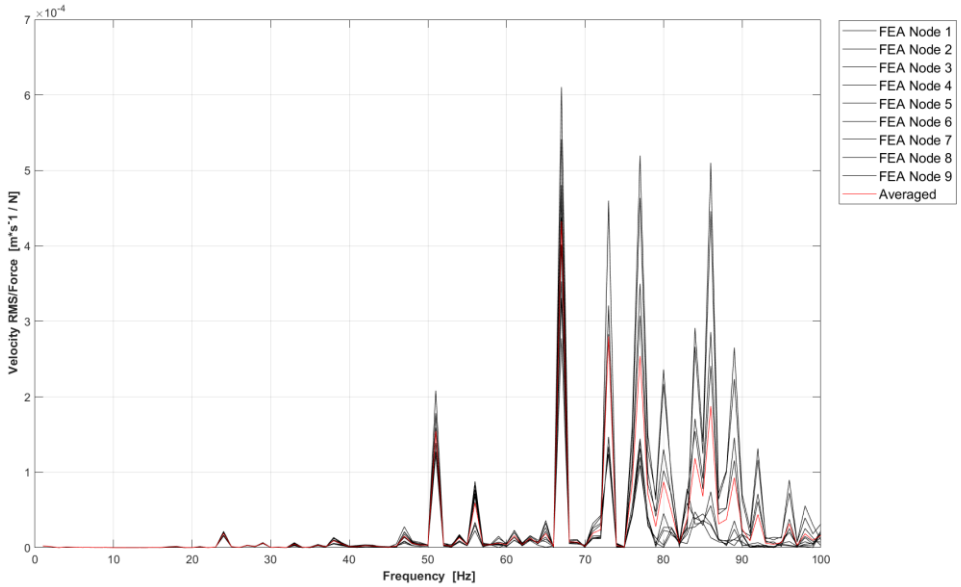

Figure B.14: Mobility - Engine to Bunker Point 2

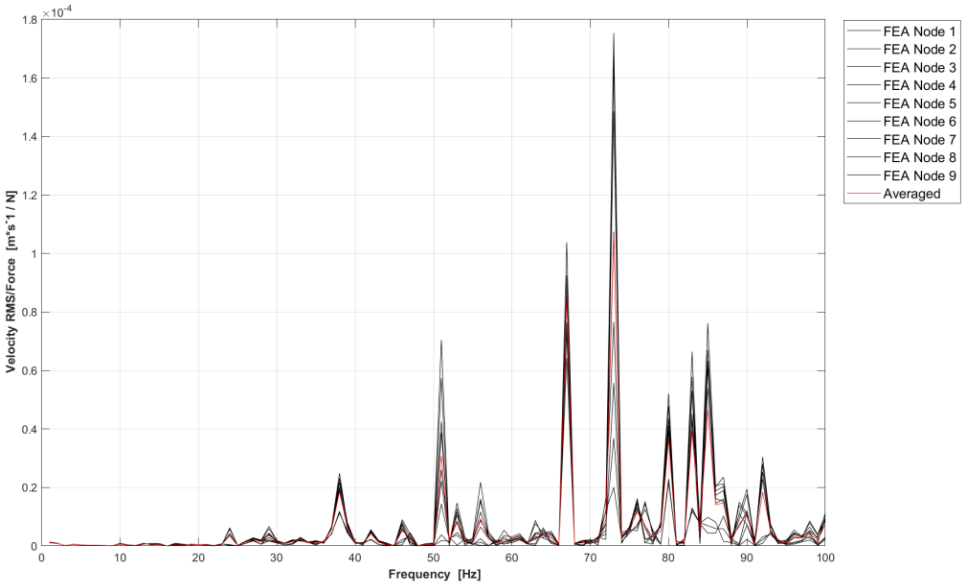

Figure B.15: Mobility - Engine to Cabin Point 1

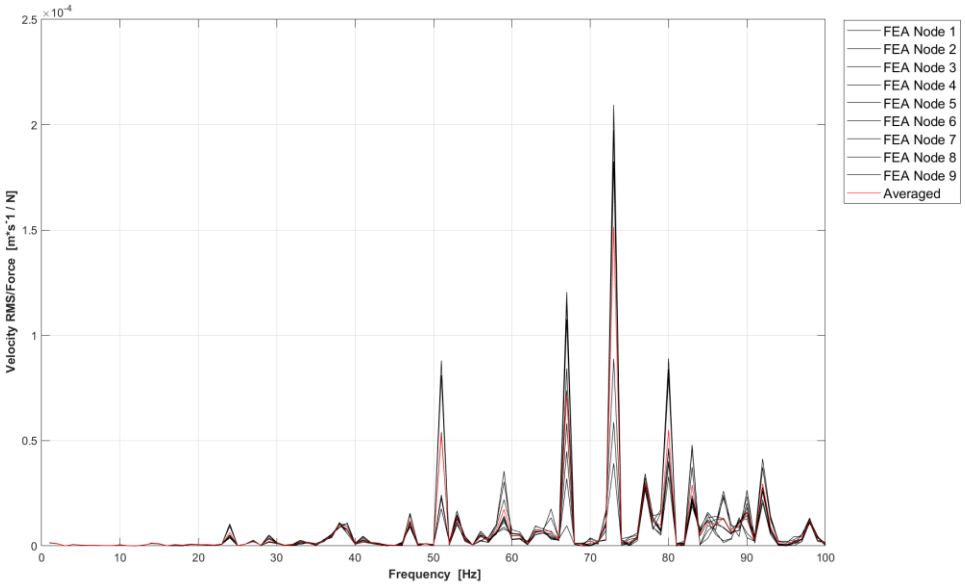

Figure B.16: Mobility - Engine to Cabin Point 2

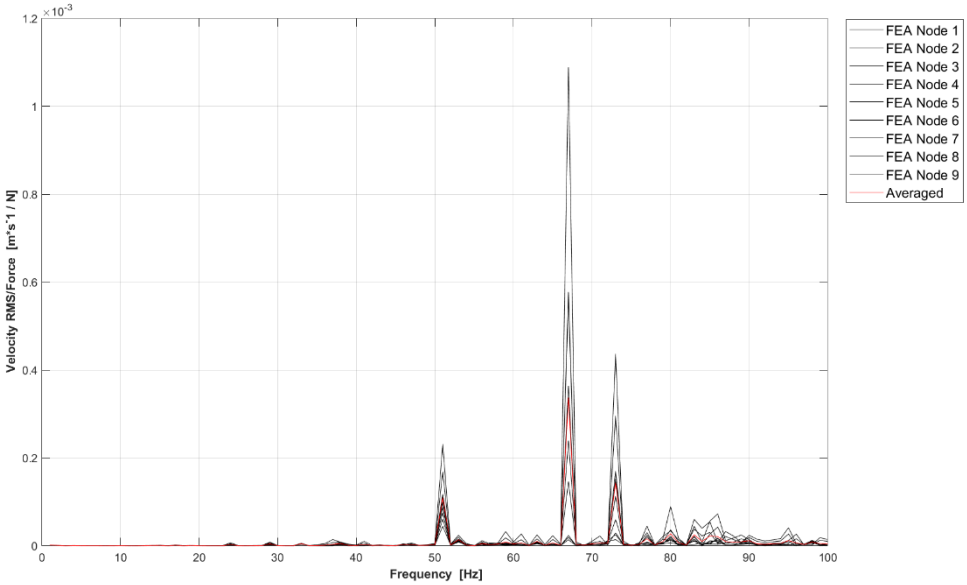

Figure B.17: Mobility - Engine to Canteen Group 1, Point 1

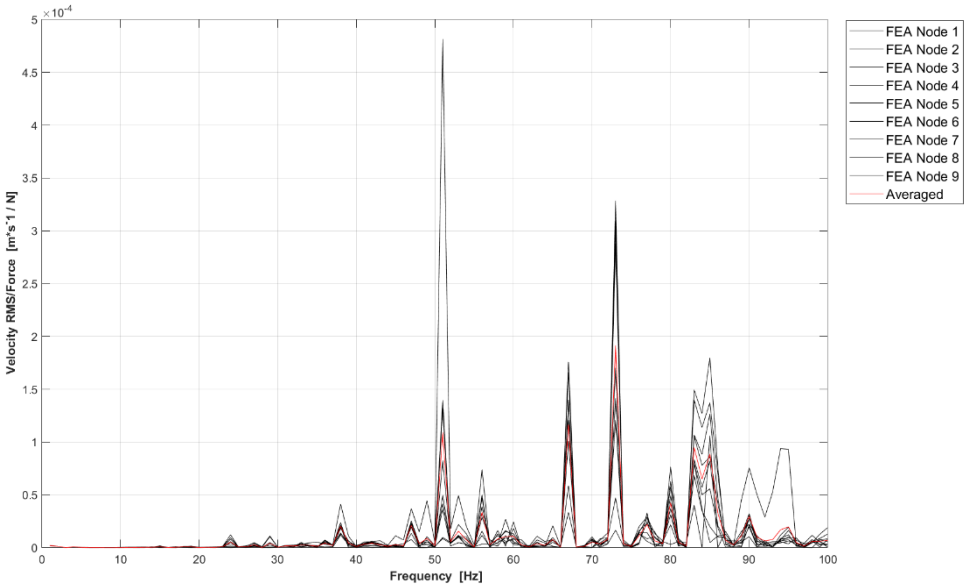

Figure B.18: Mobility - Engine to Canteen Group 1, Point 2

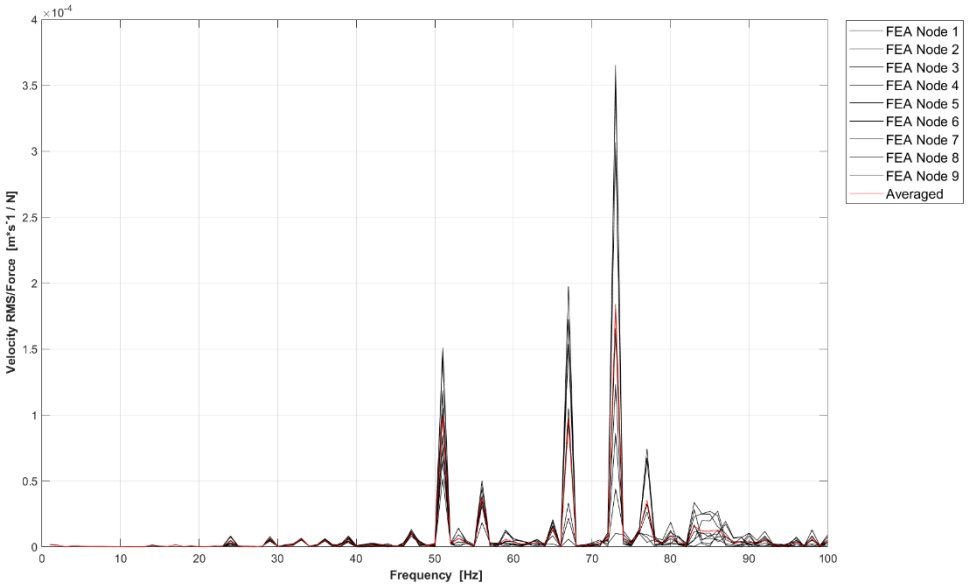

Figure B.19: Mobility - Engine to Canteen Group 2, Point 1

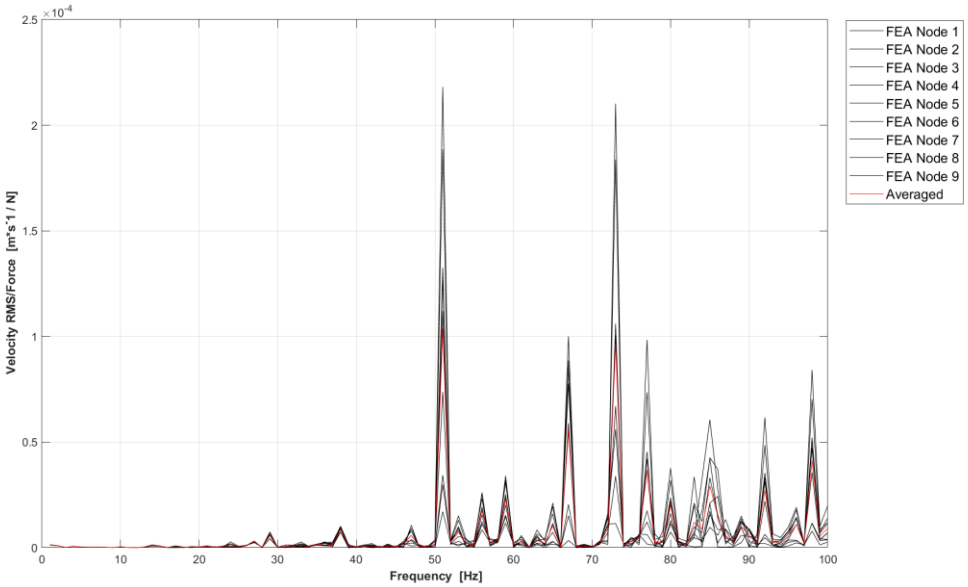

Figure B.20: Mobility - Engine to Canteen Group 2, Point 2

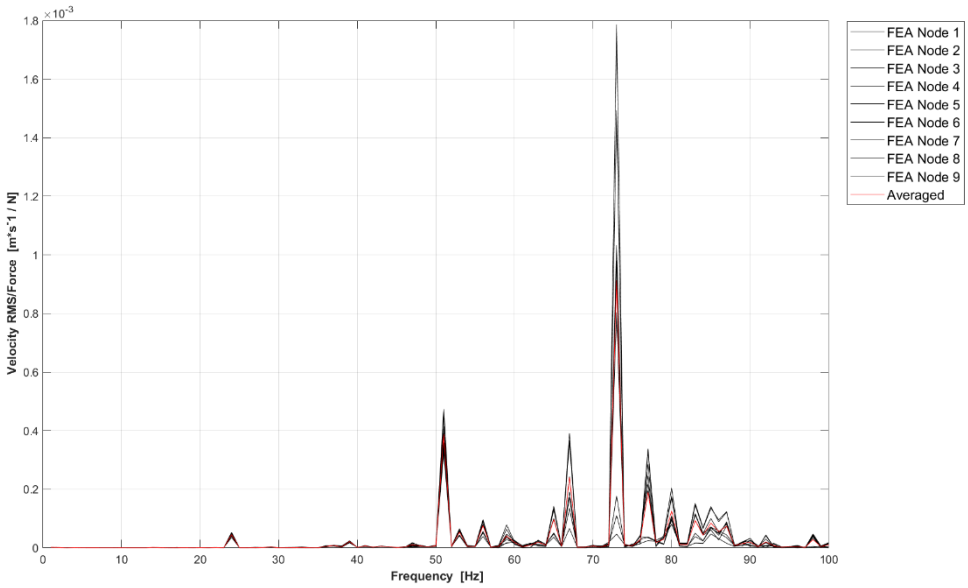

Figure B.21: Mobility - Engine to Wheelhouse Group 1, Point 1

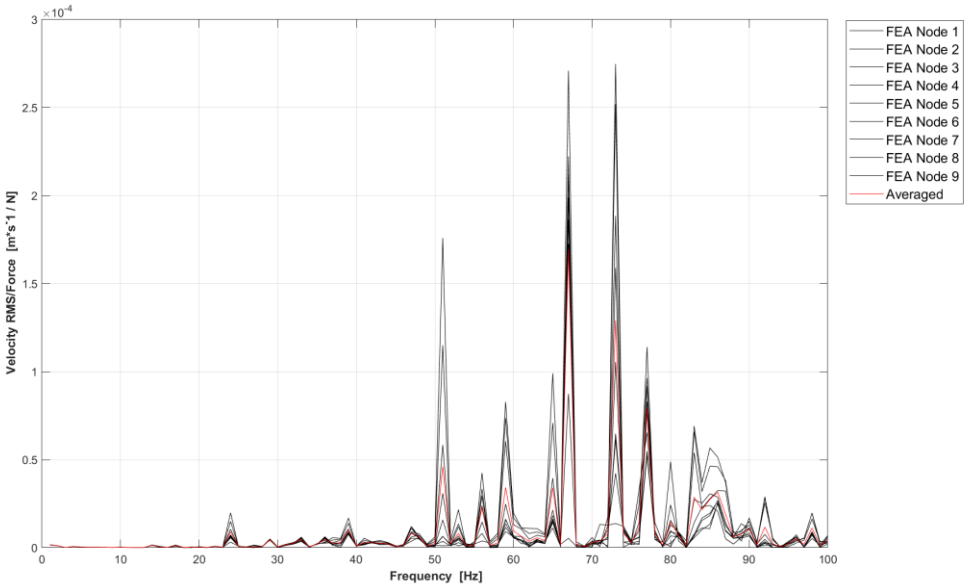

Figure B.22: Mobility - Engine to Wheelhouse Group 1, Point 2

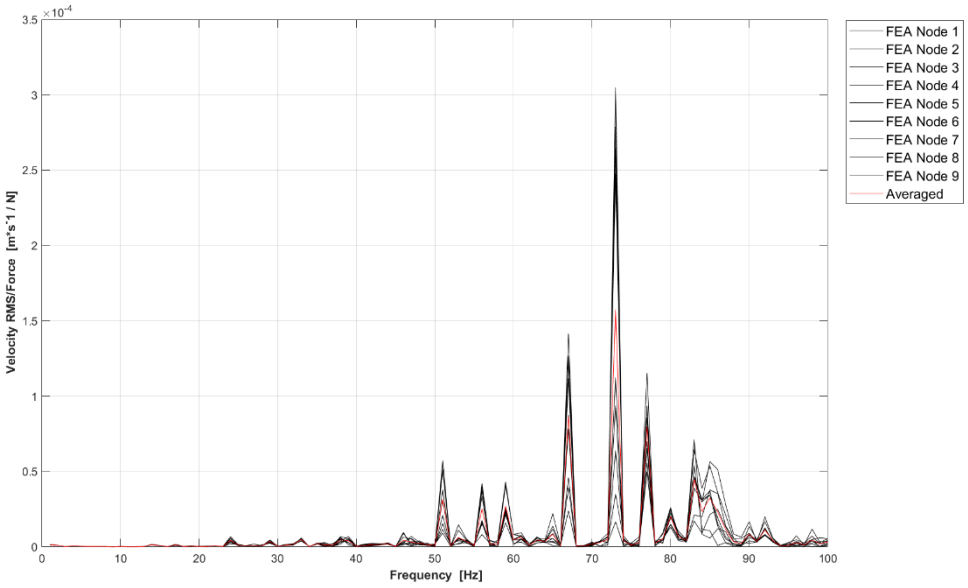

Figure B.23: Mobility - Engine to Wheelhouse Group 2, Point 1

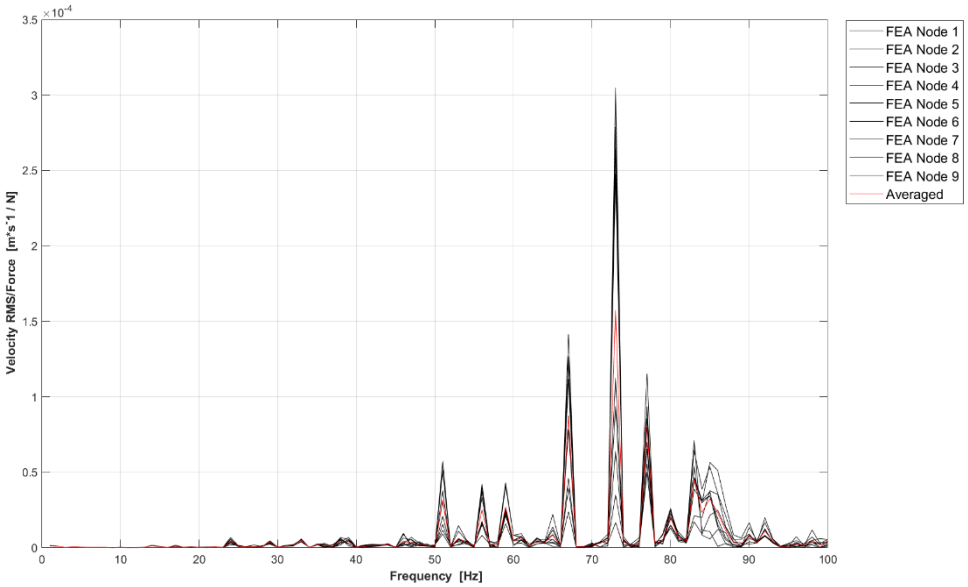

Figure B.24: Mobility - Engine to Wheelhouse Group 2, Point 2

Appendix B.3. Generator Mobility

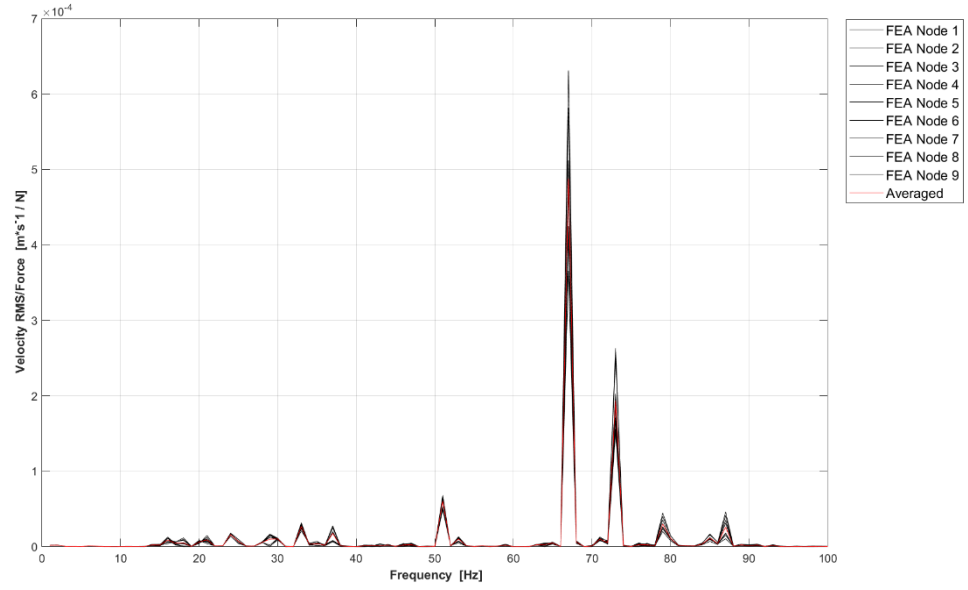

Figure B.25: Mobility - Generator to Bunker Point 1

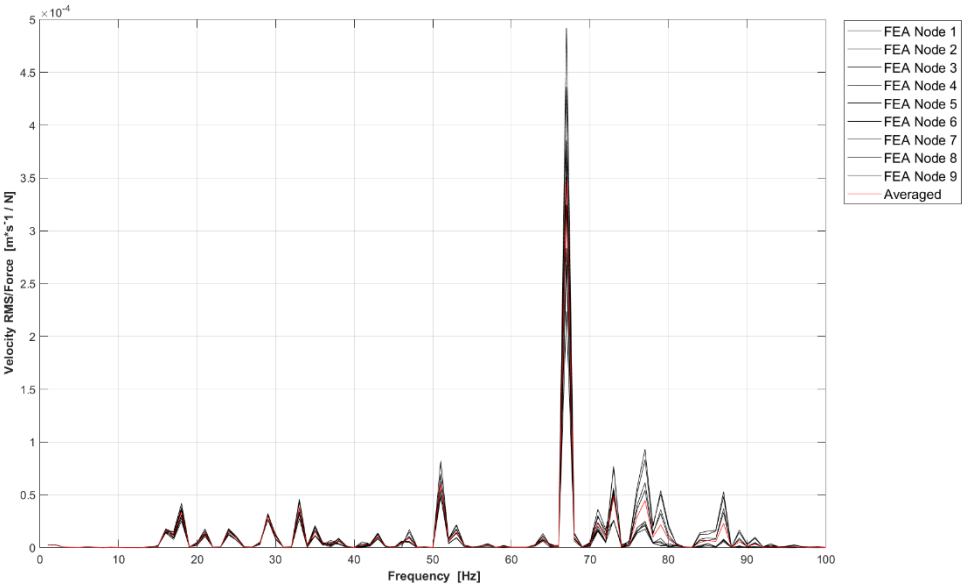

Figure B.26: Mobility - Generator to Bunker Point 2

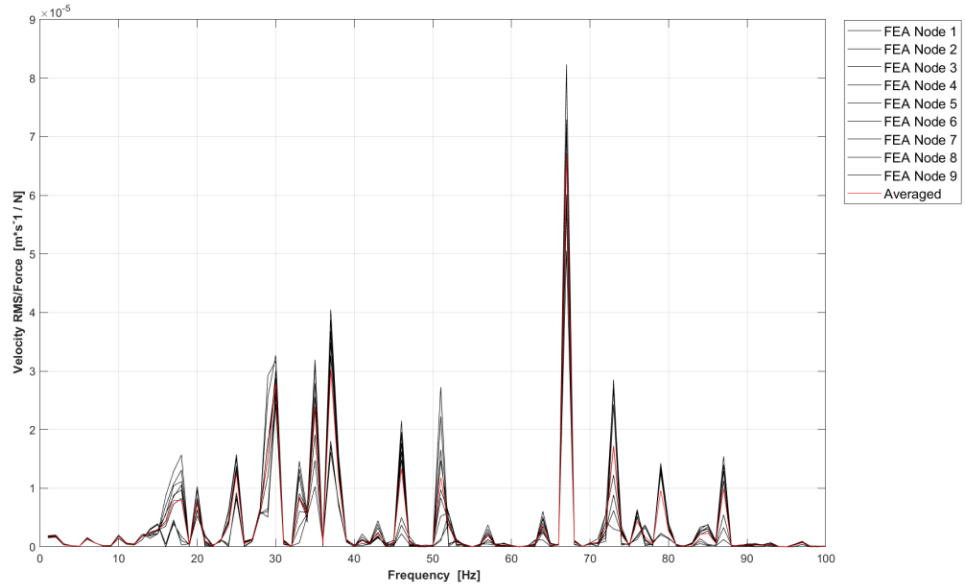

Figure B.27: Mobility - Generator to Cabin Point 1

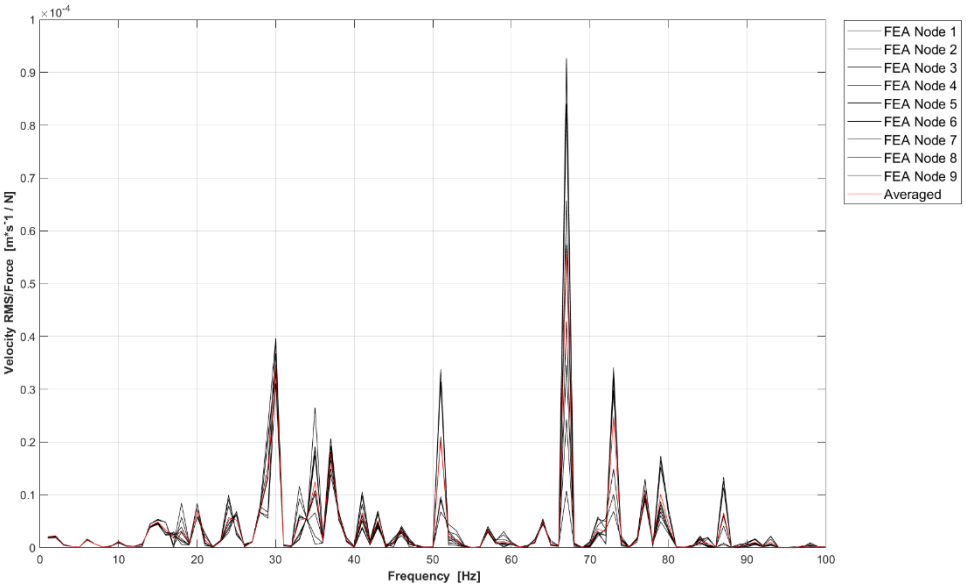

Figure B.28: Mobility - Generator to Cabin Point 2

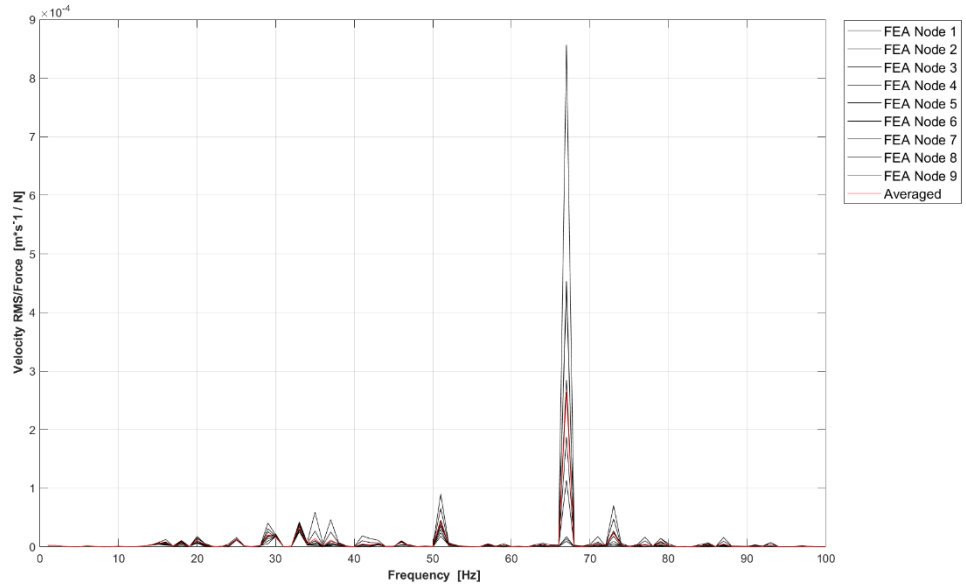

Figure B.29: Mobility - Generator to Canteen Group 1, Point 1

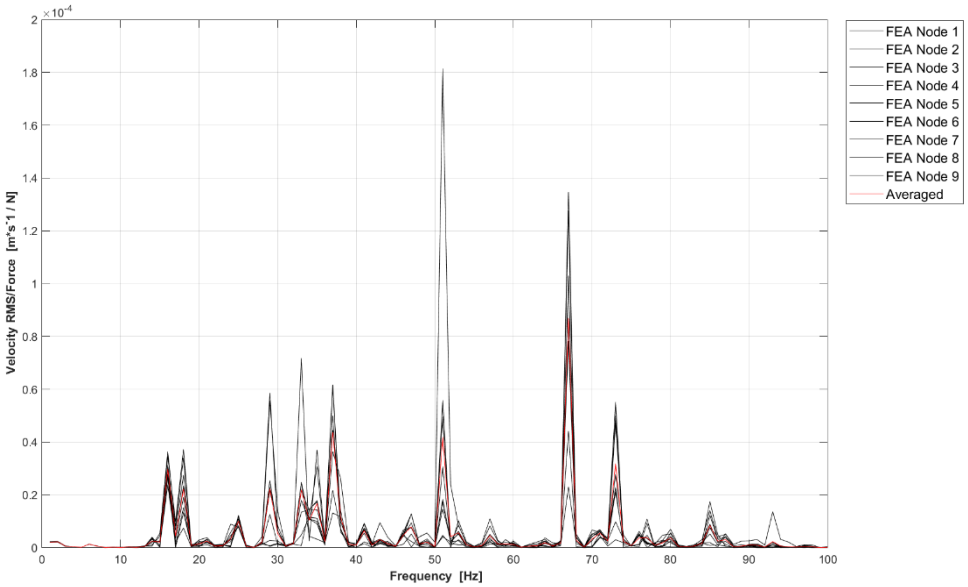

Figure B.30: Mobility - Generator to Canteen Group 1, Point 2

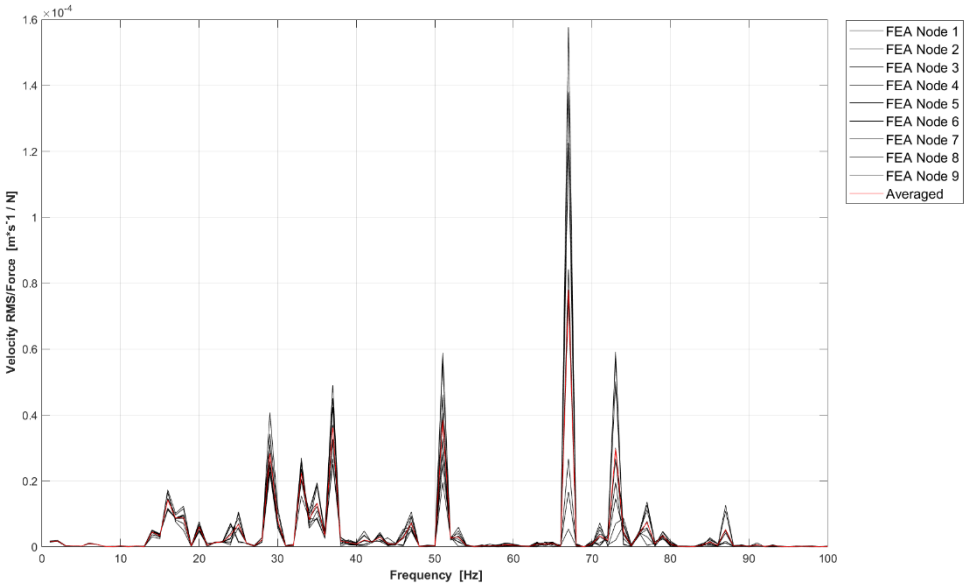

Figure B.31: Mobility - Generator to Canteen Group 2, Point 1

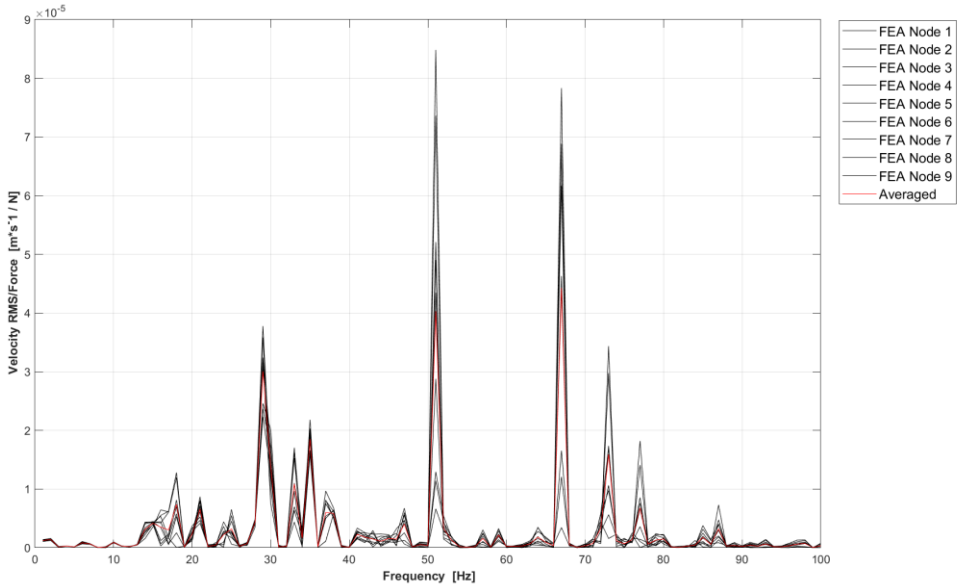

Figure B.32: Mobility - Generator to Canteen Group 2, Point 2

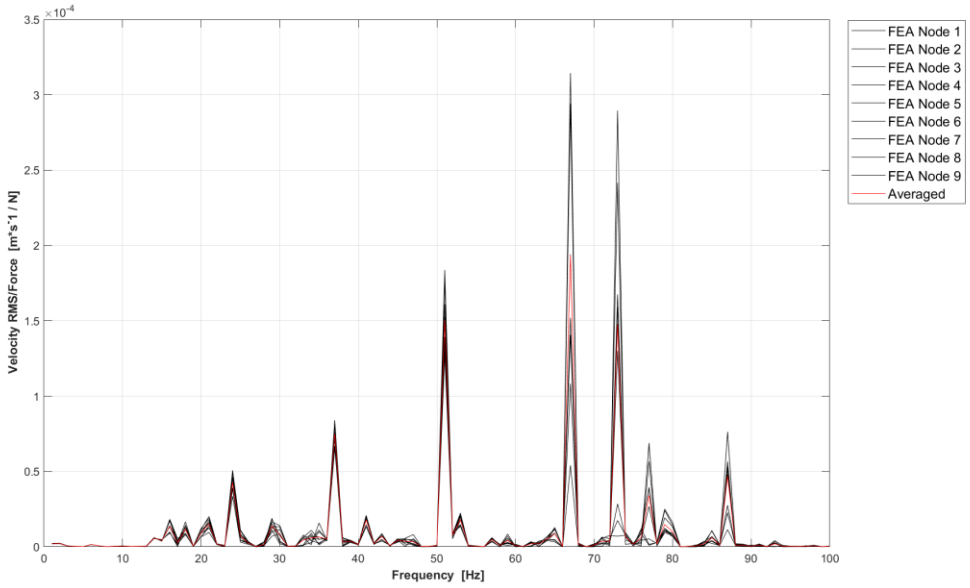

Figure B.33: Mobility - Generator to Wheelhouse Group 1, Point 1

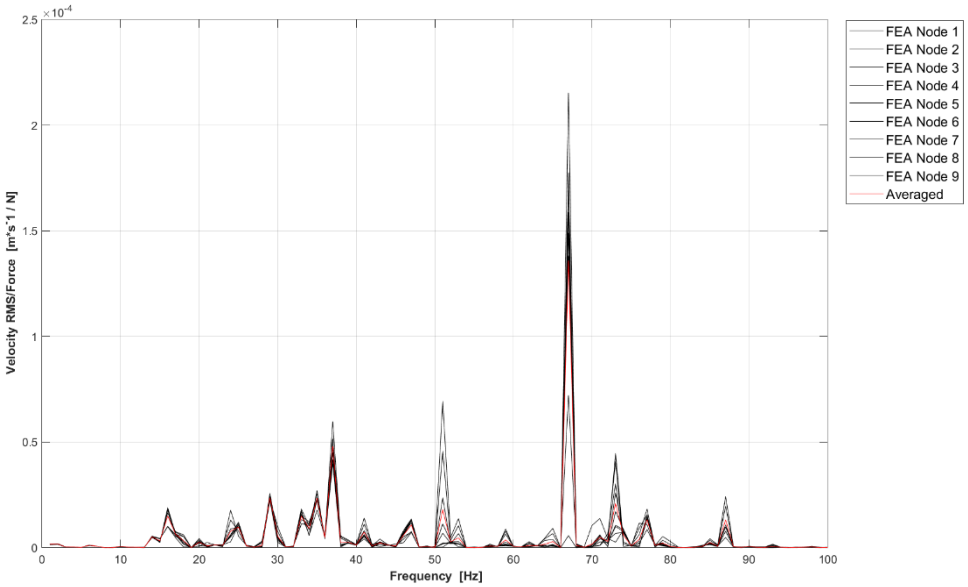

Figure B.34: Mobility - Generator to Wheelhouse Group 1, Point 2

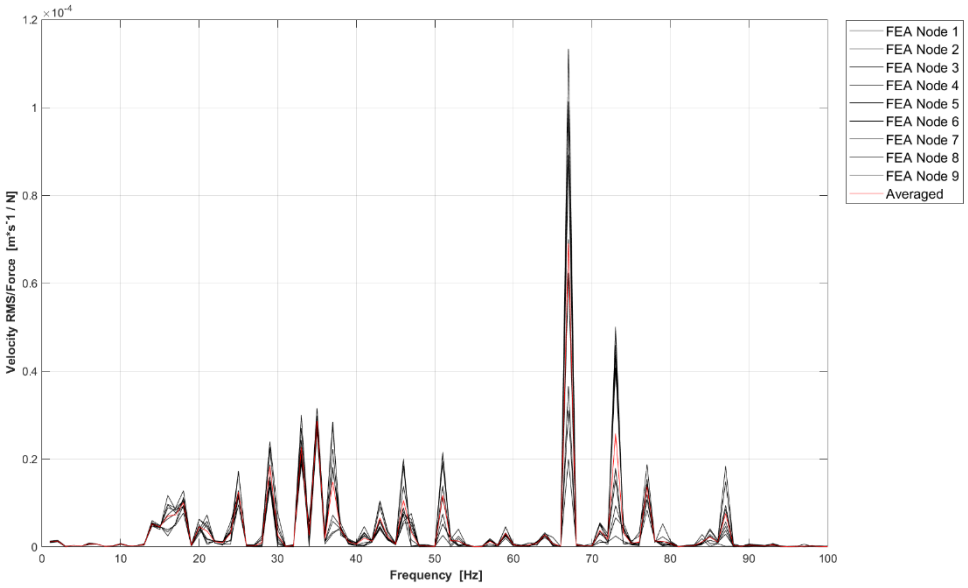

Figure B.35: Mobility - Generator to Wheelhouse Group 2, Point 1

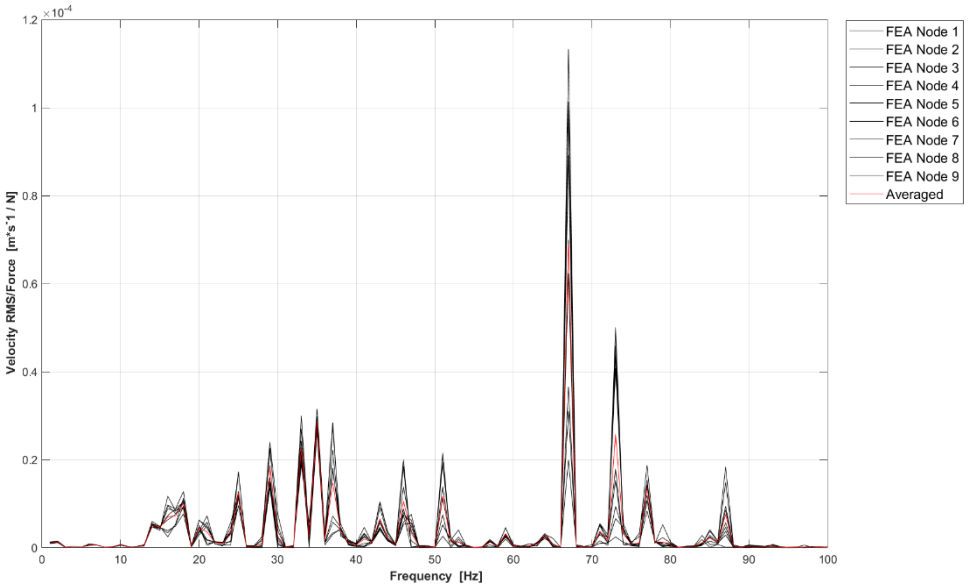

Figure B.36: Mobility - Generator to Wheelhouse Group 2, Point 2

Appendix C: Damping Determination Analysis

Appendix C.1. Engine Damping Determination

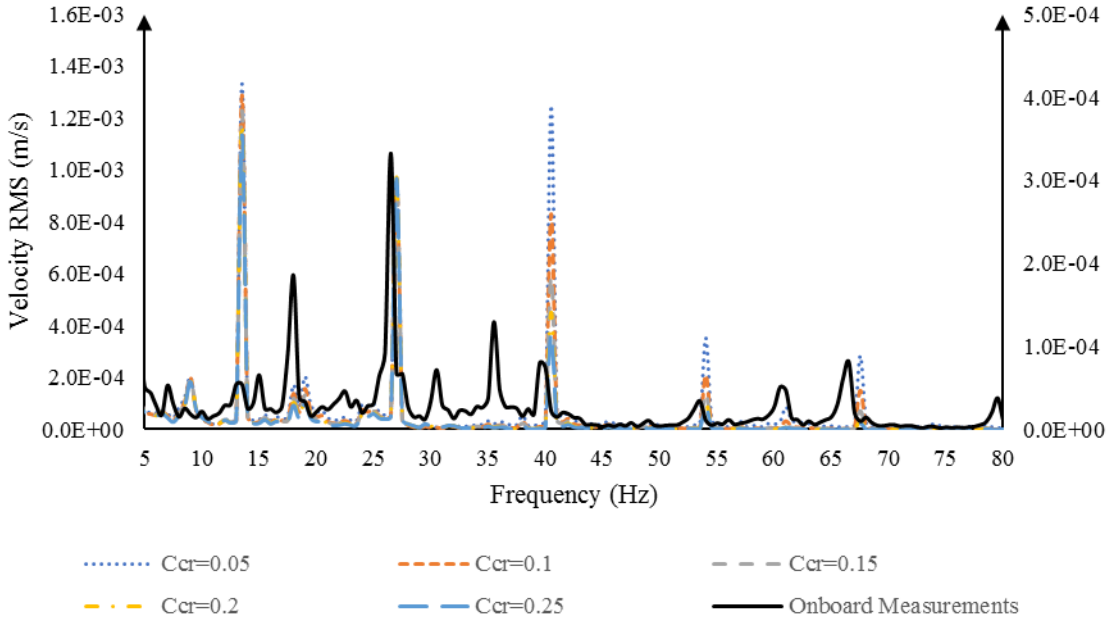

Figure C.1: Onboard Measurements against Finite Element with Varying Damping (Engine Excitation) - Wheelhouse G1 P1

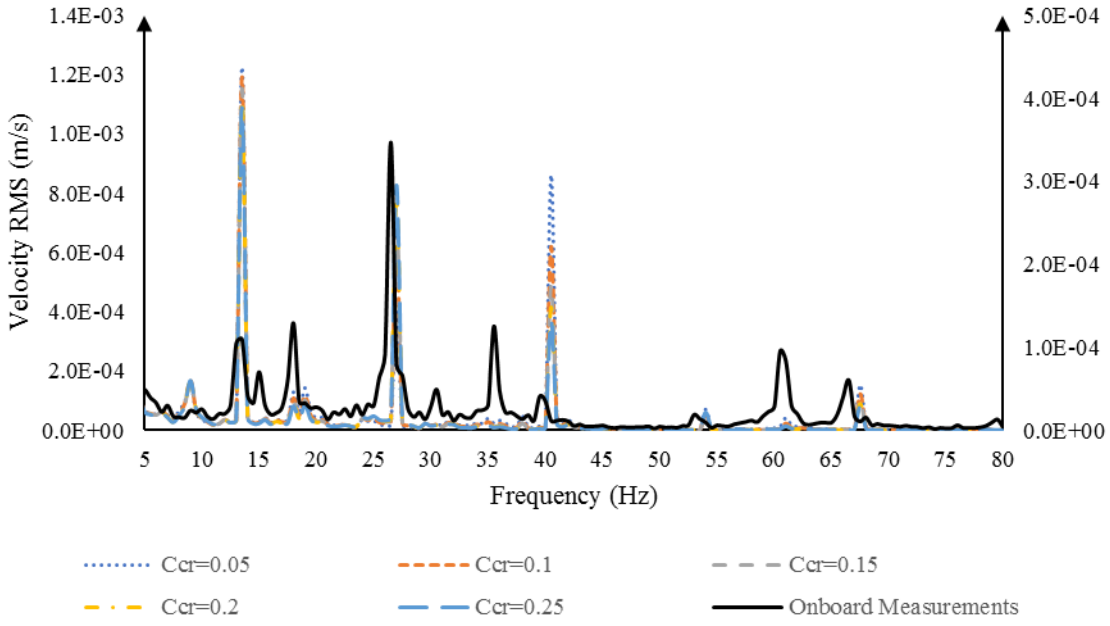

Figure C.2: Onboard Measurements against Finite Element with Varying Damping (Engine Excitation) - Wheelhouse G1 P2

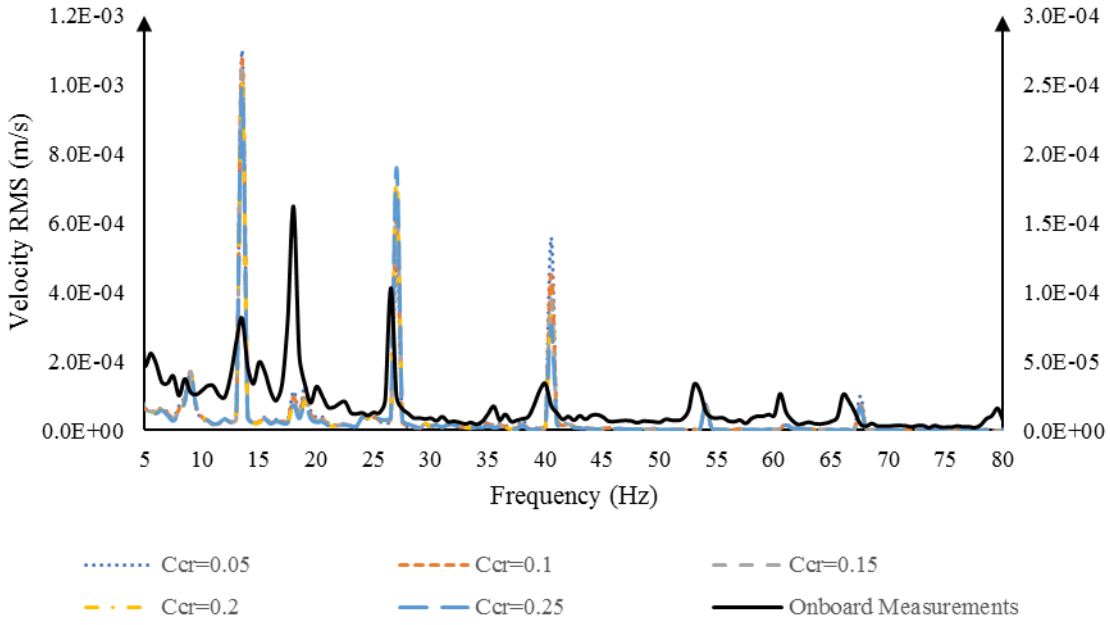

Figure C.3: Onboard Measurements against Finite Element with Varying Damping (Engine Excitation) - Wheelhouse G2 P1

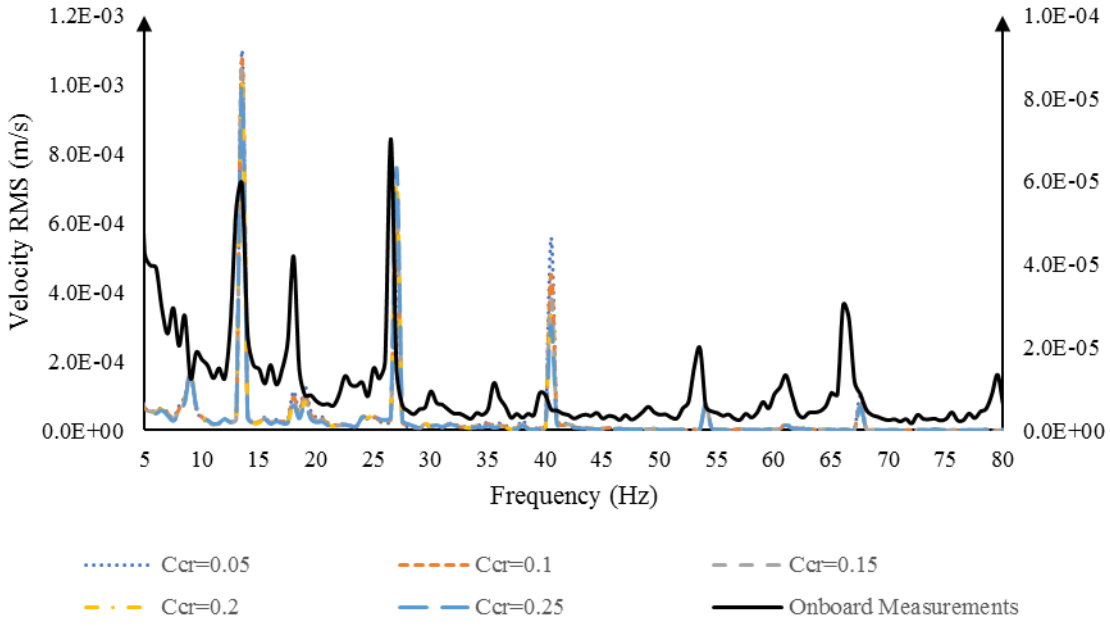

Figure C.4: Onboard Measurements against Finite Element with Varying Damping (Engine Excitation) - Wheelhouse G2 P2

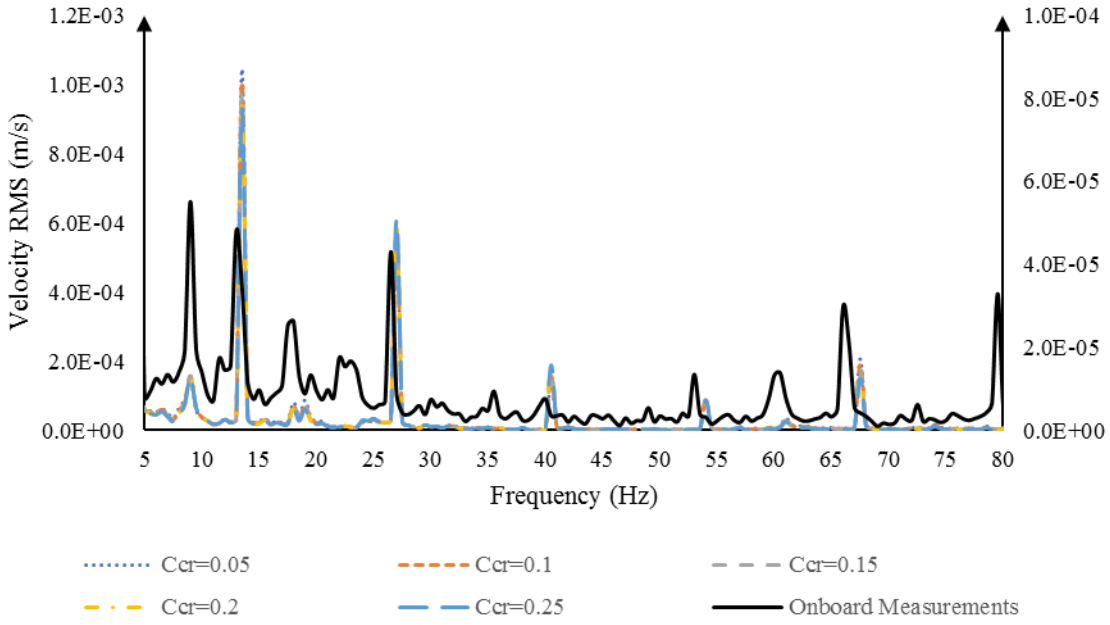

Figure C.5: Onboard Measurements against Finite Element with Varying Damping (Engine Excitation) - Canteen G1 P1

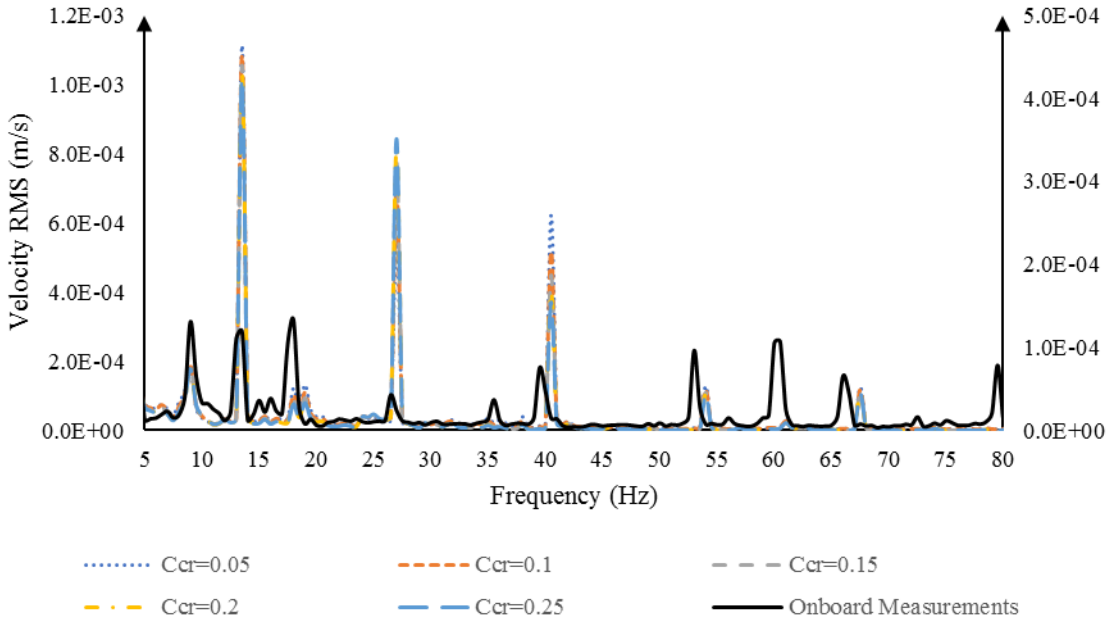

Figure C.6: Onboard Measurements against Finite Element with Varying Damping (Engine Excitation) - Canteen G1 P2

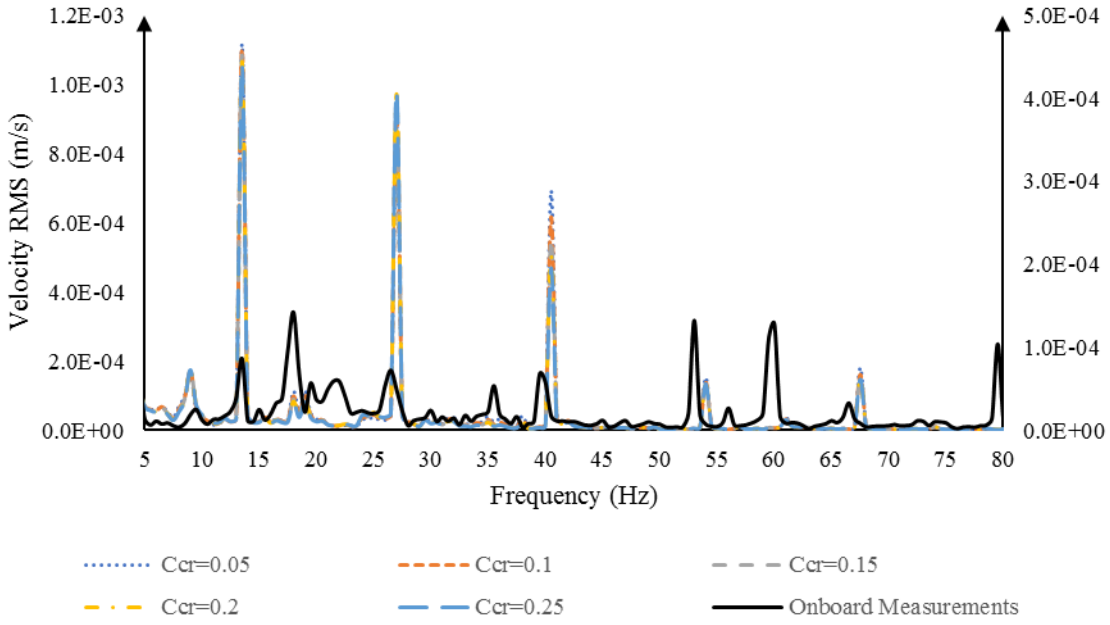

Figure C.7: Onboard Measurements against Finite Element with Varying Damping (Engine Excitation) - Canteen G2 P1

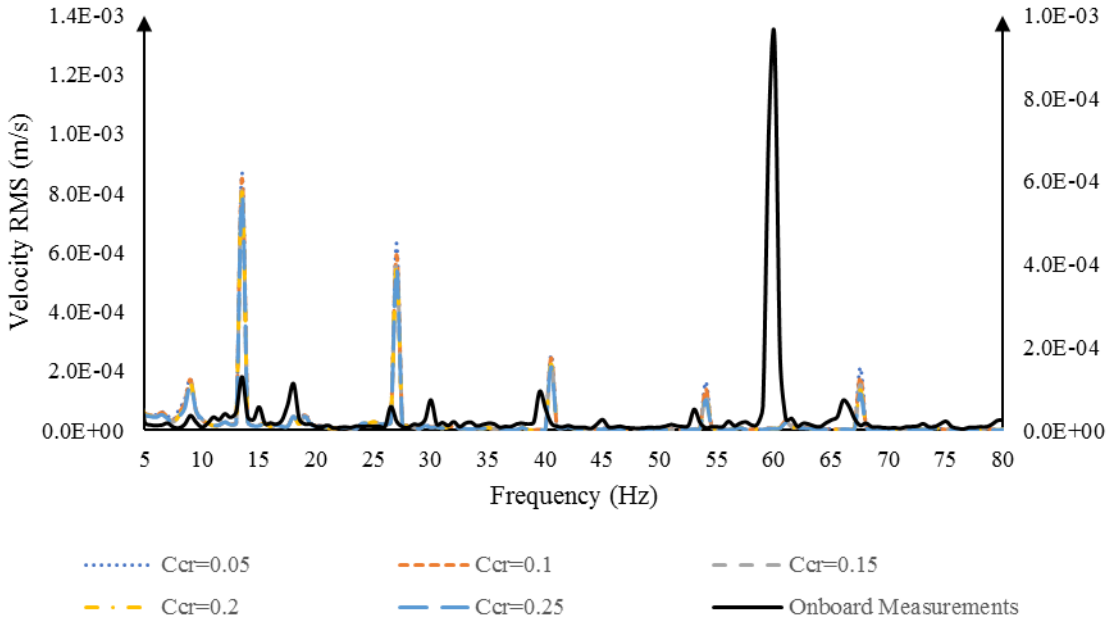

Figure C.8: Onboard Measurements against Finite Element with Varying Damping (Engine Excitation) - Canteen G2 P2

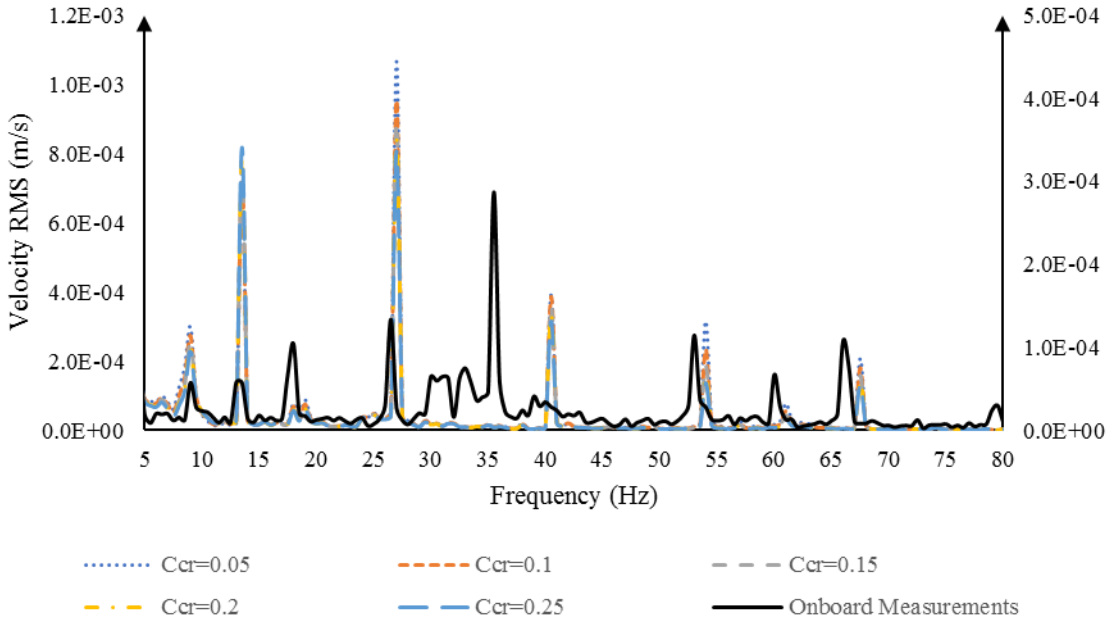

Figure C.9: Onboard Measurements against Finite Element with Varying Damping (Engine Excitation) - Bunker P1

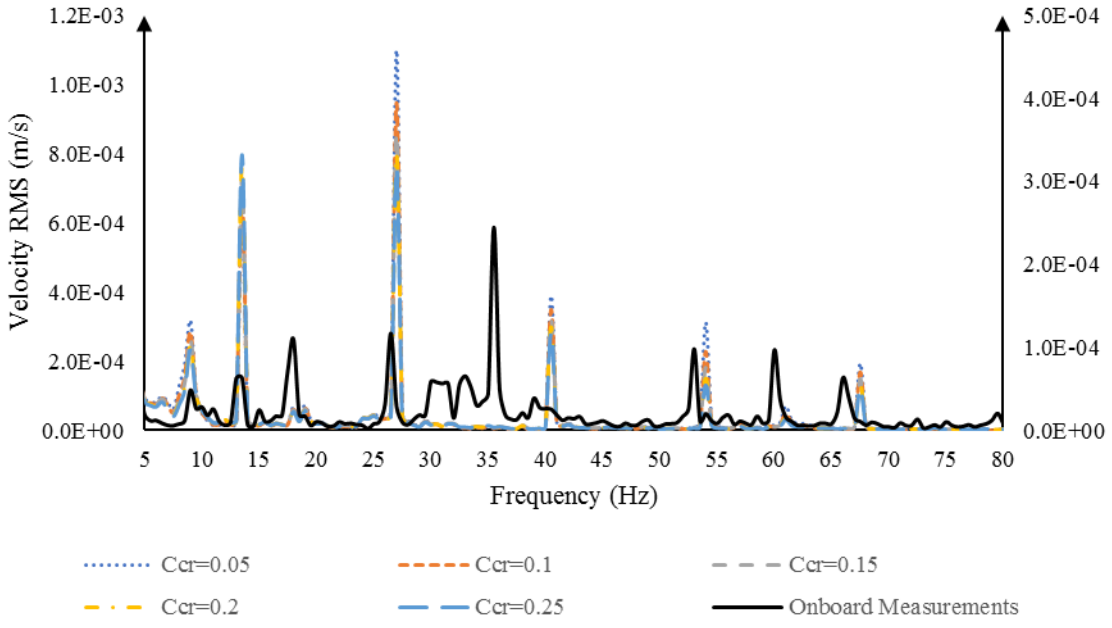

Figure C.10: Onboard Measurements against Finite Element with Varying Damping (Engine Excitation) - Bunker P2

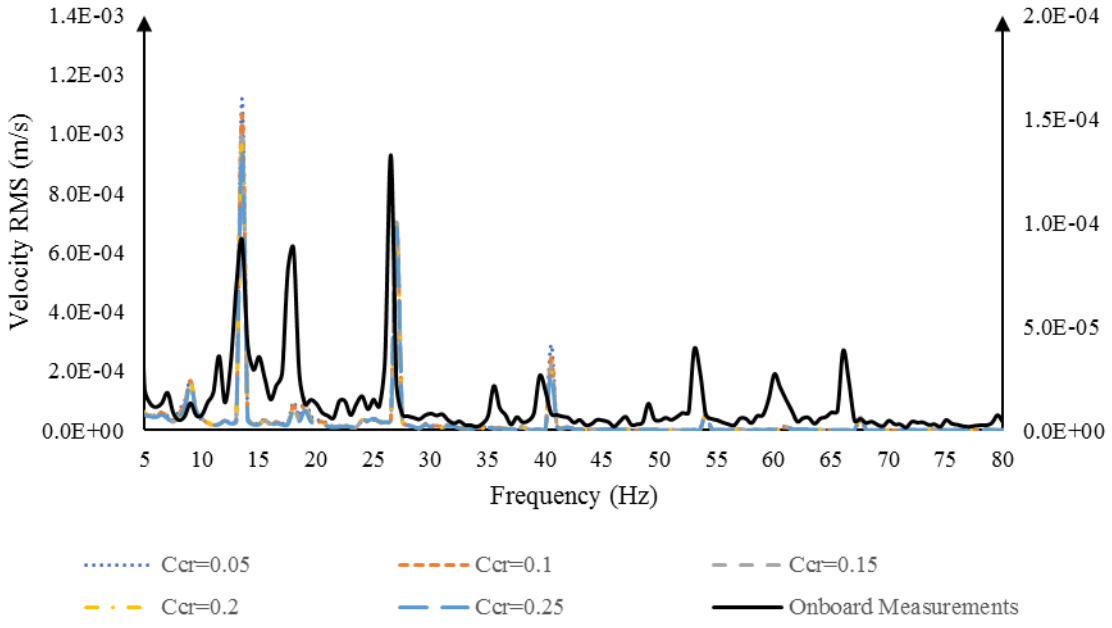

Figure C.11: Onboard Measurements against Finite Element with Varying Damping (Engine Excitation) - Cabin P1

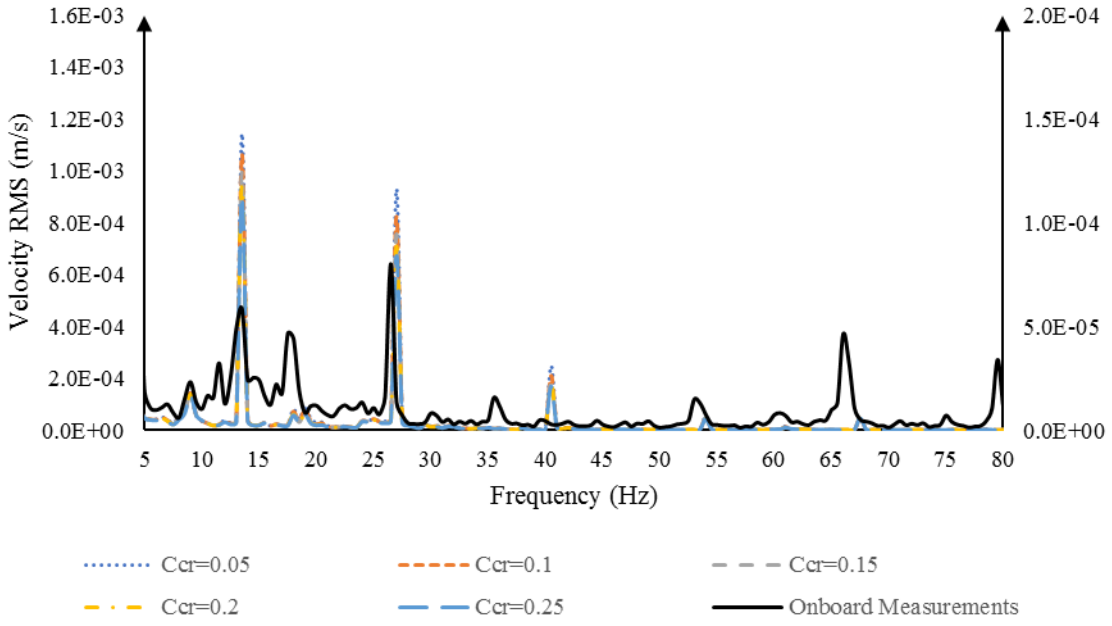

Figure C.12: Onboard Measurements against Finite Element with Varying Damping (Engine Excitation) - Cabin P2

Appendix C.2. Generator Damping Determination

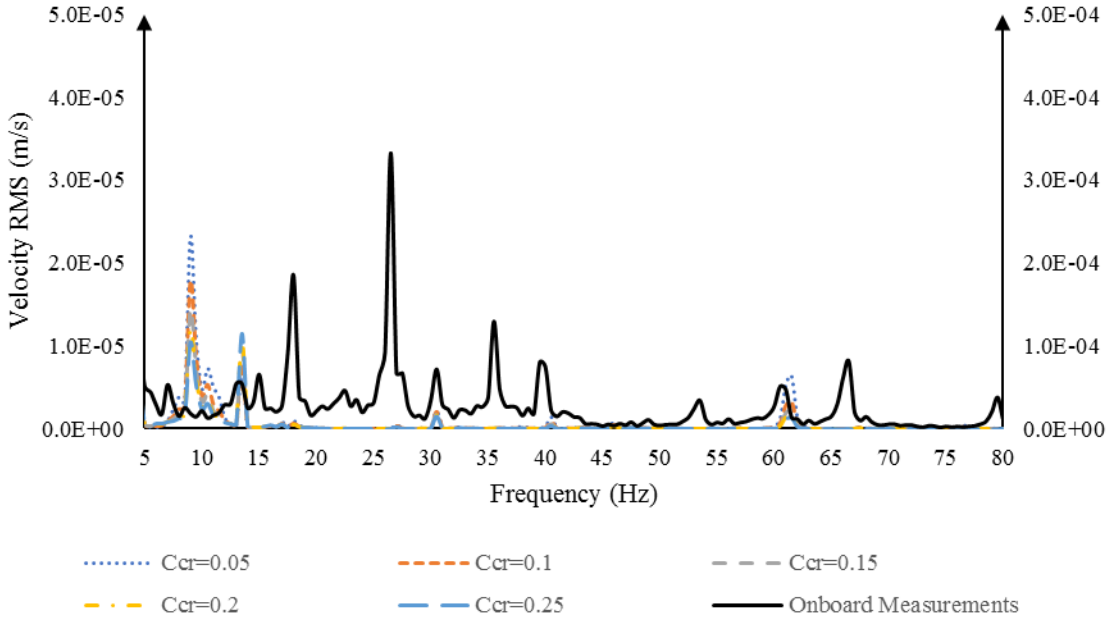

Figure C.13: Onboard Measurements against Finite Element with Varying Damping (Generator Excitation) - Wheelhouse G1 P1

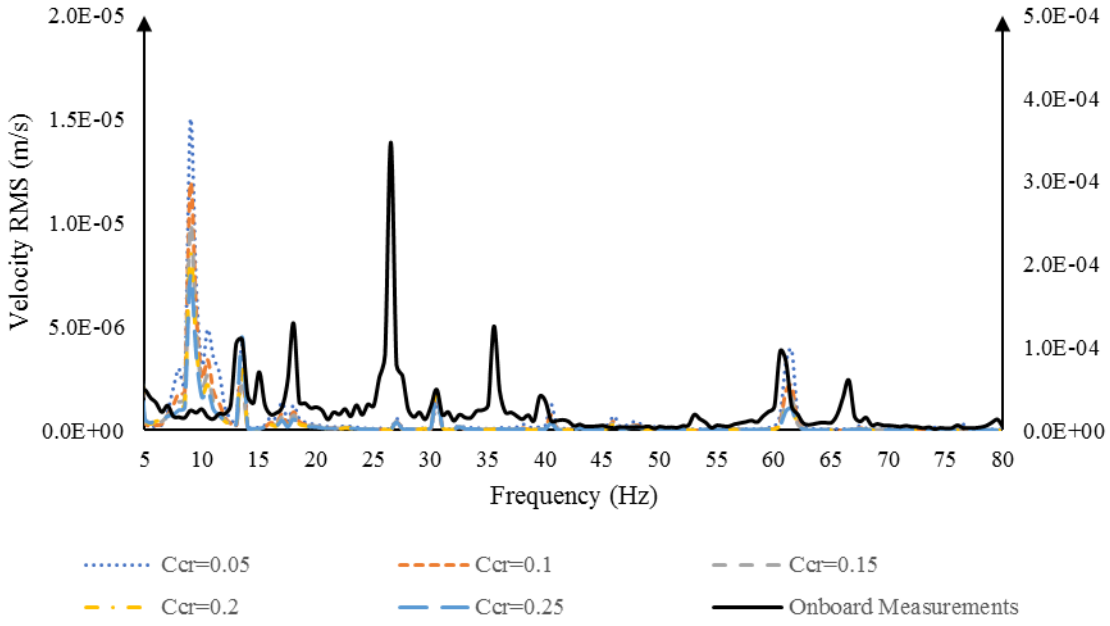

Figure C.14: Onboard Measurements against Finite Element with Varying Damping (Generator Excitation) - Wheelhouse G1 P2

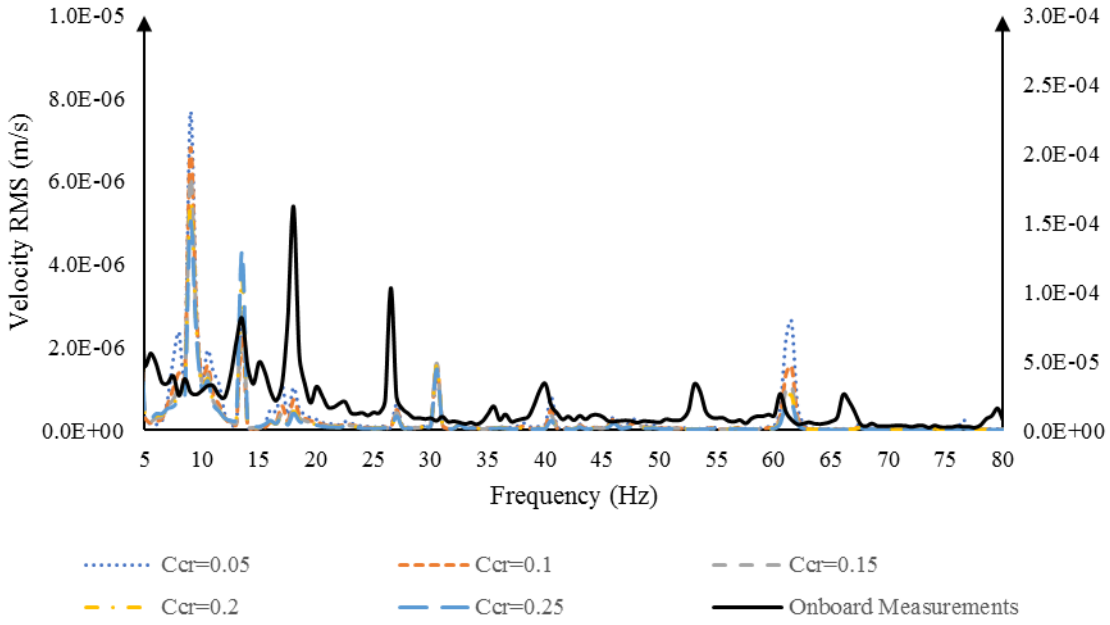

Figure C.15: Onboard Measurements against Finite Element with Varying Damping (Generator Excitation) - Wheelhouse G2 P1

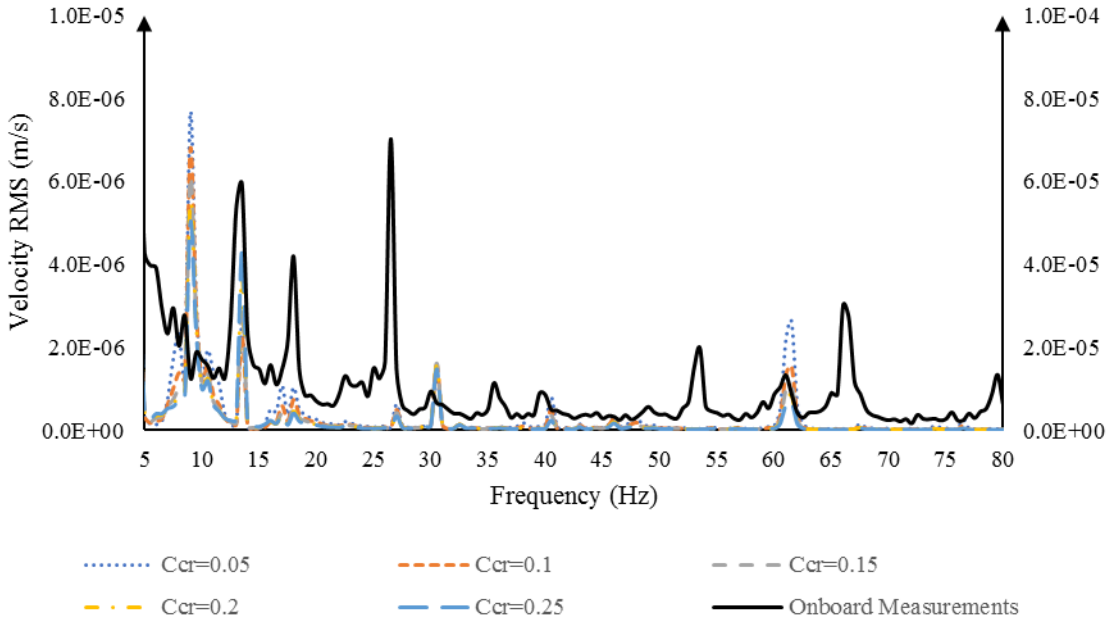

Figure C.16: Onboard Measurements against Finite Element with Varying Damping (Generator Excitation) - Wheelhouse G2 P2

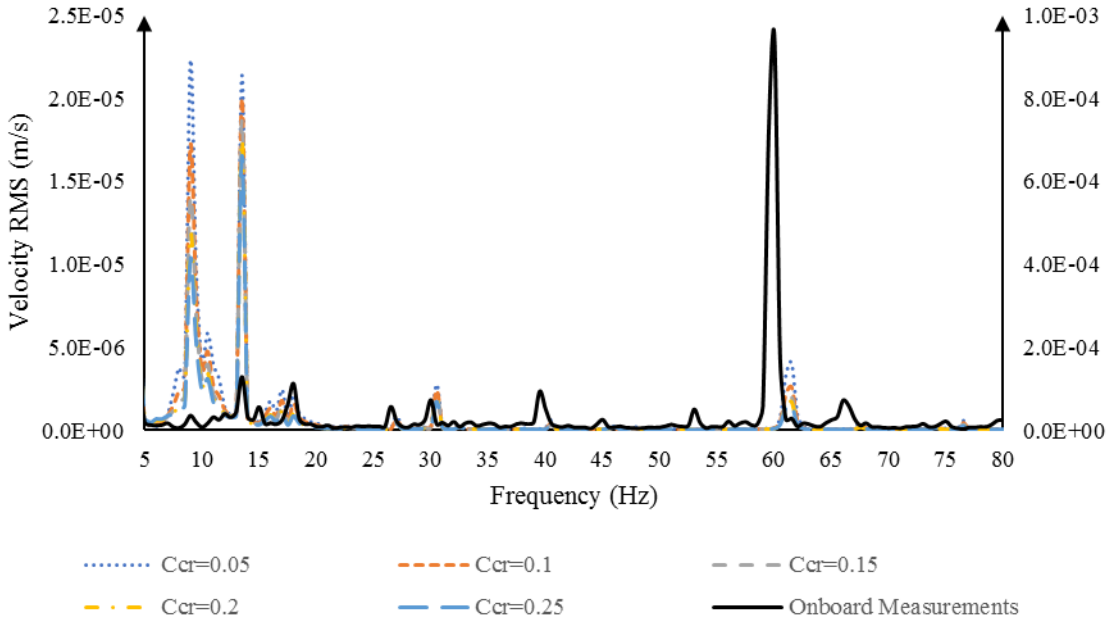

Figure C.17: Onboard Measurements against Finite Element with Varying Damping (Generator Excitation) - Canteen G1 P1

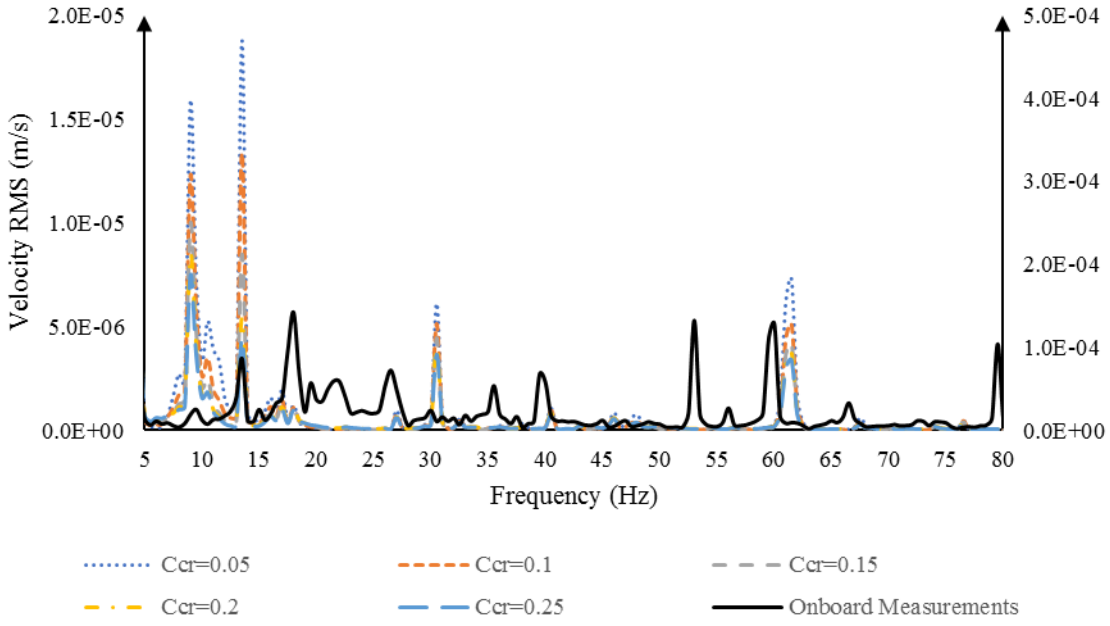

Figure C.18: Onboard Measurements against Finite Element with Varying Damping (Generator Excitation) - Canteen G1 P2

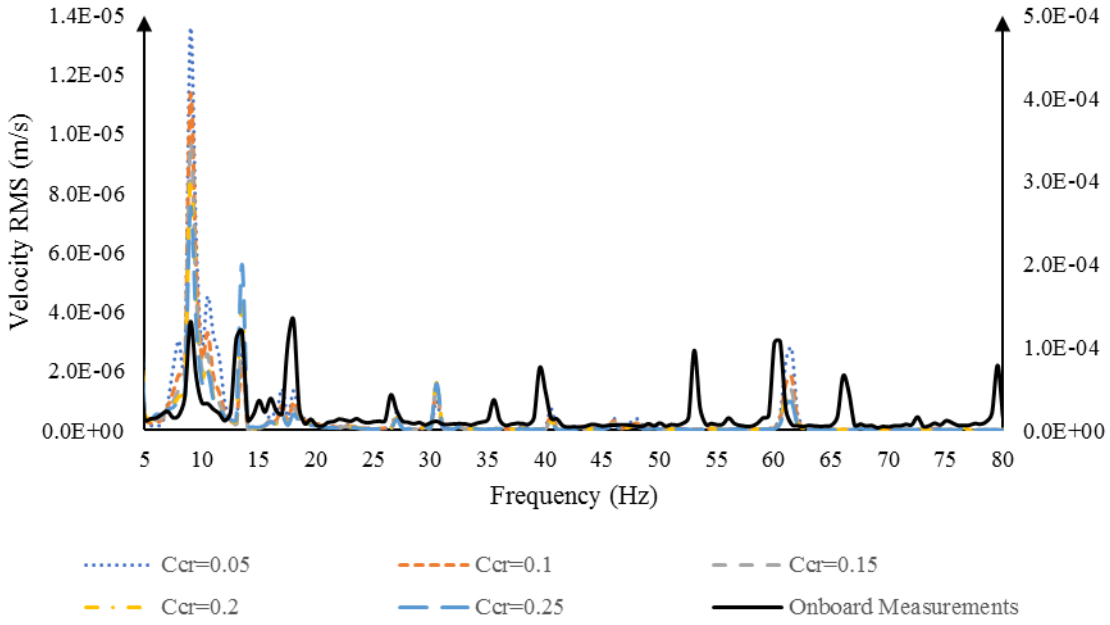

Figure C.19: Onboard Measurements against Finite Element with Varying Damping (Generator Excitation) - Canteen G2 P1

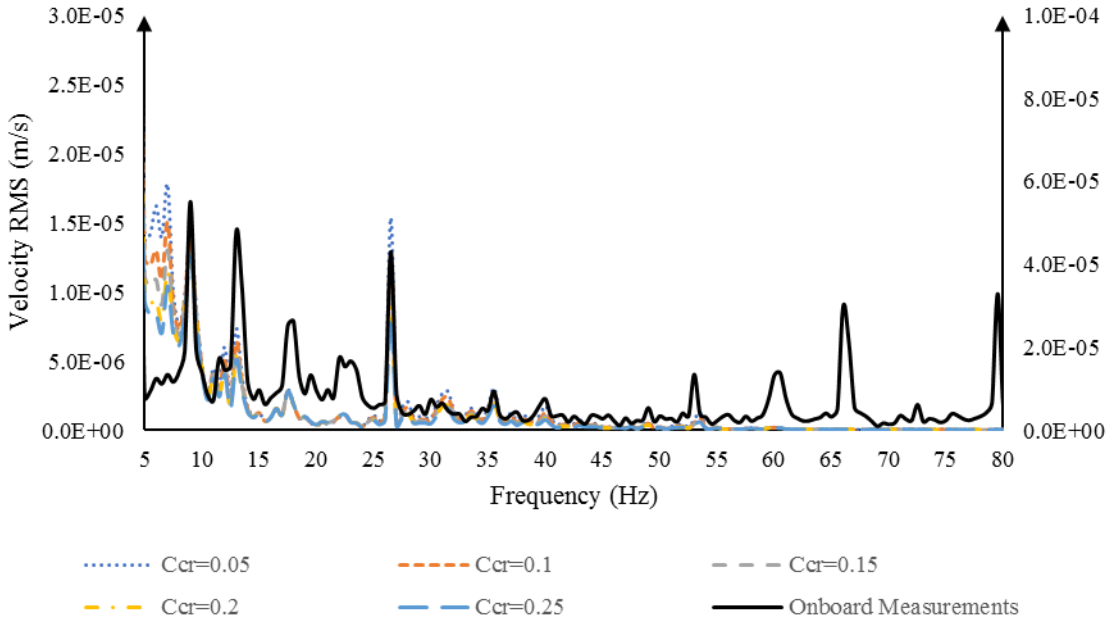

Figure C.20: Onboard Measurements against Finite Element with Varying Damping (Generator Excitation) - Canteen G2 P2

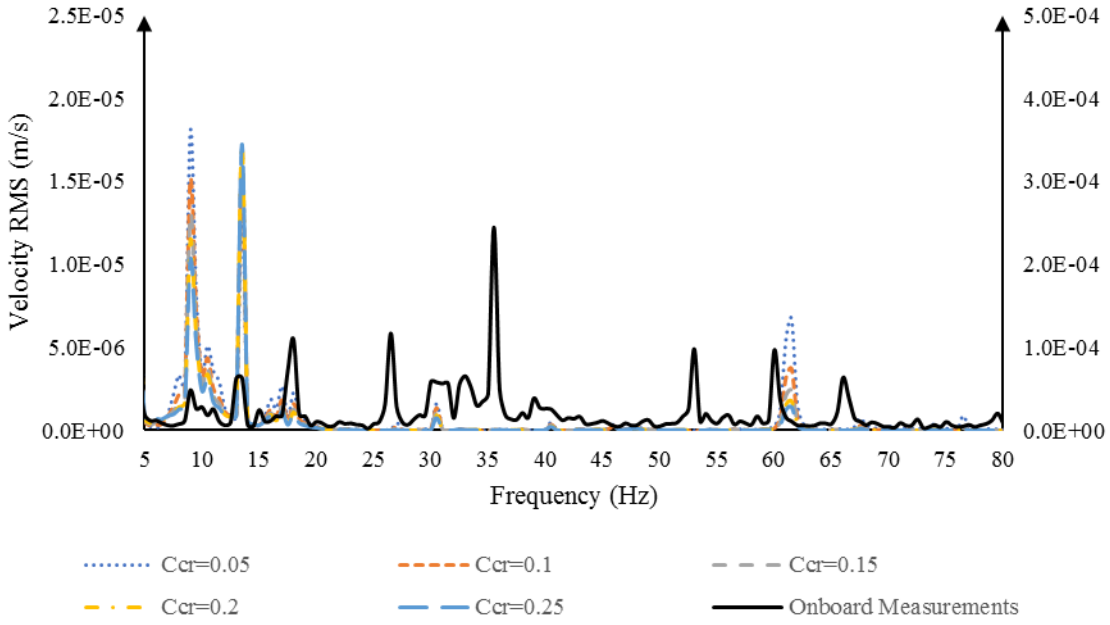

Figure C.21: Onboard Measurements against Finite Element with Varying Damping (Generator Excitation) - Bunker P1

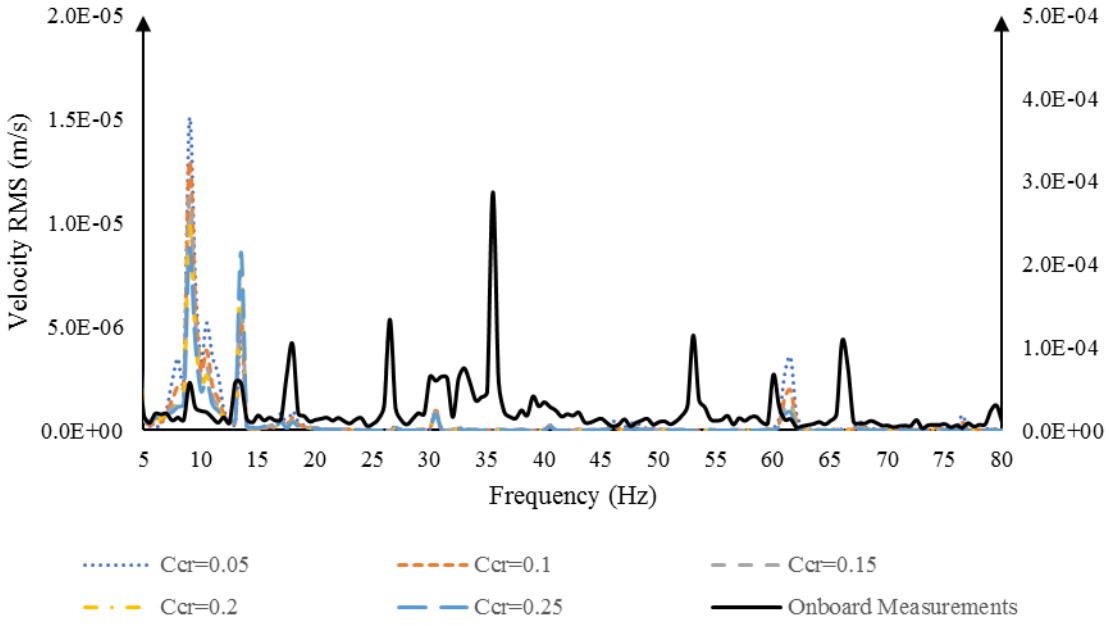

Figure C.22: Onboard Measurements against Finite Element with Varying Damping (Generator Excitation) - Bunker P2

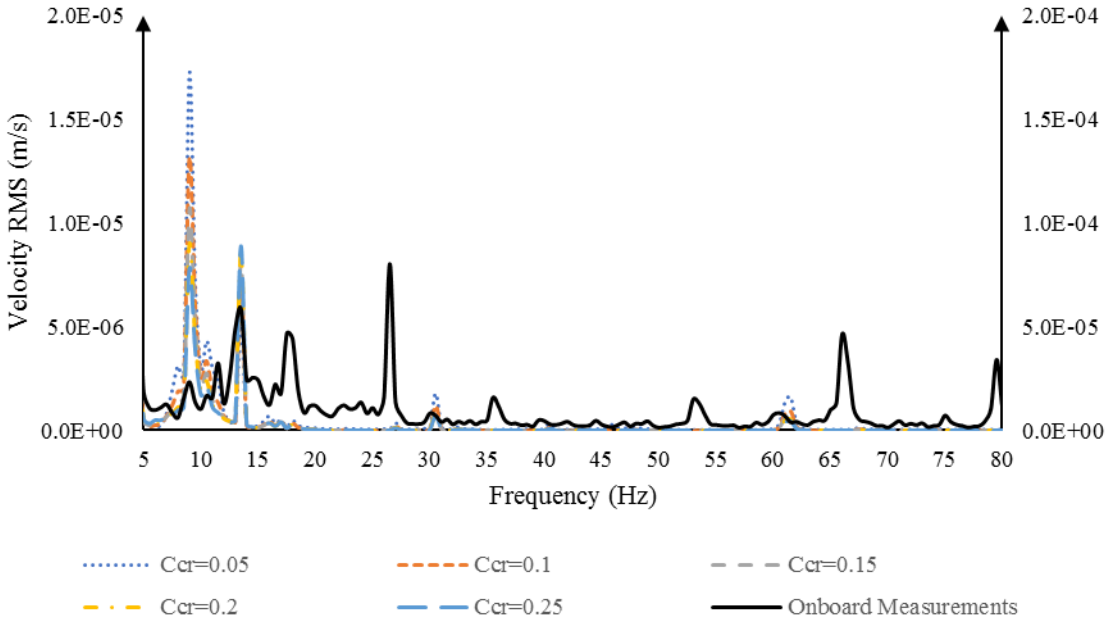

Figure C.23: Onboard Measurements against Finite Element with Varying Damping (Generator Excitation) - Cabin P1

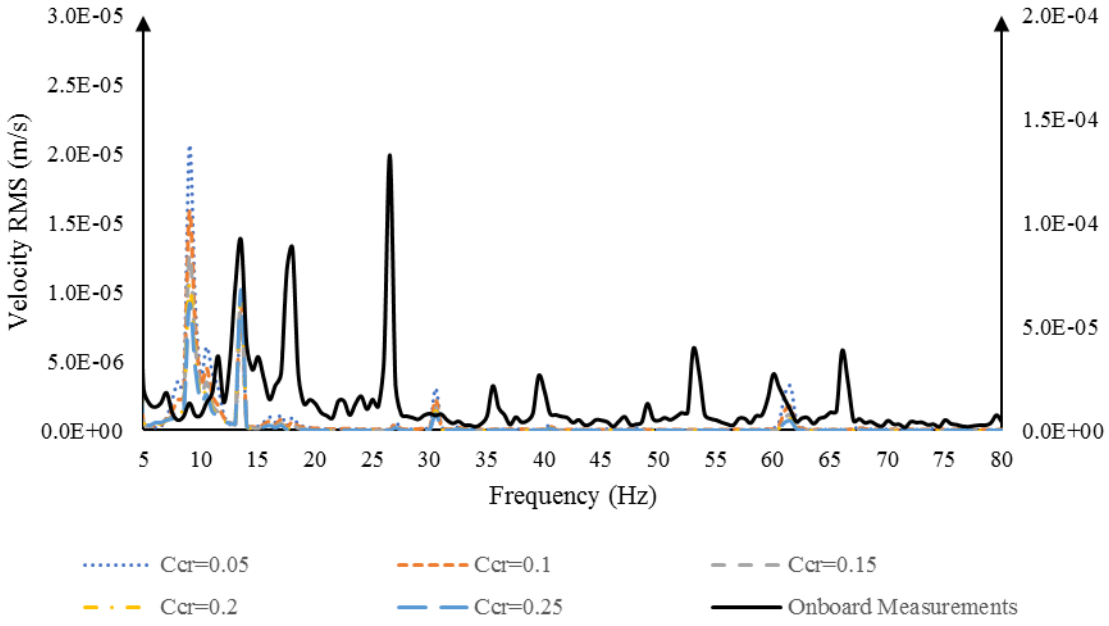

Figure C.24: Onboard Measurements against Finite Element with Varying Damping (Generator Excitation) - Cabin P2

Appendix C.3. Propeller Damping Determination

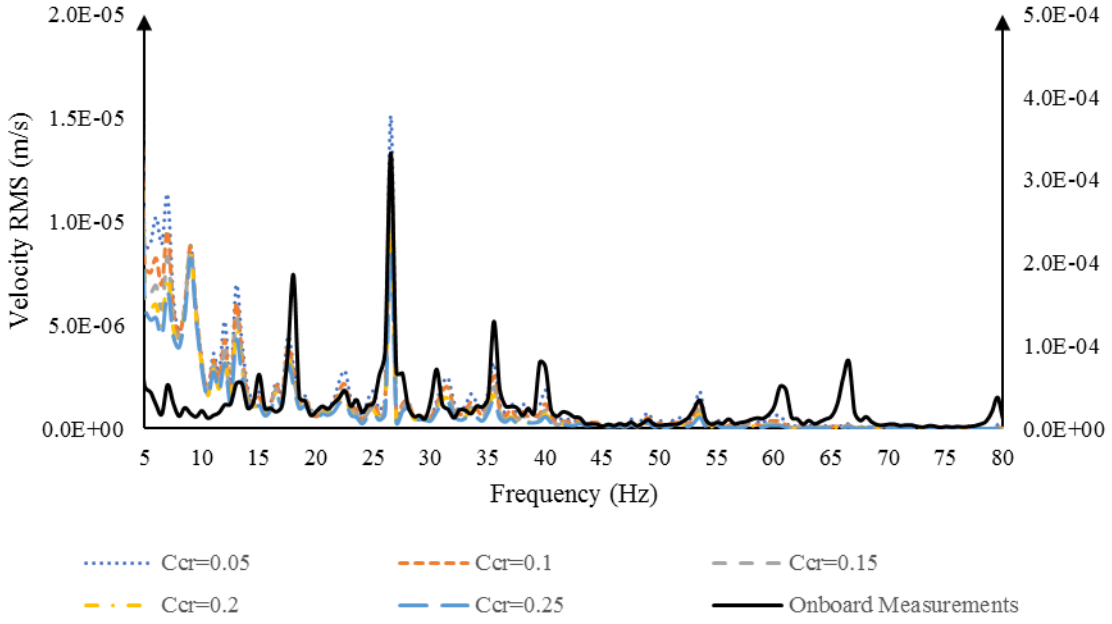

Figure C.25: Onboard Measurements against Finite Element with Varying Damping (Propeller Excitation) - Wheelhouse G1 P1

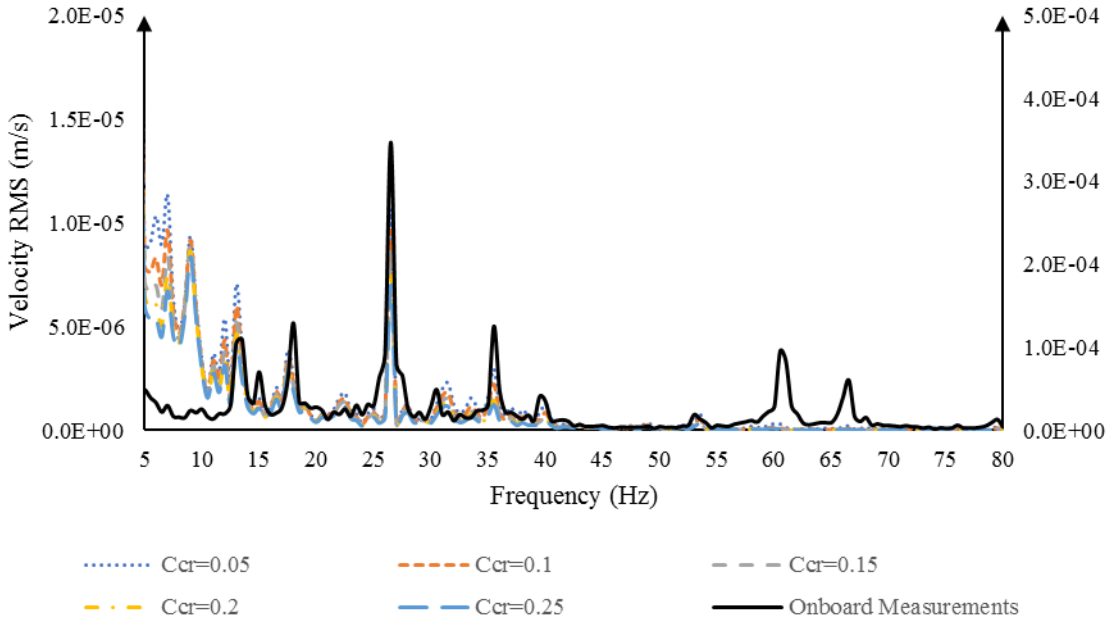

Figure C.26: Onboard Measurements against Finite Element with Varying Damping (Propeller Excitation) - Wheelhouse G1 P2

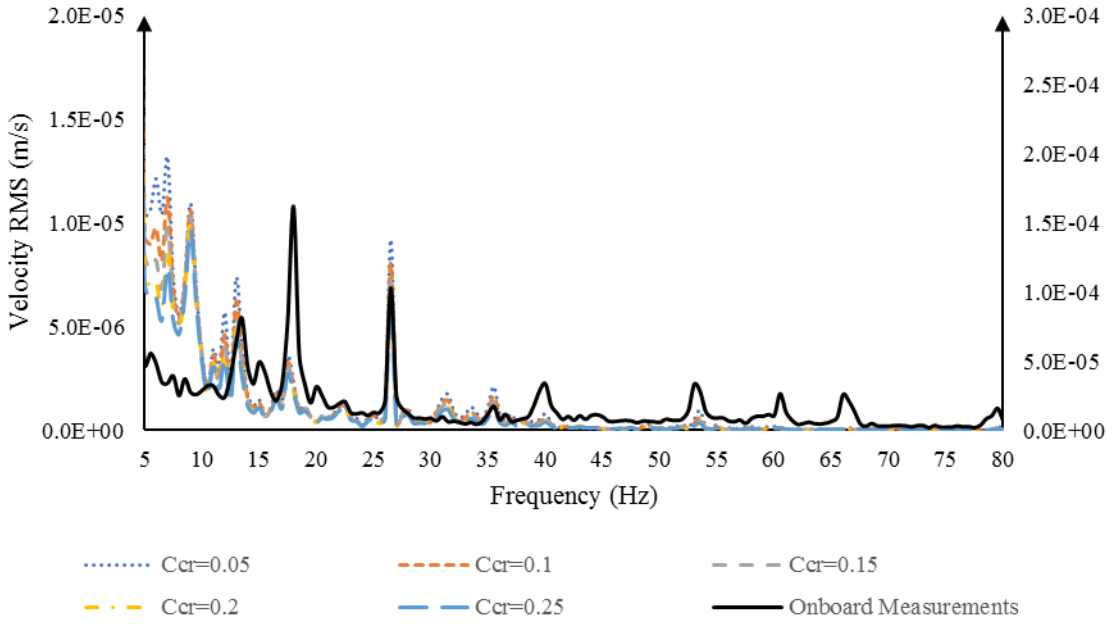

Figure C.27: Onboard Measurements against Finite Element with Varying Damping (Propeller Excitation) - Wheelhouse G2 P1

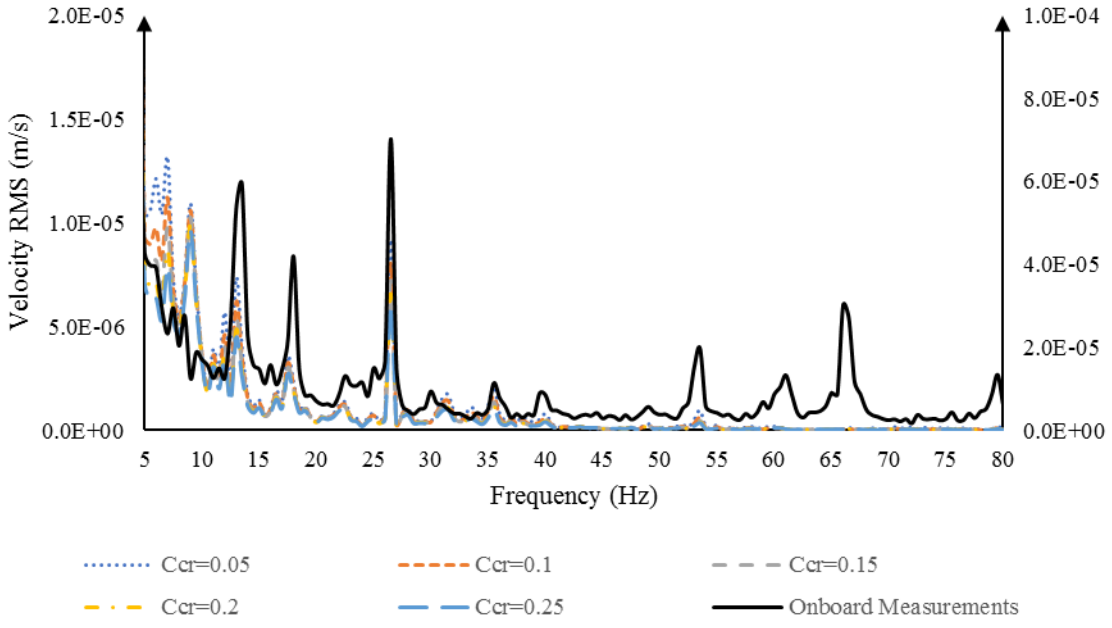

Figure C.28: Onboard Measurements against Finite Element with Varying Damping (Propeller Excitation) - Wheelhouse G2 P2

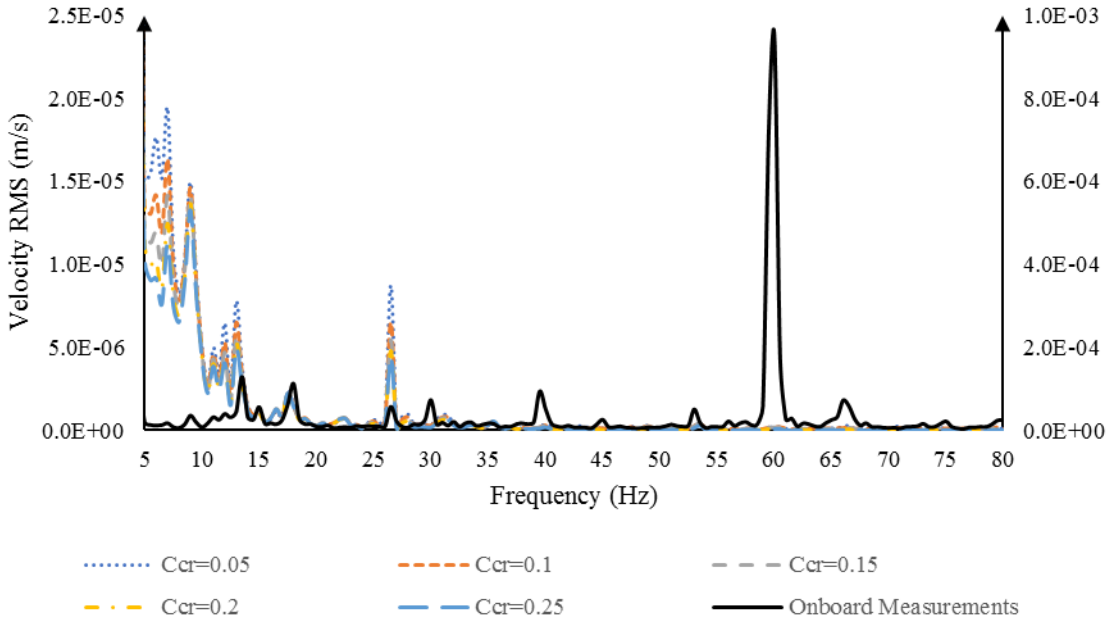

Figure C.29: Onboard Measurements against Finite Element with Varying Damping (Propeller Excitation) - Canteen G1 P1

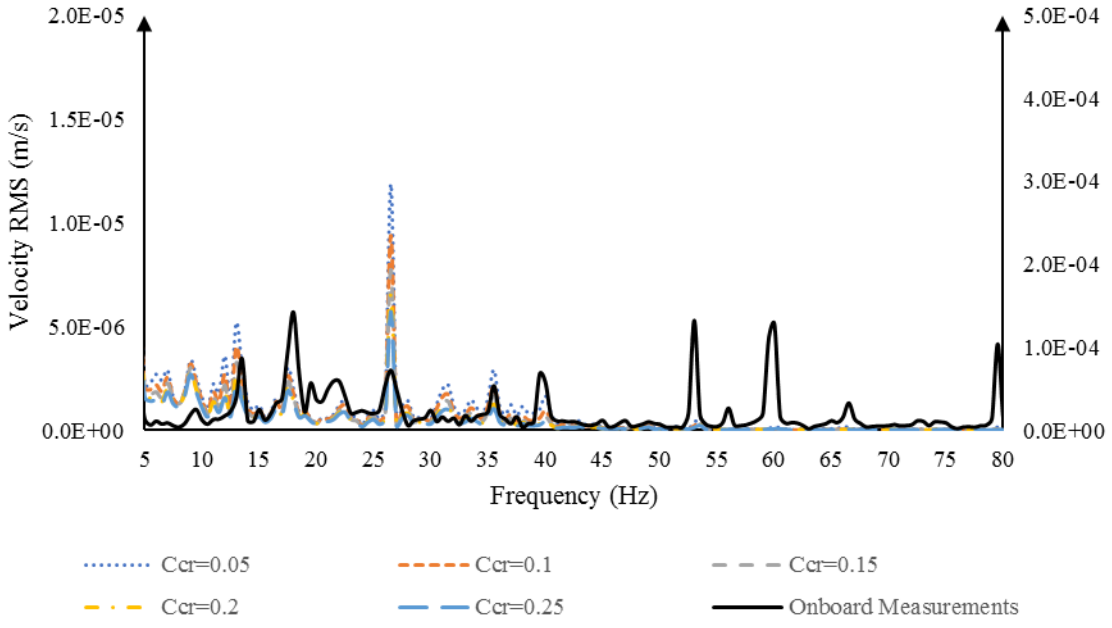

Figure C.30: Onboard Measurements against Finite Element with Varying Damping (Propeller Excitation) - Canteen G1 P2

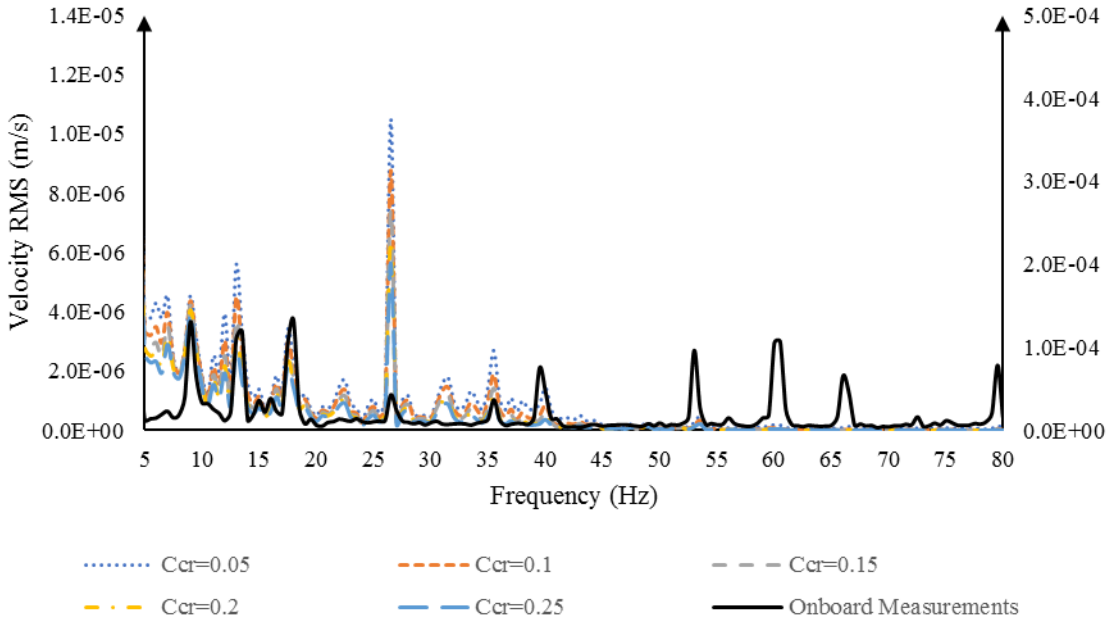

Figure C.31: Onboard Measurements against Finite Element with Varying Damping (Propeller Excitation) - Canteen G2 P1

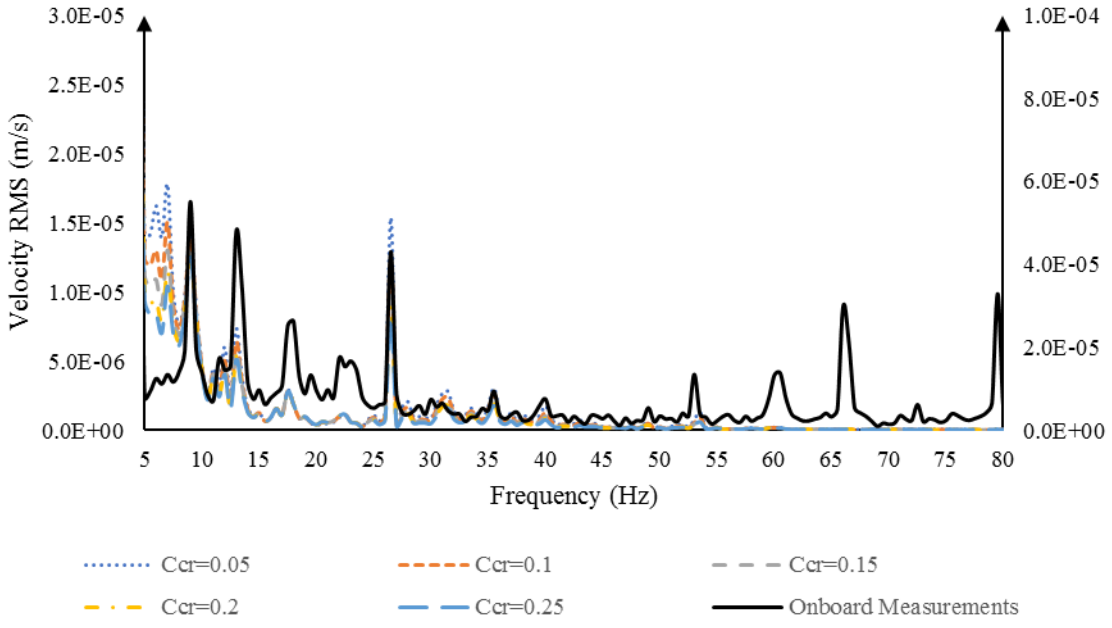

Figure C.32: Onboard Measurements against Finite Element with Varying Damping (Propeller Excitation) - Canteen G2 P2

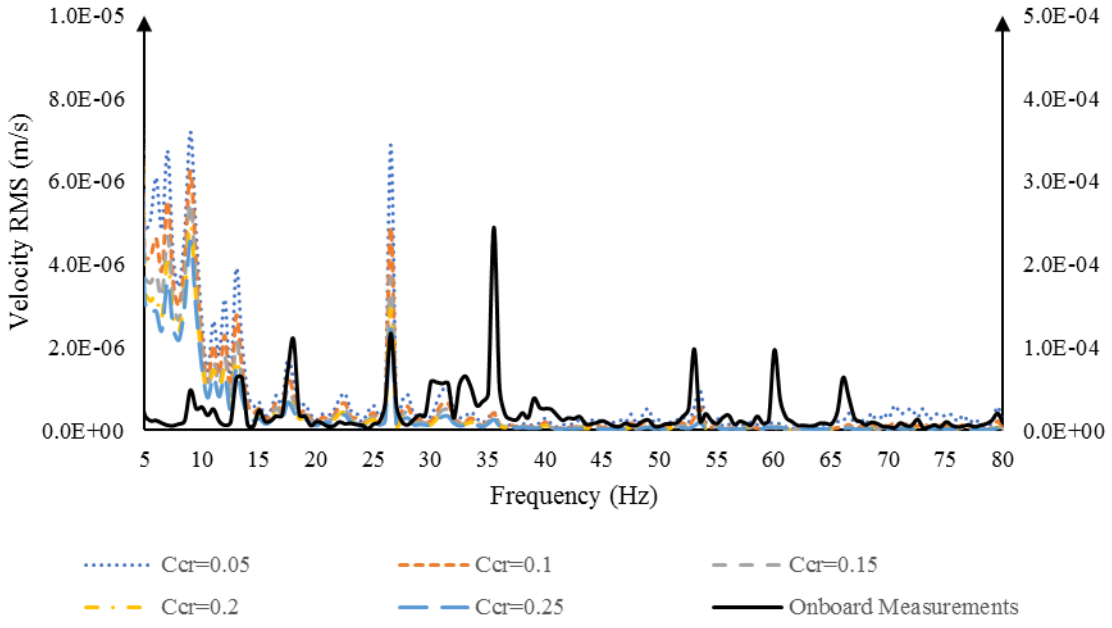

Figure C.33: Onboard Measurements against Finite Element with Varying Damping (Propeller Excitation) - Bunker P1

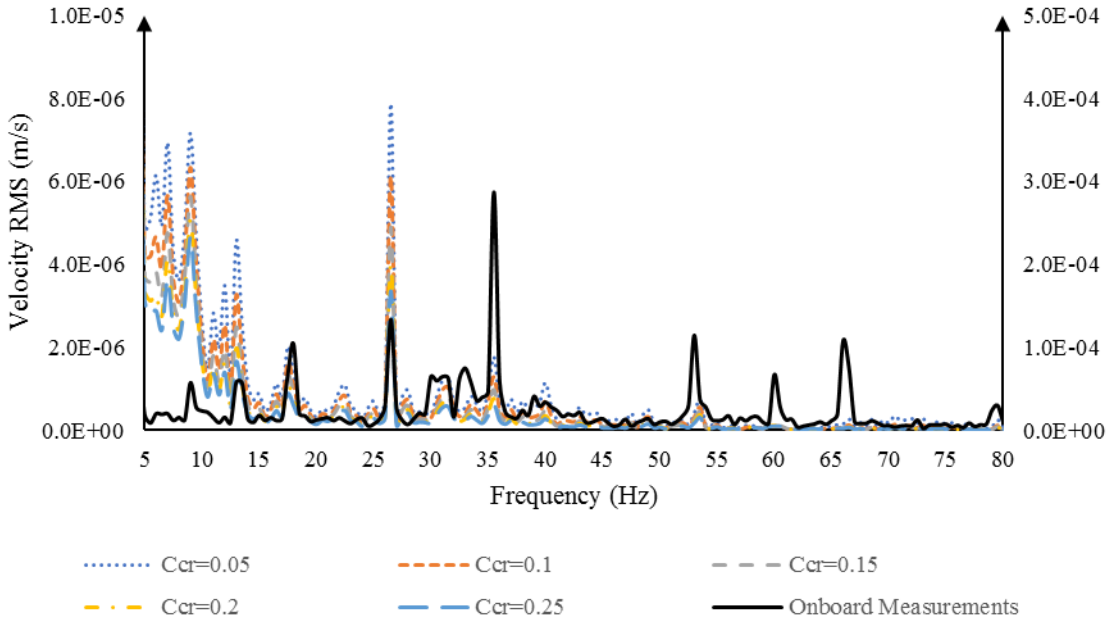

Figure C.34: Onboard Measurements against Finite Element with Varying Damping (Propeller Excitation) - Bunker P2

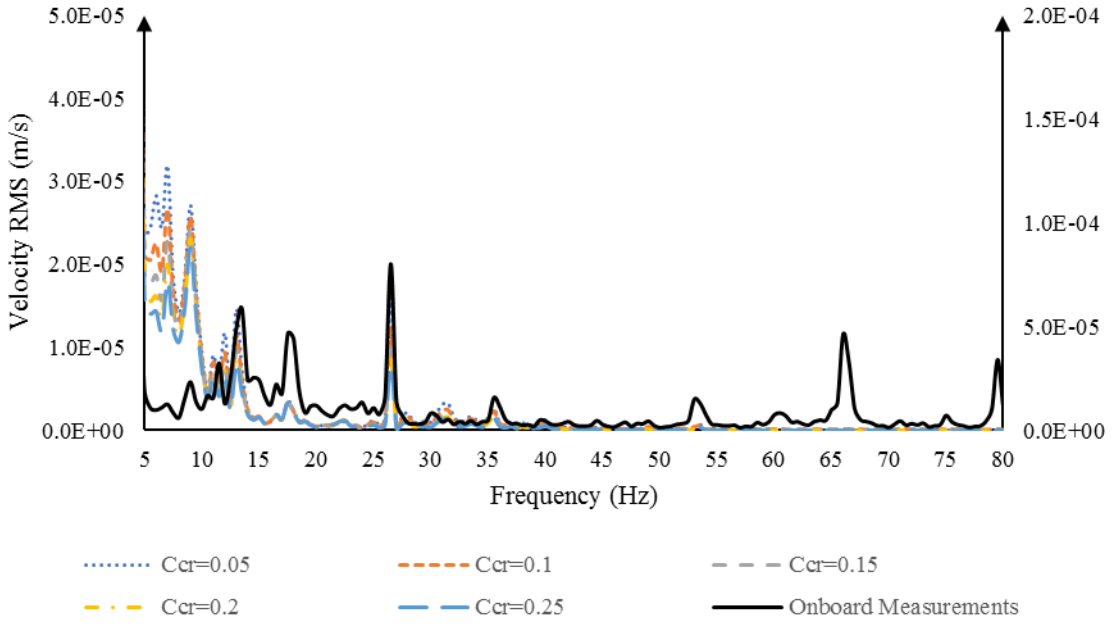

Figure C.35: Onboard Measurements against Finite Element with Varying Damping (Propeller Excitation) - Cabin P1

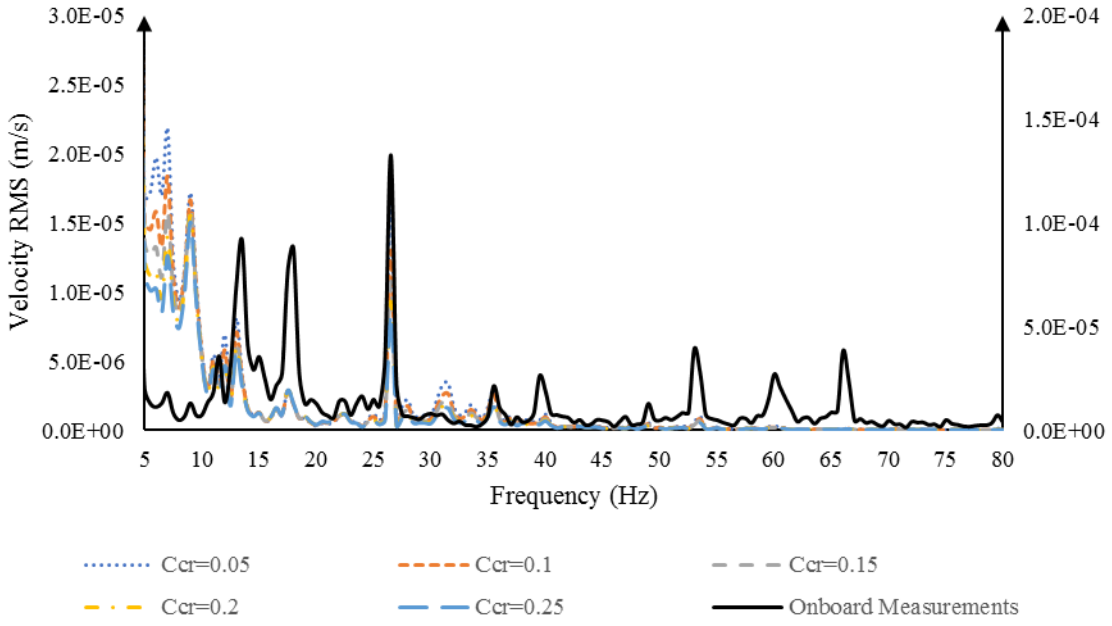

Figure C.36: Onboard Measurements against Finite Element with Varying Damping (Propeller Excitation) - Cabin P2

Appendix C.4. All Excitation Sources Damping Determination

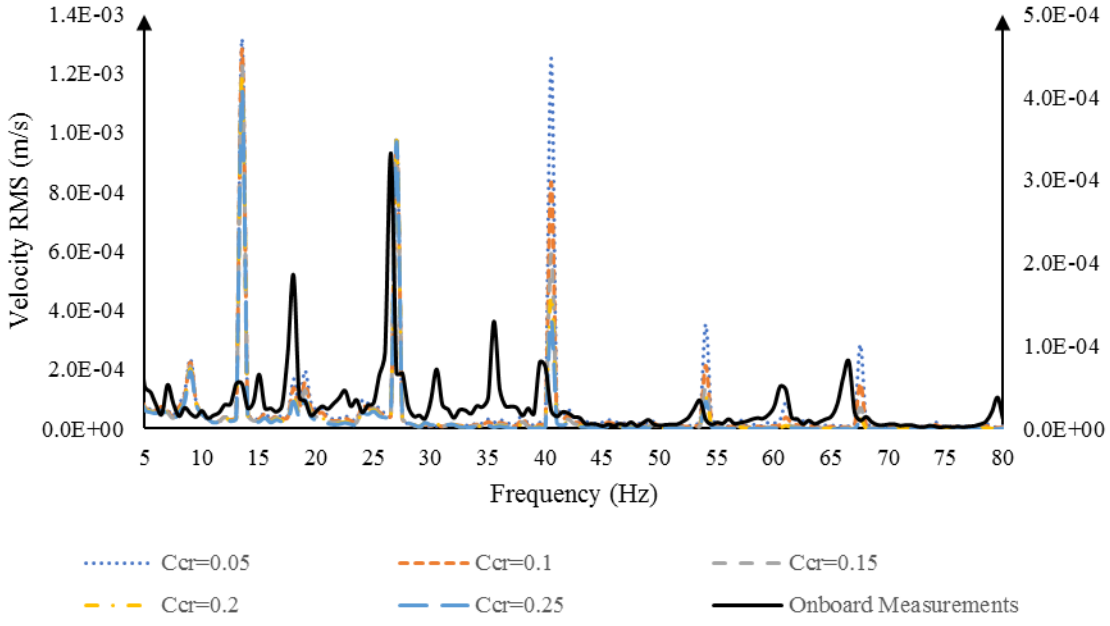

Figure C.37: Onboard Measurements against Finite Element with Varying Damping (All Excitation) - Wheelhouse G1 P1

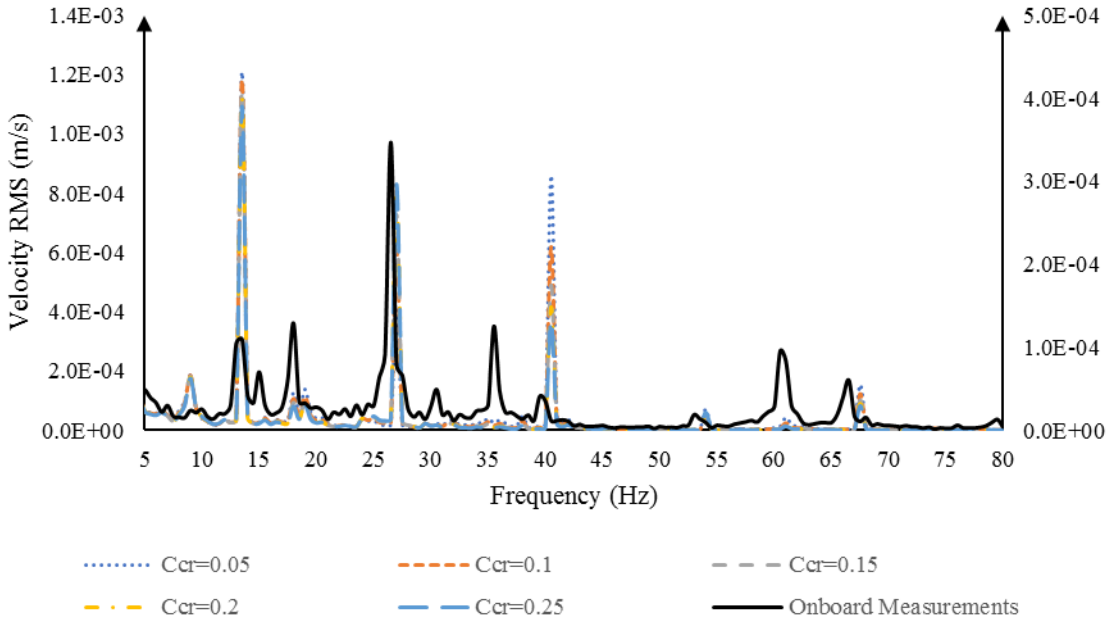

Figure C.38: Onboard Measurements against Finite Element with Varying Damping (All Excitation) - Wheelhouse G1 P2

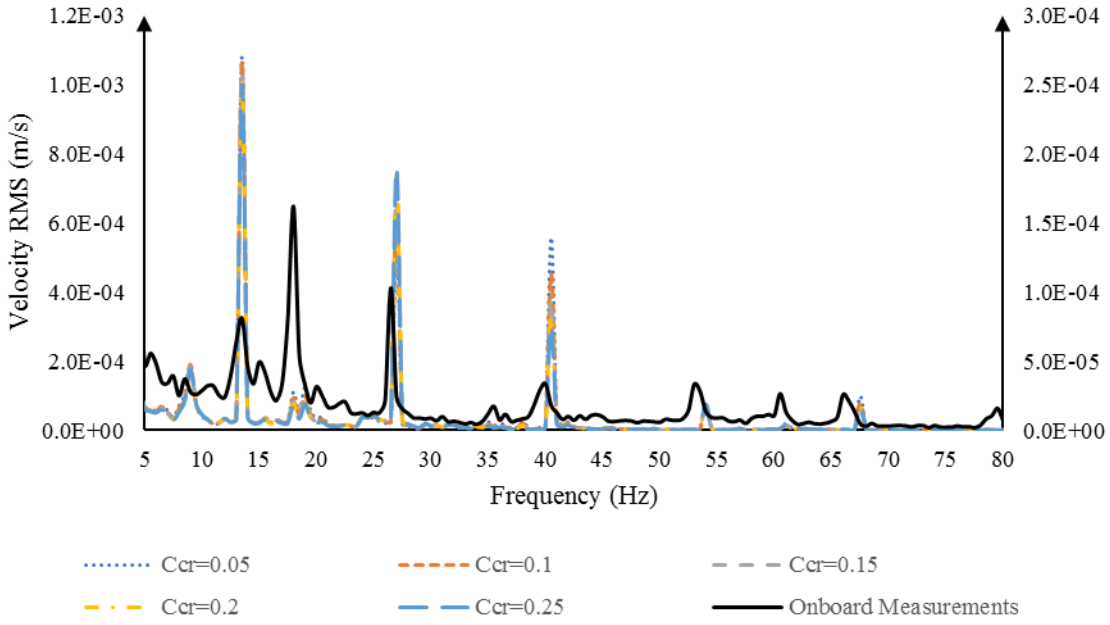

Figure C.39: Onboard Measurements against Finite Element with Varying Damping (All Excitation) - Wheelhouse G2 P1

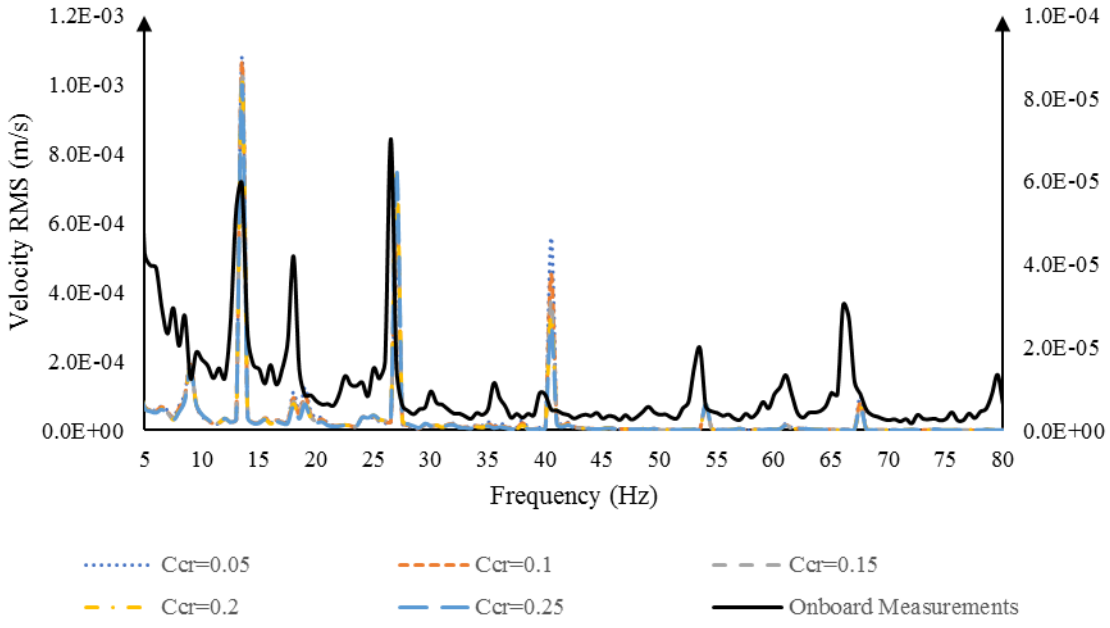

Figure C.40: Onboard Measurements against Finite Element with Varying Damping (All Excitation) - Wheelhouse G2 P2

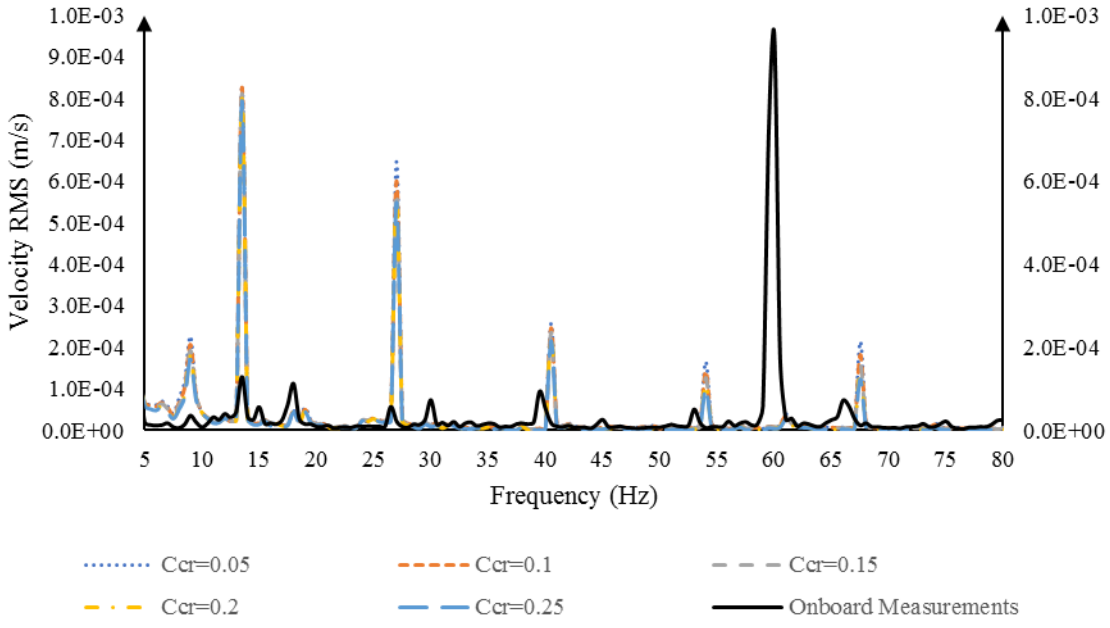

Figure C.41: Onboard Measurements against Finite Element with Varying Damping (All Excitation) - Canteen G1 P1

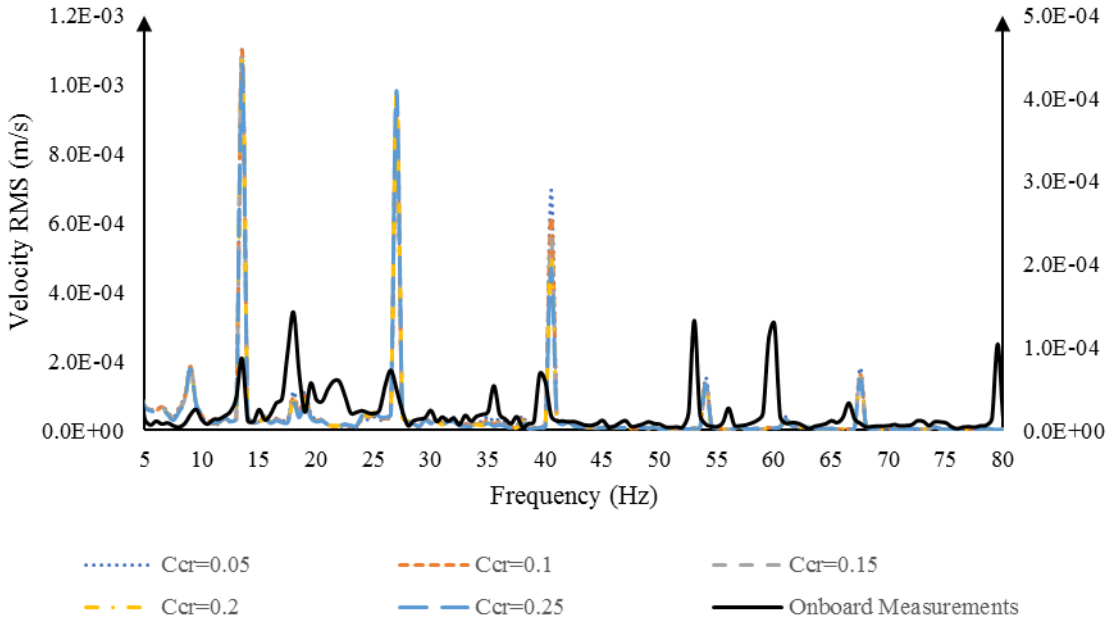

Figure C.42: Onboard Measurements against Finite Element with Varying Damping (All Excitation) - Canteen G1 P2

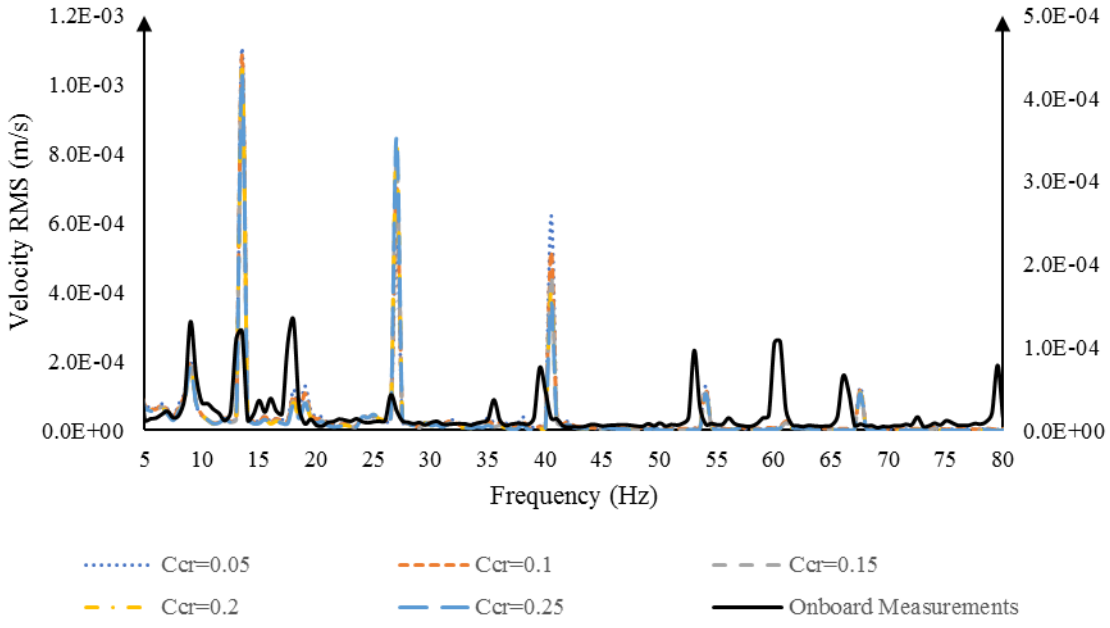

Figure C.43: Onboard Measurements against Finite Element with Varying Damping (All Excitation) - Canteen G2 P1

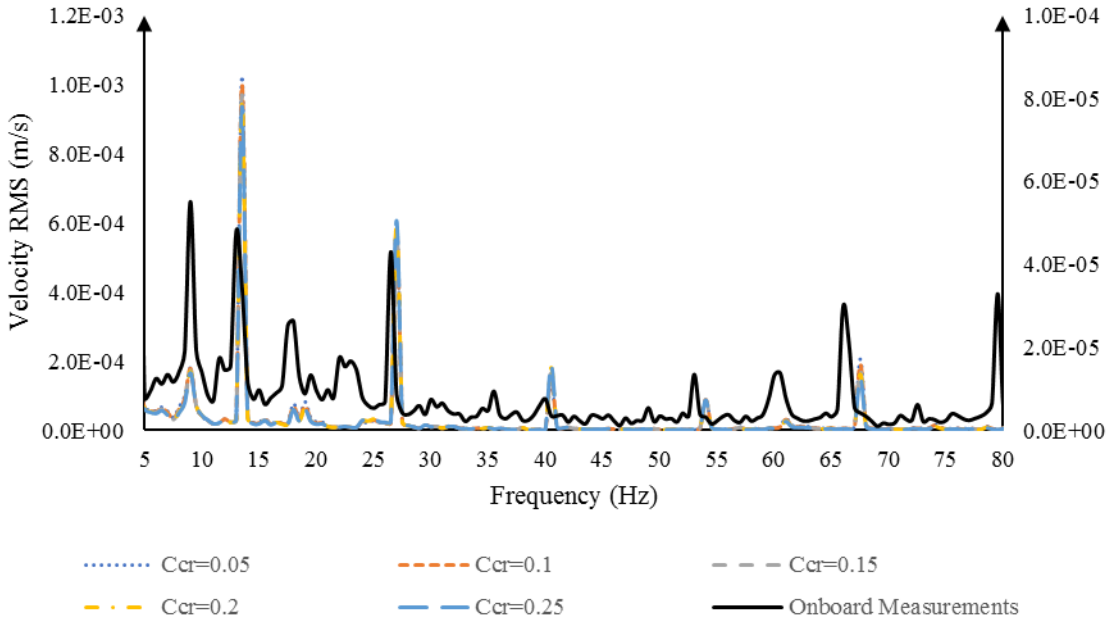

Figure C.44: Onboard Measurements against Finite Element with Varying Damping (All Excitation) - Canteen G2 P2

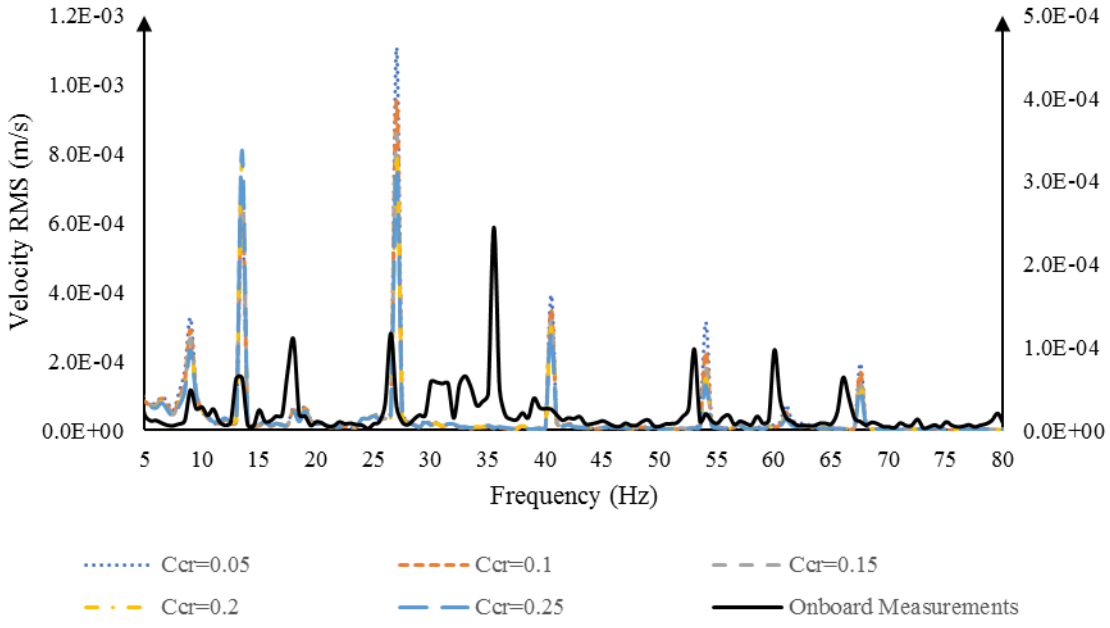

Figure C.45: Onboard Measurements against Finite Element with Varying Damping (All Excitation) - Bunker P1

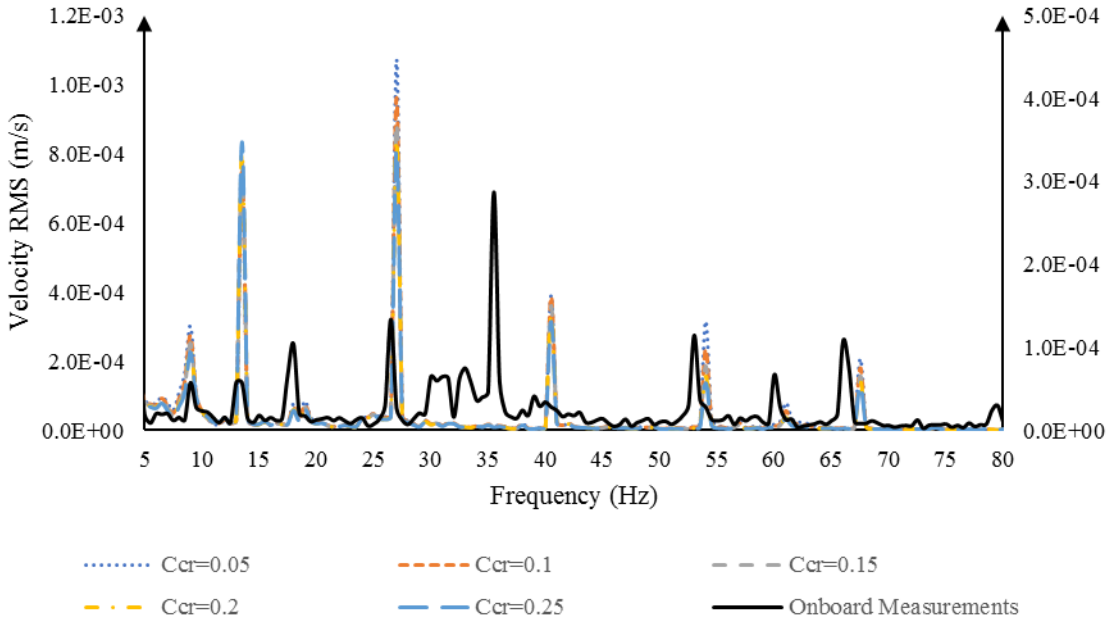

Figure C.46: Onboard Measurements against Finite Element with Varying Damping (All Excitation) - Bunker P2

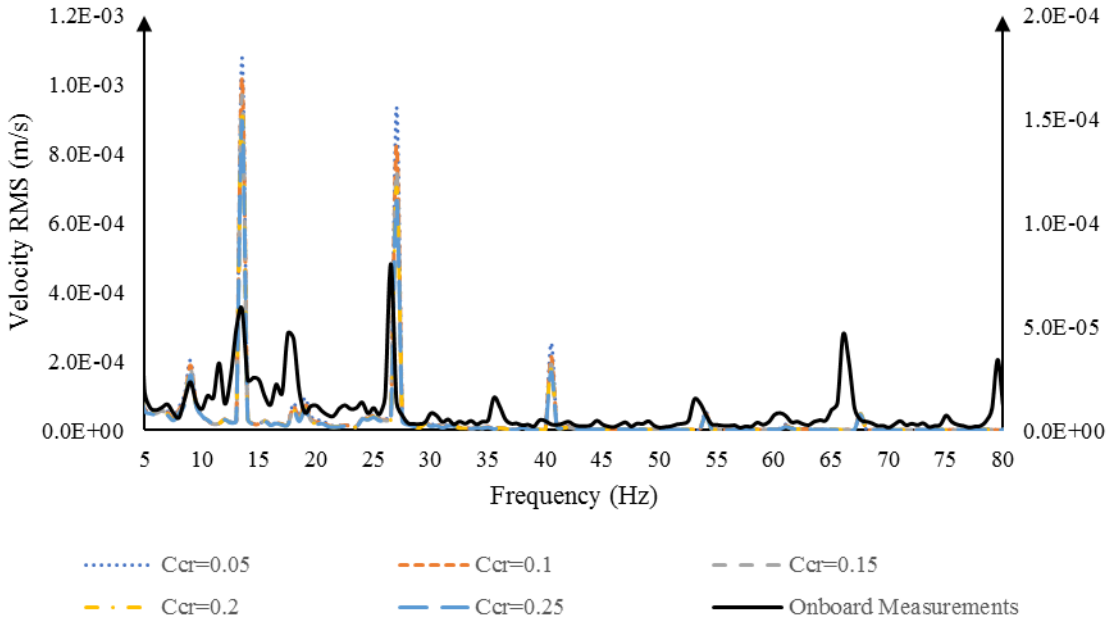

Figure C.47: Onboard Measurements against Finite Element with Varying Damping (All Excitation) - Cabin P1

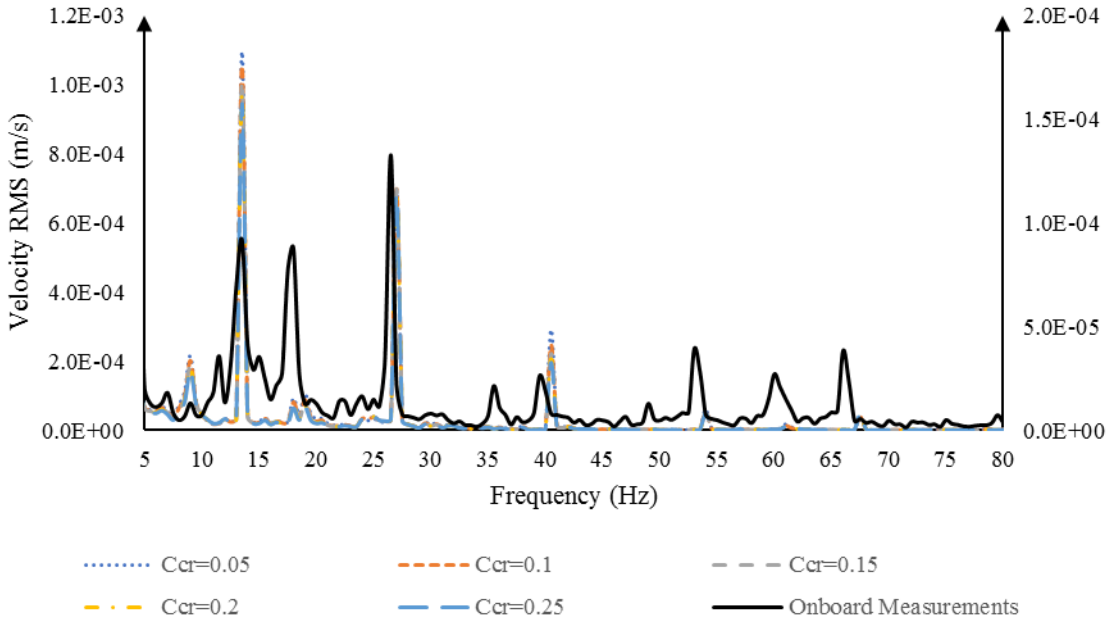

Figure C.48: Onboard Measurements against Finite Element with Varying Damping (All Excitation) - Cabin P2